WADC TECHNICAL NOTE 56-320

A STUDY OF HIGH DRAG CONFIGURATIONS AS FIRST STAGE DECELERATORS

HARRY W. WIANT
RAYMOND O. FREDETTE

COOK RESEARCH LABORATORIES
A DIVISION OF COOK ELECTRIC COMPANY
CHICAGO, ILLINOIS

JULY 1956

PARACHUTE BRANCH, EQUIPMENT LABORATORY

AF 33(616)-2345

WRIGHT AIR DEVELOPMENT CENTER
AIR RESEARCH AND DEVELOPMENT COMMAND
UNITED STATES AIR FORCE
WRIGHT-PATTERSON AIR FORCE BASE, OHIO

Carpenter Litho & Prtg. Co., Springfield, O.
100 - January 1957

FOREWORD

This report was prepared by the Cook Research Laboratories, a Division of the Cook Electric Company, Chicago, Illinois in compliance with Item I of Contract No. AF 33(616)-3346. Work by these Laboratories was initiated by the Equipment Laboratory, Wright Air Development Center, with Mr. John Kiker as Project Officer. The work at Cook Research Laboratories was conducted under the supervision of Dr. J. R. Downing, Director; Dr. H. V. Hawkins, Assistant Director; and Mr. R. O. Fredette, Assistant Director, with Mr. H. W. Wiant, as Project Engineer. Other Cook personnel contributing to the operation of the project included Messrs. W. Henricks, A. Tamosaitis, A. H. Solarski, and F. Doerr.

This report, a technical note, covers the study phase of the subject contract.

ABSTRACT

A study of high drag configurations is performed to determine their suitability as first stage decelerators for guided missiles and target drone aircraft. The report considers devices which are applicable in Mach number ranges from 1.0 to 5.0 and at altitudes from sea level to 250,000 feet. It is concluded that, for cases where the area of the brake can be less than the cross-sectional area of the vehicle, dive brakes are most suitable. For those conditions where the braking area required exceeds the cross-sectional area of the vehicle, a parachute system is most desirable. In order to withstand the effects of aerodynamic heating, the parachute should be constructed of metal. Sled tests are recommended to explore the operational characteristics of metal canopy parachutes.

PUBLICATION REVIEW

This report has been reviewed and is approved:

FOR THE COMMANDER:

Warren P. Shepardson

WARREN P. SHEPARDSON
Chief, Parachute Branch
Equipment Laboratory
Directorate of Development
Wright Air Development Center

TABLE OF CONTENTS

LIST OF ILLUSTRATIONS

Figure Page

CHAPTER 1

INTRODUCTION

During the testing and utilization of guided missiles and target aircraft, it is often either necessary or economically advisable to recover these bodies after the preplanned termination of their flight or in the event of a malfunction.

To date, recovery has generally been effected through the use of nylon parachutes. However, due to aerodynamic heating, nylon parachutes are reaching their strength limitation as velocities exceed Mach 2.0. Therefore, it is the object of this project to provide adequate first stage recovery drag devices which can be used at speeds from Mach 1.0 to Mach 5.0, and at altitudes from sea level to 250,000 feet. The project specifies that a brake drag area of 16 square feet be taken as the basis for the studies.

Probably the two most desirable characteristics of any first stage recovery drag device are that it be an efficient producer of drag and be able to withstand aerodynamic heating. There is also the inherent requirement of all missile and aircraft components that dictates they be light in weight and compact. The purpose of this study is to investigate known, or conceive of new drag devices and principles, and compare the above mentioned characteristics of each.

The number of potential devices is rather large; therefore, the devices treated in this study were considered in two broad categories. These are: (1) devices which are towed by or trail the missile and (2) devices which are immediately attached to the vehicle.

Manuscript released by the author 1 August 1956 for publication as a WADC Technical Note.

This report investigates quantitatively the drag and temperature characteristics of braking devices that are potentially applicable. It also determines, generally, the structural requirements, i.e., weight and bulk of various devices, and qualitatively considers their suitability to packaging.

CHAPTER 2

CLASSIFICATION OF DRAG PRINCIPLES

Drag devices may be classified into the following two broad categories:

(1) Towed or trailing devices, e.g., parachute or streamer with drag plates spaced along its length

(2) Devices attached immediately and rigidly to the vehicle, which enter the airstream either by translation or rotation. The dive brake and the spoiler are examples of such devices.

The specific principles, applicable in either category, which can be employed to produce drag are:

(1) Bluff configuration having inherently high drag due to its shape

(2) Impluse or momentum exchange, e.g., deflection of the airstream through a large angle

(3) Chemically stored energy, as,

(a) Retrorockets

(b) Motor thrust reversal.

(4) Generation of "lift" force in direction opposite the velocity, as by means of a rotochute.

Devices selected for study in this program must be considered on the basis of the following characteristics:

(1) Effectiveness in producing drag

(2) Capability of withstanding elevated temperatures

(3) Suitability of materials

(4) Weight and bulk

(5) Stowage or packageability.

Subsequent sections of this report discuss these characteristics and compare the relative advantages of various braking devices.

Although the contract specifically calls for consideration of a given drag area, the first part of this report examines drag devices in terms of their characteristic drag coefficient. This approach is employed since only devices having high values of drag coefficient are suitable for purposes of the contract. Thus drag coefficient and methods for its estimation are considered first.

CHAPTER 3

AERODYNAMICS

A. General Considerations

The subsonic drag of bodies producing no lift is made up of skin friction and pressure or form drag. The subsonic drag of bodies of various configurations including many types of braking devices has been experimentally investigated and presented in various publications by the NACA and other sources. Thus the drag performance of braking devices in the subsonic range of operation can be predicted quite well by making use of the available experimental data.

Usually, the supersonic drag of bodies is divided into fore drag, base drag, and skin friction drag. The fore and base drags are the integrals of the pressure forces acting on the forward and rearward parts of the body. The skin friction of braking devices at supersonic speeds amounts only to a small percentage of the total drag and therefore it is of little significance compared to fore drag and base drag.

At the present time there are relatively little experimental drag data on the supersonic drag of braking devices per se; however, there exist considerable data and physical understanding of supersonic flow about objects of similar configurations. Thus the drag performance of supersonic braking devices can be estimated satisfactorily in many instances from theoretical considerations and available drag data on similar shapes. Since braking devices usually imply blunt objects with a high drag-producing ability, the following sections will consider the prediction of supersonic drag on such shapes as flat disks and blunt wedges.

There are basically two approaches which are used in the determination of supersonic nose drag of blunt bodies. The first one, set forth in Chapter XII of Ref. 1, is based on the assumption that the nose drag of a blunt

body can be taken as a percentage of compressible impact pressure. This assumption implies that the drag is proportional to the compressible impact pressure, the constant of proportionately K_3 being a shape factor. Thus the drag coefficient is:

$$C_{D_N} = \frac{D_N}{q S_N} = \frac{K_3 (p_{t2} - p_\infty) S_N}{q S_N} = K_3 \frac{q_c}{q}$$

$$= \frac{2K_3}{\gamma M^2} \left[\left(\frac{\gamma + 1}{2\gamma M^2 - \gamma + 1} \right)^{\frac{1}{\gamma - 1}} \left(\frac{\gamma + 1}{2} M^2 \right)^{\frac{\gamma}{\gamma - 1}} - 1 \right] \qquad (1)$$

where:

$$q = \frac{\gamma}{2} M^2 p_\infty$$

A more direct method of estimating the shape factor is to make use of measurements of pressure on the face of the body. The drag coefficient is calculated from the integral of the pressure distribution over the face as follows:

$$C_{D_N} = \frac{1}{q S_N} \int_{S_N} \left[p(x, y) - p_\infty \right] dS$$

$$= \frac{p_\infty}{q} \cdot \frac{1}{S_N} \int_{S_N} \frac{p(x, y)}{p_\infty} dS - \frac{p_\infty}{q}$$

$$= \frac{2}{\gamma M^2} \left[\frac{1}{S_N} \int_{S_N} \frac{p(x, y)}{p_\infty} dS - 1 \right] \qquad (2)$$

If the pressure, $p(x, y)$ at any point on the face is written as a fraction, K'_2, of stagnation pressure, p_{t2}, behind the normal shock, then

$$C_{D_N} = \frac{2}{\gamma M^2} \left[\frac{Pt2}{P\infty} \frac{1}{S_N} \int_{S_N} K'_2 (x, y)\, dS - 1 \right]$$

The shape factor, K_2 in this case is defined as

$$K_2 = \frac{1}{S_N} \int_{S_N} K'_2 (x, y)\, dS$$

Thus:

$$C_{D_N} = \frac{2}{\gamma M^2} \left(K_2 \frac{Pt2}{P\infty} - 1 \right)$$

The ratio $\frac{Pt2}{P\infty}$ is determined from flow relations across a normal shock as a function of Mach number; see, for example, Ref. 2. The quantity, K_2 may be determined from measurements of the pressure distribution on the face of two-dimensional wedges of varying semivertex angle such as those given in Ref. 3. K_2 is plotted in Figure 1 as a function of wedge semivertex angle. In particular the limiting wedge, semivertex angle 90 degrees, is of interest here for purposes of comparison with the three-dimensional values given by Equation (1).

Using Equation (3) the fore drag coefficient over a semi-infinite flat plate is plotted in Figure 2 as a function of Mach number, along with a similar plot of the fore drag coefficient given by Equation (1) for a circular disk for which the shape factor $K_3 = 0.9$ as shown in Figure 12.10 of Ref. 1. The two-dimensional values of drag coefficient are only about 6% greater than the three-dimensional values.

The approach given by Equation (3) is considered to be the more accurate since the factor K_2, operates only on the stagnation-to-static pressure ratio behind the normal shock and should be less dependent on Mach number, for bodies with well detached shock waves; whereas the factor, K_3 of Equation (1) also relates to the free stream static pressure, which, in reality is unaffected by the presence of a body. However, in the following sections, the supersonic fore drag of braking devices will be computed from Equation (1) for finite cross sections and from Equation (3) for two-dimensional shapes.

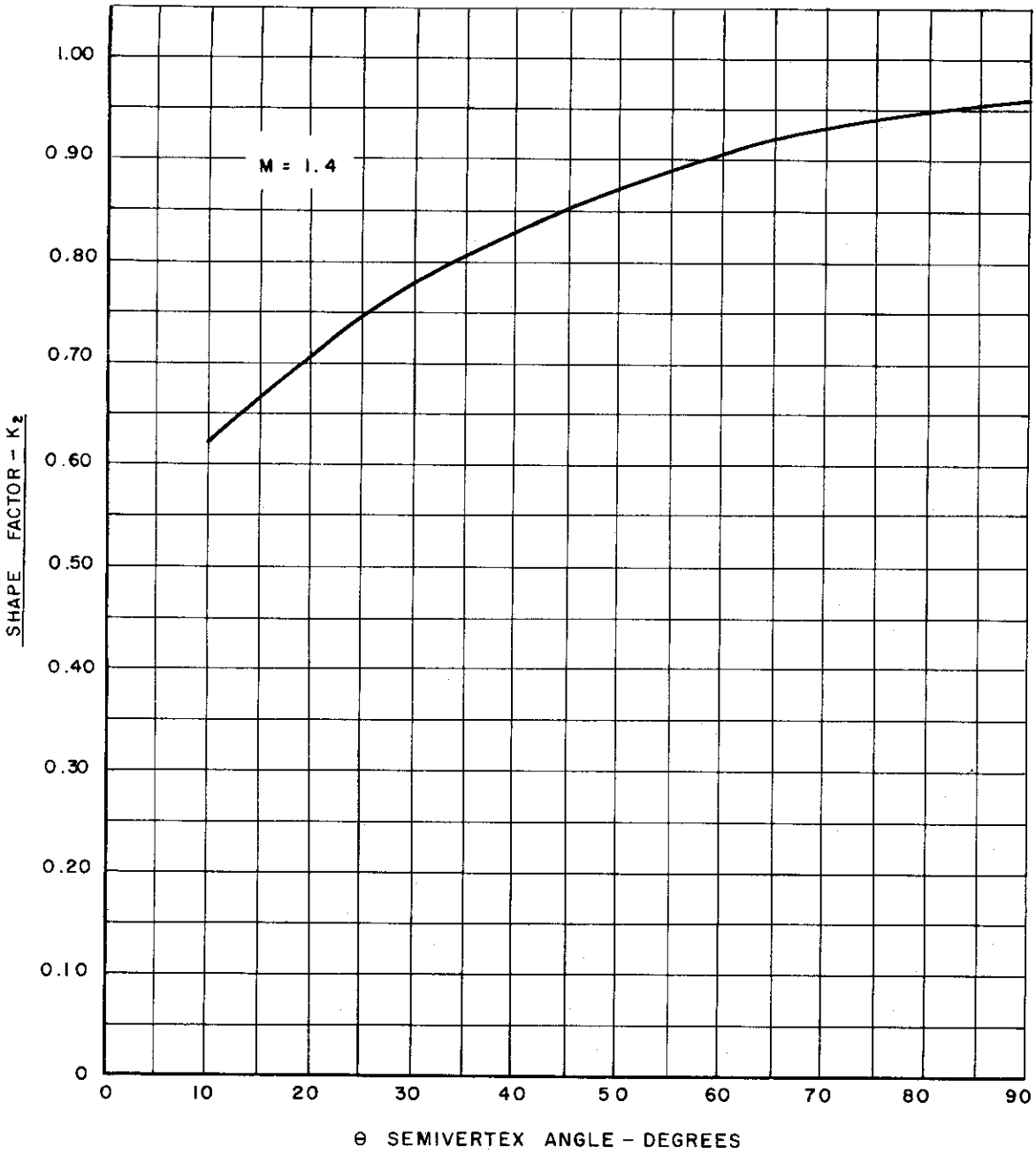

Figure 1. Shape Factor, K_2, as a Function of Deflection Angle Determined from Pressure Distribution on Two Dimensional Bodies

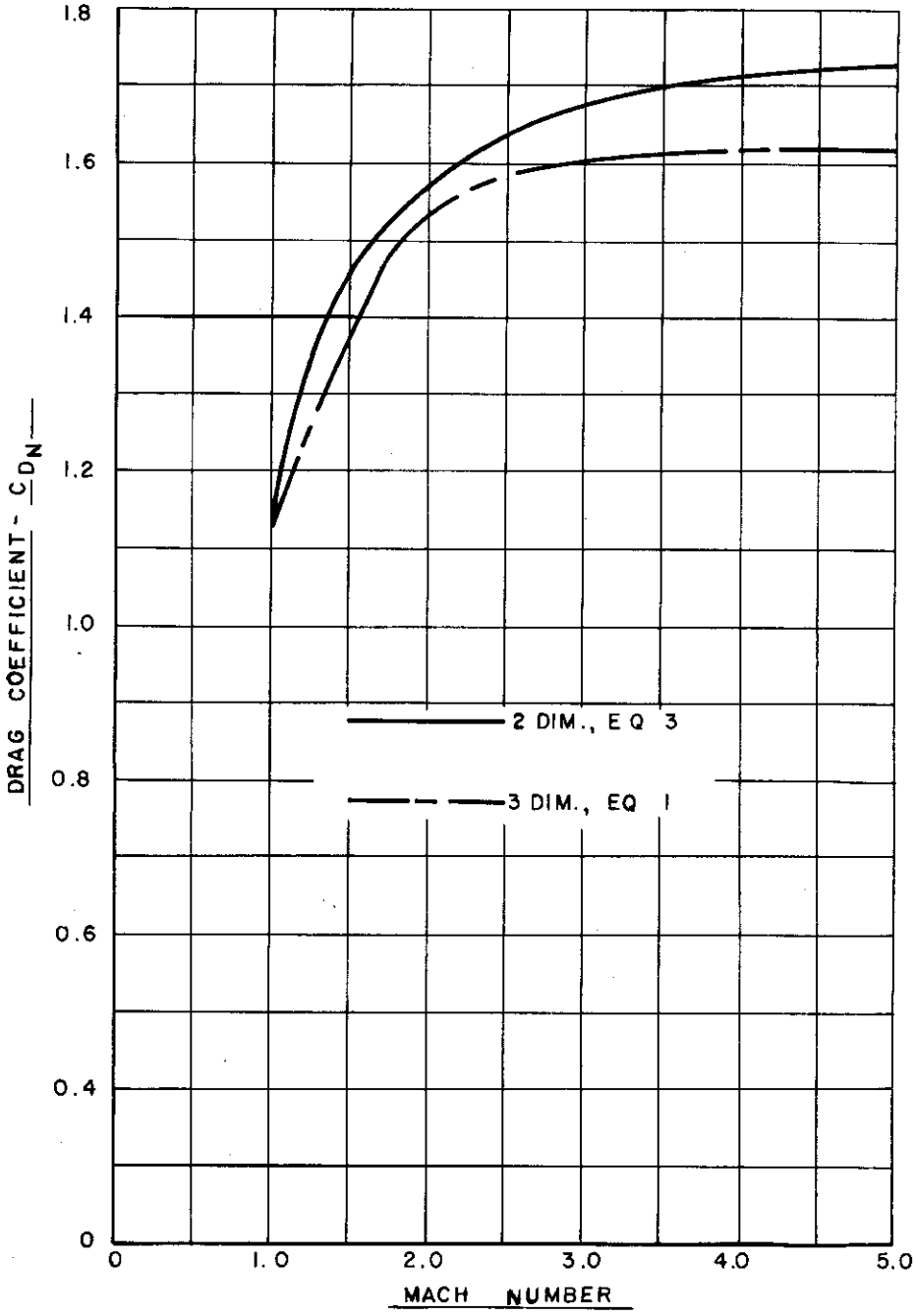

Figure 2. Comparison of Fore Drag Coefficient Computed from Equations (1) and (3) for Three and Two Dimensional Bodies Respectively

Base drag is caused by considerably reduced static pressure at the base of the missile. Although the base drag coefficient is influenced by both Mach number and Reynolds number, results plotted from data in Figure 12.5 of Ref. 1 and shown in Figure 3 indicate pressure ratio of $\frac{p_B}{p_\infty} = 0.42$ can be

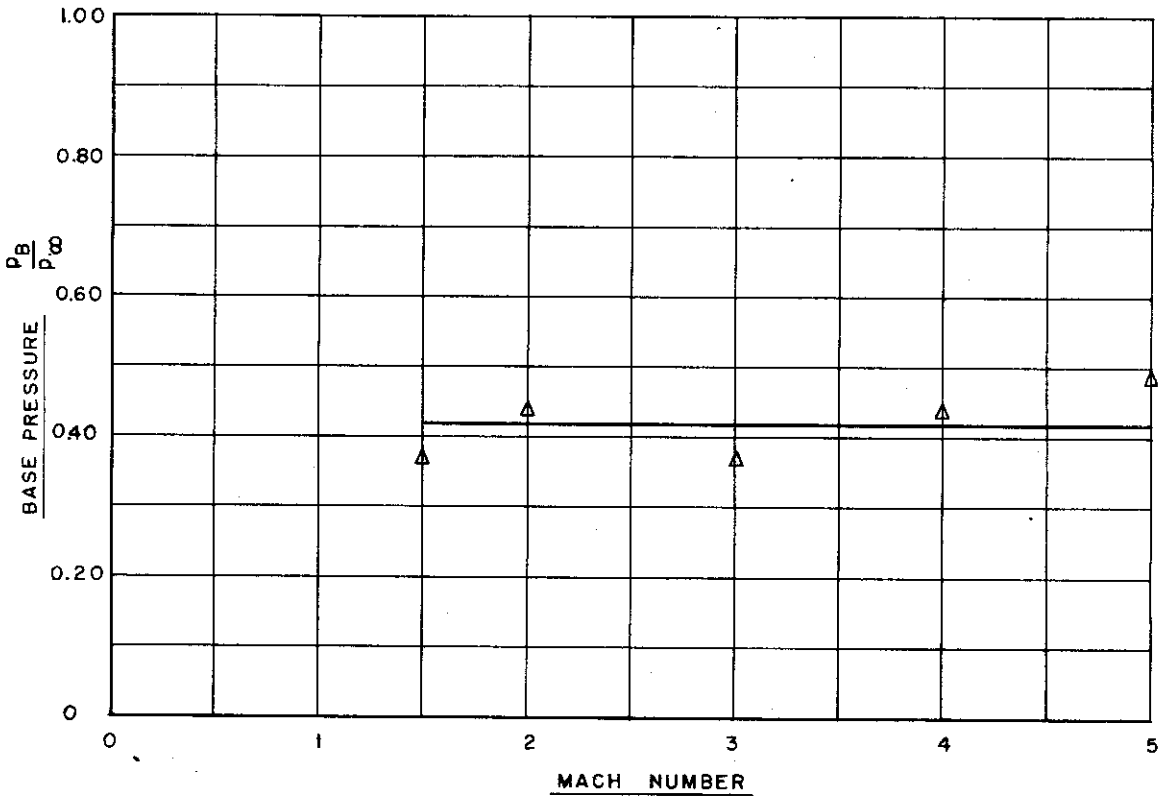

Figure 3. Base Pressure vs. Mach Number from Ref. 1

used as a satisfactory average value over a wide range of supersonic velocities. This same tendency is also noted in Figure 28 of Ref. 4. The base drag coefficient based on the frontal area and $\frac{p_B}{p_\infty} = 0.42$ is given by

$$C_{D_B} = \frac{2}{\gamma M^2} \left(1 - \frac{p_B}{p_\infty}\right) = \frac{0.83}{M^2} \qquad (4)$$

In addition to drag considerations, the wake effects are also of great importance in determining the relative locations of braking devices. In case of trailing devices the wake characteristics are the deciding factor in the spacing of the disks and, in case of fuselage mounted devices, the wake properties determine the optimum location of dive brakes and spoilers to minimize interference with the flow over the fins of a vehicle.

The wake effects cannot be calculated theoretically, and experimental data are very scarce at higher Mach numbers. However, Ref. 5 has some results of wake survey at the core of the wake. The tests were conducted in a 4-1/2 inch induction type wind tunnel at a Mach number of about 1.33. The model fineness ratio was $\frac{l}{d} = 4.0$ with a diameter of d = 0.3 inches. The average static pressure in the wind tunnel during operation was 11 inches of mercury. Results of these tests are shown in Figure 4 as total pressure recovery in the wake. Computing the ratio of dynamic pressure in the wake to

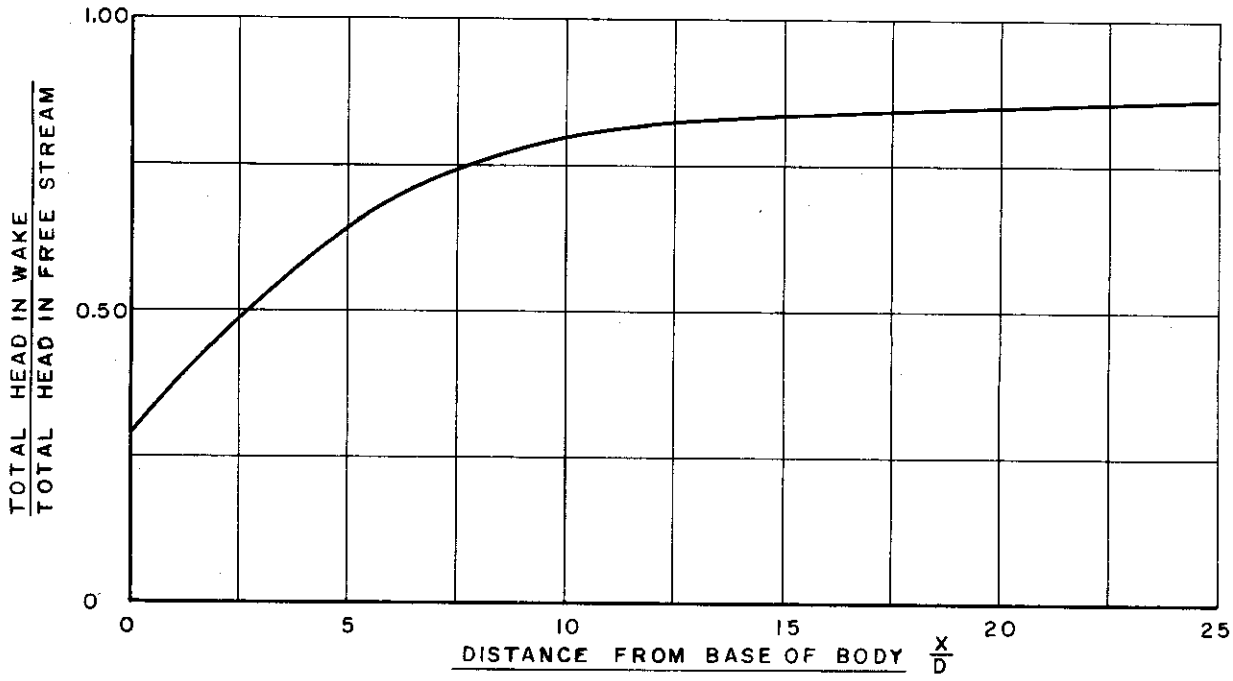

Figure 4. Total Head Recovery on the Centerline of the Wake of Body at Mach 2.86

that in free stream from the data in Figure 4 it is found that at $\frac{x}{d} = 5.0$, $\frac{q_w}{q} = 0.45$; $\frac{x}{d} = 10.0$, $\frac{q_w}{q} = 0.67$: and $\frac{x}{d} = 25$, $\frac{q_w}{q} = 0.85$ where $\frac{x}{d}$ is the caliber distance down stream from the base.

The results of a survey of the wake behind a circular cylinder, conducted at M = 2.86, (Ref. 6) are presented in Figure 5. The dynamic pressure at the core is less than 20 per cent of free stream at 2 body diameters,

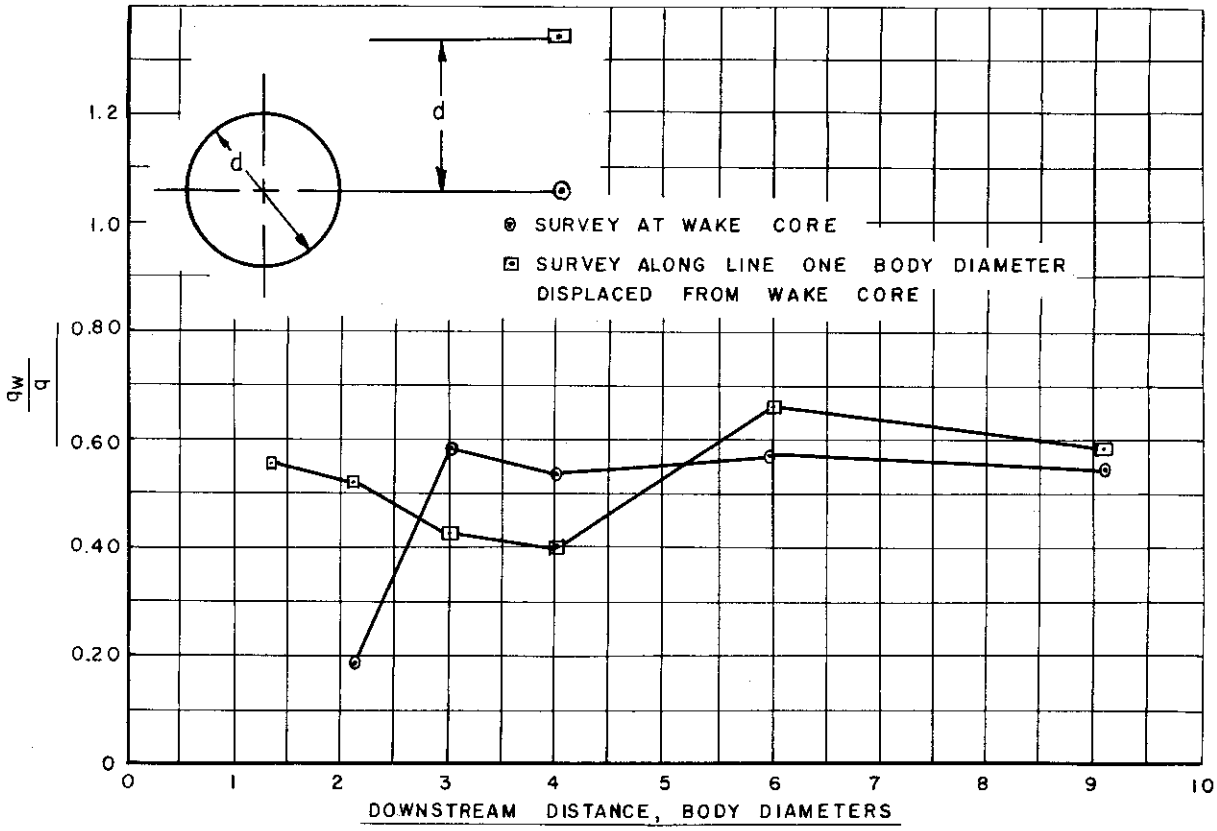

Figure 5. Ratio of Dynamic Pressure in Wake to Free Stream Dynamic Pressure Behind a Two-Dimensional Cylinder at Mach 2.86

and rises to about 60 per cent of free stream between 3 and 9 body diameters. At 1 body diameter displacement from the core, the dynamic pressure is

more variable but hovers about the value of dynamic pressure ratio of 0.6 from 2 to 9 diameters down stream. Discrepancies between the wake characteristics obtained from Ref. 5 and those contained in Ref. 6 are due, probably, to the differences in the wake producing bodies. The data of Figure 5 imply that the pressure ratio in the wake one caliber displaced from the wake core is approximately equivalent to that of the core. Hence, on the basis of these limited data, trailing devices can be expected to operate in a fairly uniform transverse pressure field determined by the value at the wake core. Thus it is seen that the wake effects must greatly influence the location and spacing of braking devices.

The preceding discussion has established methods which will be used in estimating drag and qualitatively the stability characteristics of specific braking devices presented in the following parts of this section.

B. Immediately Attached Devices

1. Dive Brakes

Dive Brakes, as used in this application, refer to fuselage mounted flaps which can be rotated out into the airstream, Figure 6. Subsonic fuselage mounted dive brakes are usually either perforated or

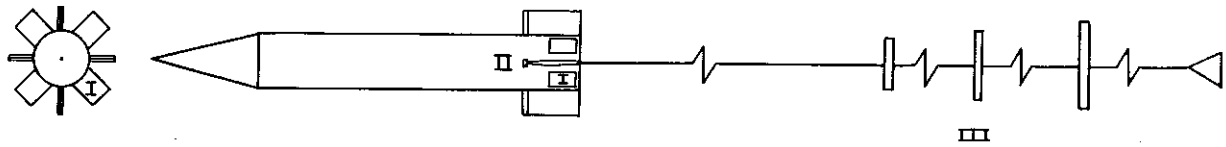

I DIVE BRAKES
II LEADING EDGE SLATS
III DRAG TRAIN

Figure 6. Sketch of Typical Drag Devices

slotted to prevent flutter caused by vortex shedding from the edges of the flap. Supersonically, however, the steady loading is high, so that the brakes must be designed for great strength. Consequently, wake

pulsations are negligible in this case, and it appears that supersonic dive brakes can be built as solid plates.

Typical high-subsonic, fuselage-mounted dive brakes are described in Ref. 7 and their subsonic drag coefficient is shown over a range of velocities. Since supersonic dive brakes will very closely resemble finite solid flat plates, their drag coefficient is assumed equal to that of a flat plate, operating at a given angle to the flow direction.

It was shown in Part A of this section that the fore drag of a flat plate at supersonic speeds is satisfactorily predicted by Equation (1) provided a suitable choice of the shape factor K_3 is used. Reference 1 indicates that a value of $K_3 = 0.9$ is satisfactory for a dive brake hinged at the rear or rotated out 90 degrees to the flow direction. For brakes which are hinged at the front, and which do not rotate fully 90 degrees into the air stream, the fore drag may be estimated by use of Equation (3) and the data of Figure 1, from which the effect of brake obliquity with the flow can be determined. The base drag of dive brakes is given by Equation (4).

The total drag for dive brakes oriented at 90 degrees to the flow direction is given in Figure 7. The drag data in the subsonic range were obtained from Ref. 7, and in the supersonic range were estimated by means of Equations (1) and (4).

The stability of a vehicle may be significantly influenced by the location of the dive brakes. As it was shown in Part A of this section, the dynamic pressure in the wake of a body is recovered only to 85% of its free stream value even at distances as great as 25 times the maximum diameter of the body. Thus it is important to avoid a location of dive brakes which would put the stabilizing fins of the missile in their wake. If the vehicle has four fins the desirable location of four dive brakes would be 45 degrees off fin centers. This arrangement would tend to concentrate the wake between the fins and reduce the wake effects of stability. An optimum brake location would be to the rear of the fins. It is indicated in Ref. 8 that, at Mach 6.5, the stability of a vehicle having dive brakes located to the rear is actually increased over that with the brakes in stowage.

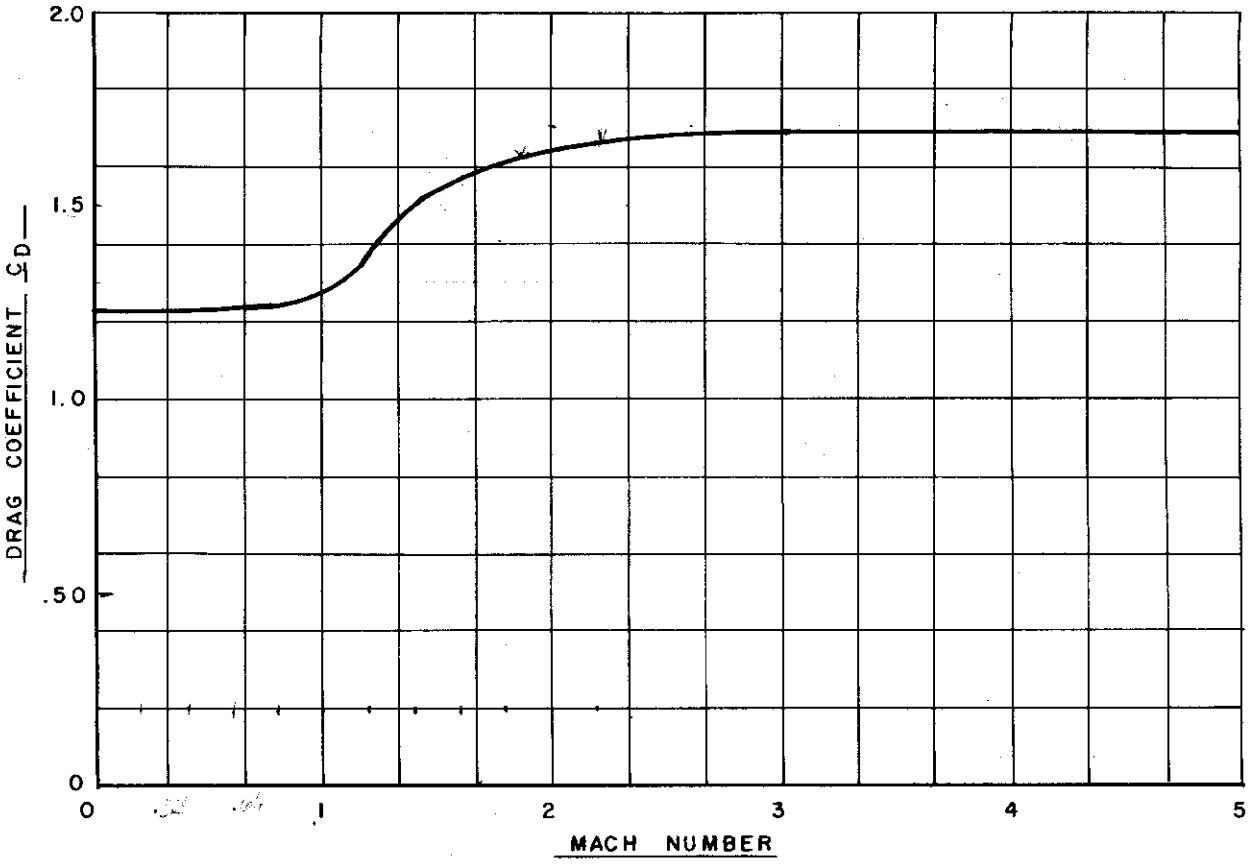

Figure 7. Drag Coefficient of Dive Brakes and Fin Leading Edge Slats vs. Mach Number

Dive brakes located between the fins will cause flow disturbances on them. The shock pattern in the wake of the brake will affect the boundary layer on the fins, probably causing flow separation, and generally reducing their lifting effectiveness.

2. Alteration of Flow Field by Blunting the Nose

In some instances it may be possible to detach or blunt the nose of a vehicle at a predetermined time thus increasing its drag coefficient.

The effects of nose blunting on the supersonic drag coefficient of a typical body of revolution have been determined by O. Walchner and are

represented in Figure 7 of Ref. 9.

Some interesting results can be deduced from the data presented in the above reference. An ogival-headed missile with an ogival radius of 6.5 calibers and a tip length of 2.5 calibers, Figure 8, is considered. Then, using the data from Figure 7 of Ref. 9, the increment in drag coefficient of the blunted body over that of the pointed body, based on the

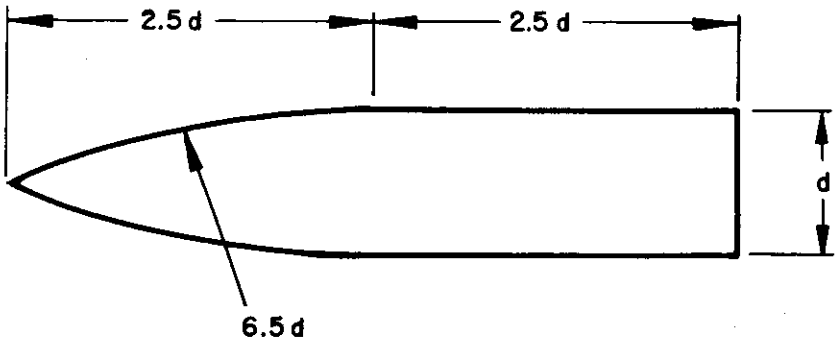

Figure 8. Typical Missile Configuration

area of the blunted nose, may be computed. These increments are plotted in Figure 9 as a function of Mach number for various amounts of nose bluntness. It is indicated that a substantial drag coefficient increment is obtained for Mach numbers above about 2.5, which is approximately independent of nose bluntness. Below M = 2.0, the increment in drag coefficient, based on blunted area, decreases as the per cent bluntness decreases, thus requiring greater amounts of blunting for a given increment in drag coefficient.

A plot of missile drag area, $C_D S_M$ can be prepared as shown in Figure 10. Figure 11 is a plot of $C_D S_M$ for the same missile with various amounts of blunting. The difference between the drag area in Figure 11 and Figure 10 represents the net increase in vehicle drag area, which is shown in Figure 12. From the standpoint of drag coefficient, nose blunting is equally effective for both small diameter and large diameter missiles. For a specified value of drag area, however, small diameter missiles may not permit a sufficient nose blunting to produce the required product of drag coefficient and area.

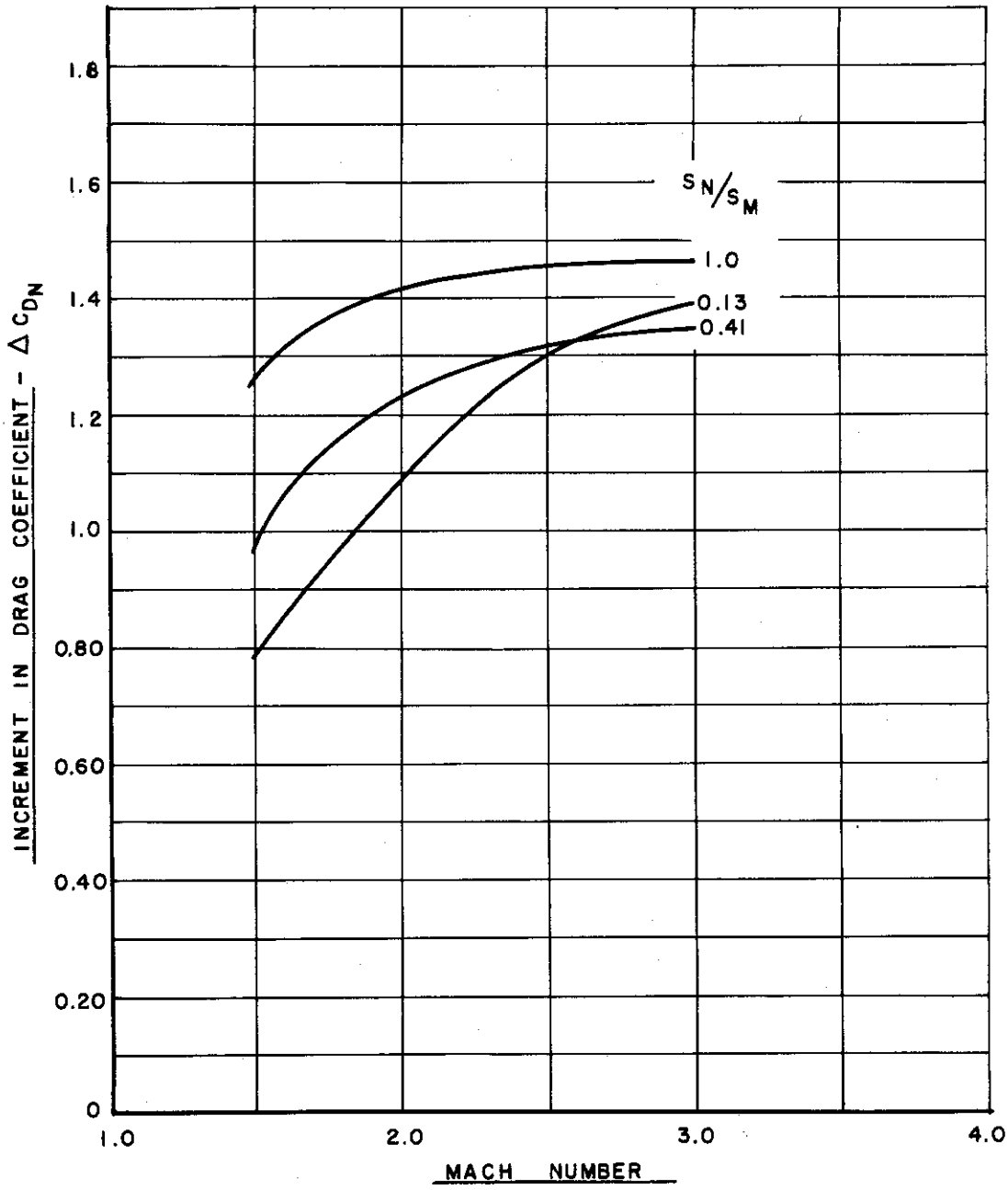

Figure 9. Increment in Drag Coefficient of Blunted Bodies over that of Pointed Body, Based on Area of Blunted Nose, as Function of Mach Number for Various Amounts of Bluntness

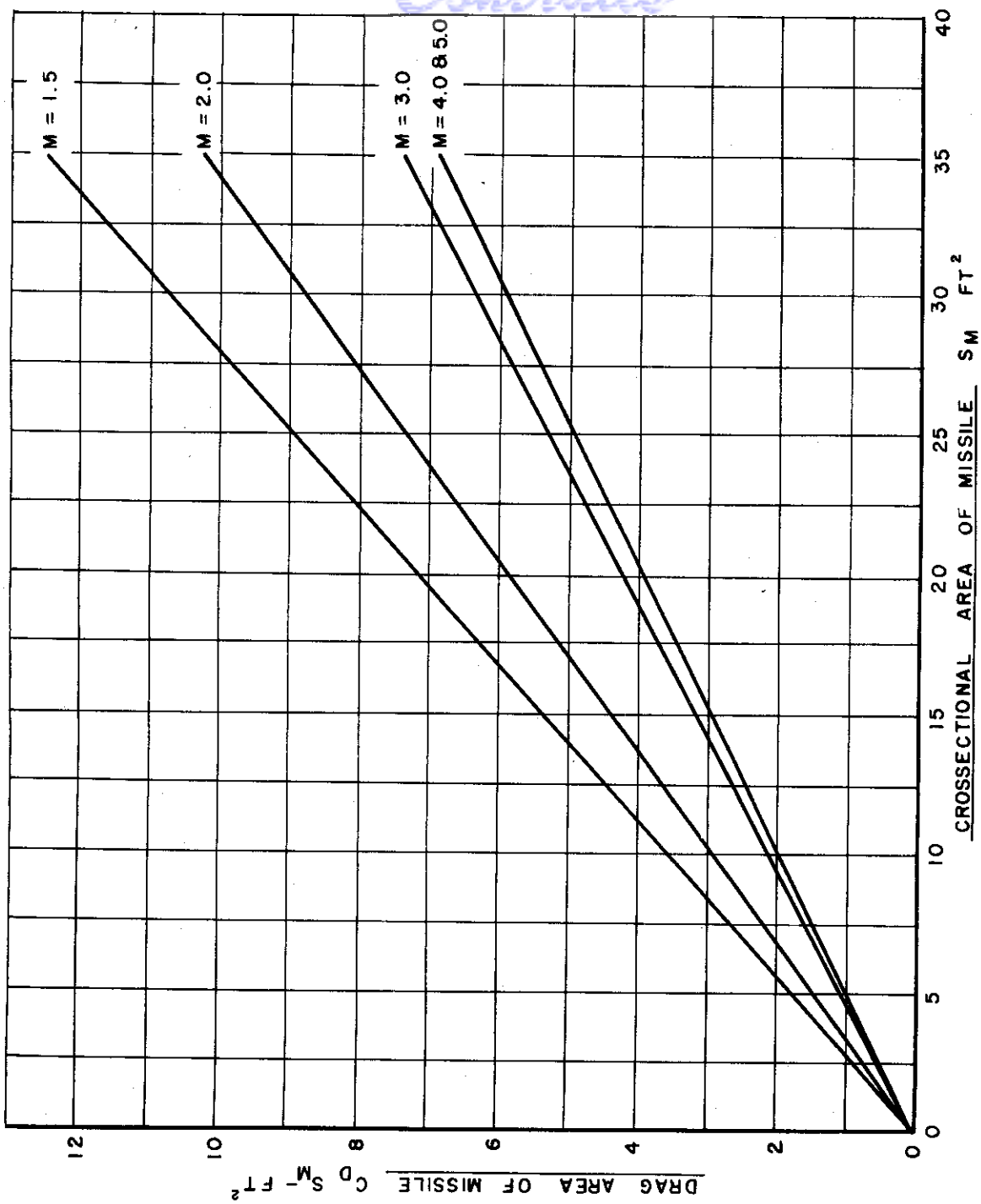

Figure 10. Basic Drag Area of a Hypothetical Missile vs. Missile Size

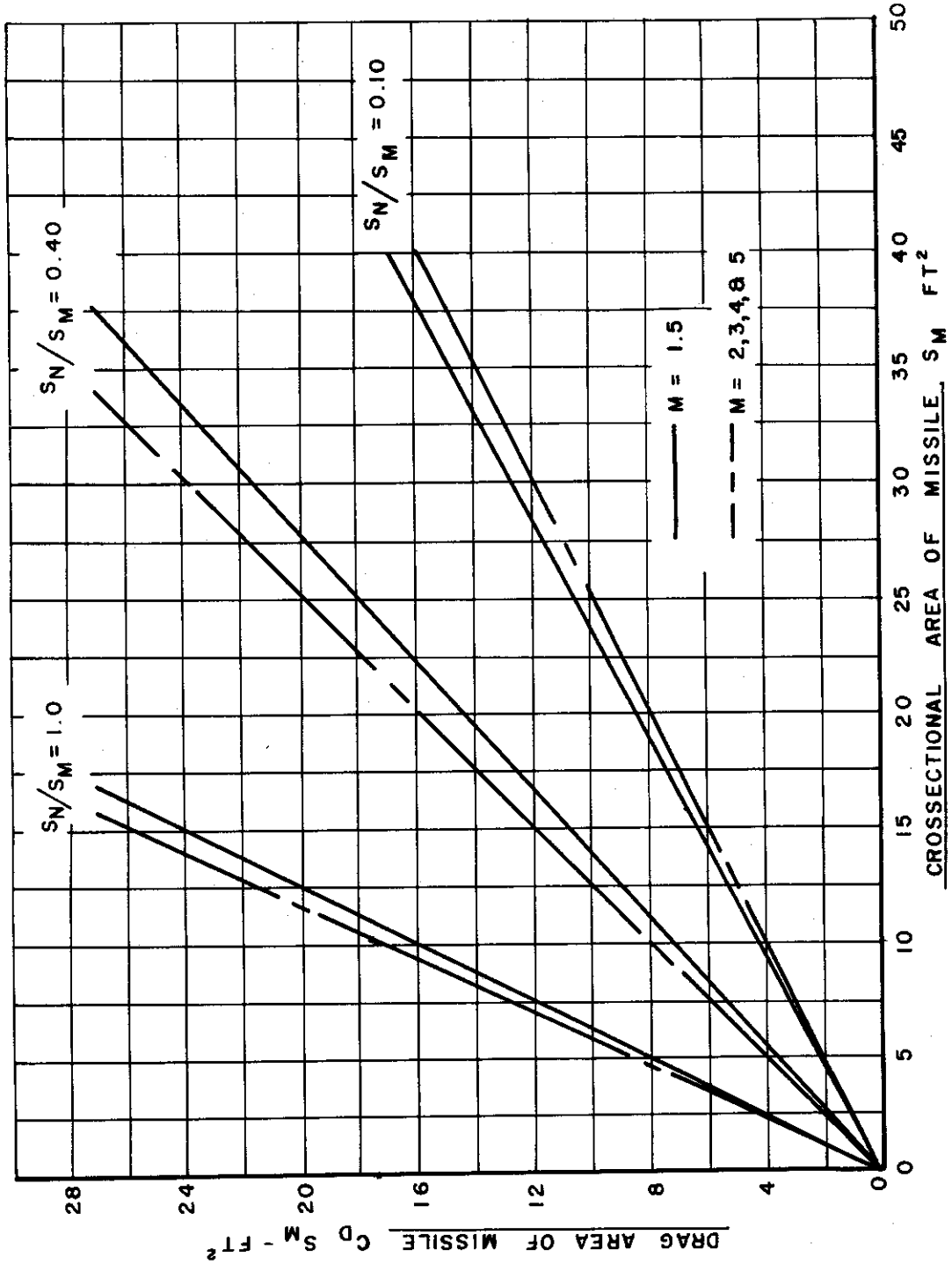

Figure 11. Drag Area of Hypothetical Missile with Various Amounts of Bluntness

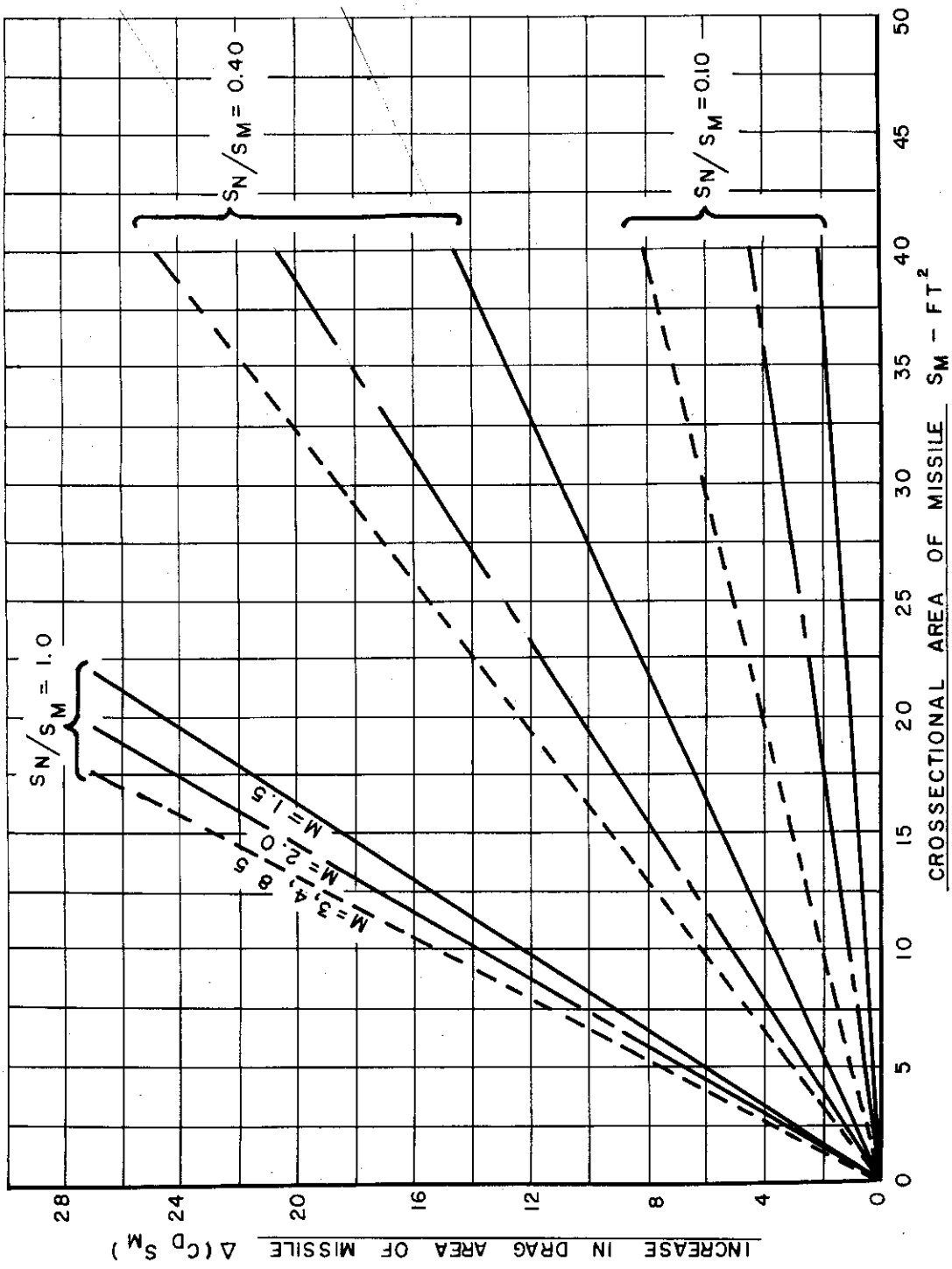

Figure 12. Net Increase in Drag Area of Hypothetical Missile with Various Amounts of Bluntness

The aerodynamic effectiveness of nose blunting decreases with Mach number, i.e., for the same percentage of bluntness a larger missile area is required to produce a drag area of 16 ft^2 at the lower Mach number. As an illustrative example a vehicle with a cross-sectional area of 47.5 ft^2 (diameter 7.78 feet) may be considered. Referring to Figure 12 a missile with this cross-sectional area and a nose bluntness of $S_N/S_M = 0.4$ is capable of producing a net increase in drag area of 28 ft^2 at M = 5.0. As the vehicle slows down this increase in drag area drops off to 16 ft^2 at M = 1.5. At Mach numbers less than M = 1.5 an additional drag producing device would be required in order to achieve a drag area of 16 ft^2.

The aerodynamic stability of a missile is improved by blunting the tip of the nose section. The blunt nose tends to destroy lift over the forward part of the nose section which in turn reduces the upsetting moment about the base of the nose section. An estimate of effect on stability due to blunted noses was made from the data of Ref. 9 and plotted in Figure 13 as the change in moment slope vs. the ratio of flat area to missile cross section, for several Mach numbers. It is apparent from Figure 13 that this effect is favorable at Mach numbers higher than M = 2 but becomes unfavorable at M = 1.5. However, as mentioned previously, the braking efficiency of the device also drops sharply at the same Mach number. But the second stage of the recovery system, probably a parachute, may be deployed at this point, and thus the characteristics of nose bluntness at Mach numbers below 1.5 are not crucial.

3. Fin Leading Edge Slats or Spoilers

The aerodynamic drag characteristics of this braking device are similar to those of dive brakes whose drag coefficient is shown in Figure 7 and therefore the drag characteristics shown there are applicable.

There are some conditions however under which fin leading edge slats (spoilers) may be of greatly diminished value. For example, if the fins are either of swept-back or of delta planform with a subsonic leading edge the drag coefficient of the slats will drop to its subsonic value and its drag producing ability will be reduced further by the cube of the cosine of the sweepback angle. Furthermore, the short span of the fins of a supersonic vehicle requires that leading edge slats be of

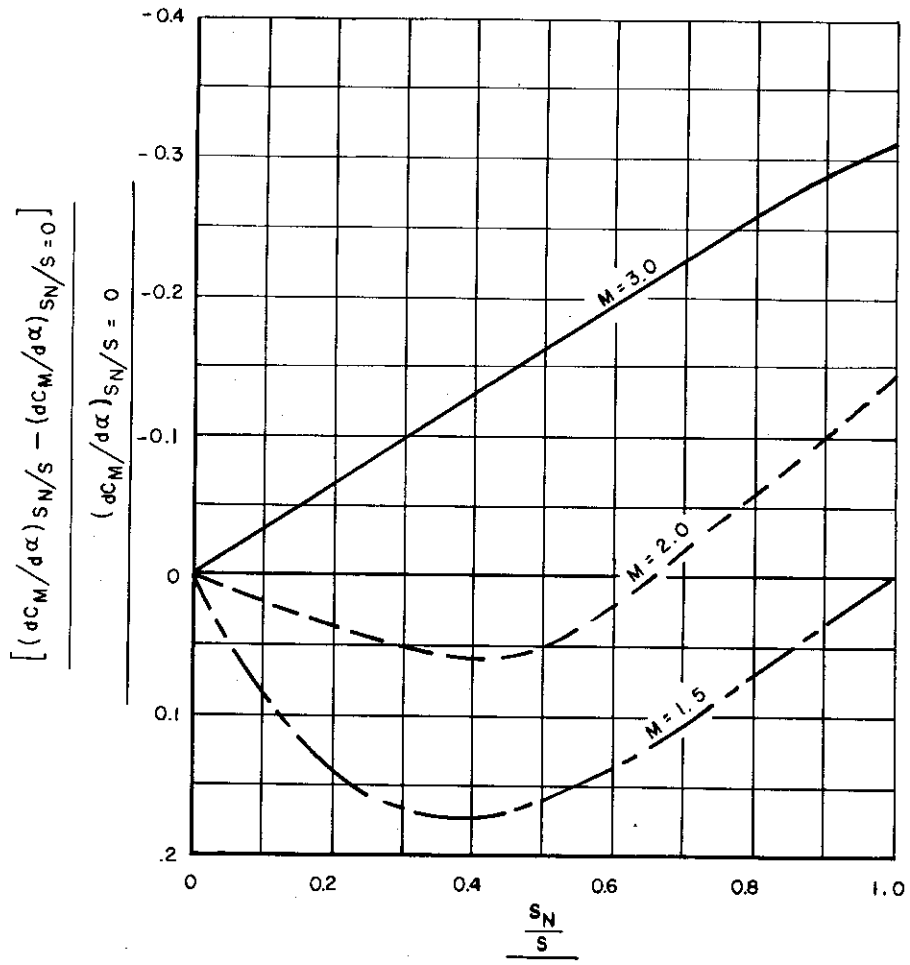

Figure 13. Effects of Nose Blunting on Destabilization Moments Due to Nose Section

great height in order to provide the required drag area. Therefore, the fin is caused to operate largely in the wake of the slat, with consequent diminished lifting effectiveness and loss in aerodynamic stability of the vehicle. Fin-mounted spoilers are likely to be used only as auxiliary drag devices in applications where the required drag area can be attained only by employing all possible means of creating drag force.

4. Momentum Exchange

A possible means of producing high drag coefficient is to cause the approaching airstream to be deflected through a large angle, for example, 90 degrees. A device capable of achieving this change in momentum may consist of an inlet and a curved channel, through which the captured air passes, to be exhausted to the outside at right angles to its initial direction. This device may be located either in the nose of the missile or along the side of the missile so as to be retractable when not in use. Figure 14 schematically illustrates this device.

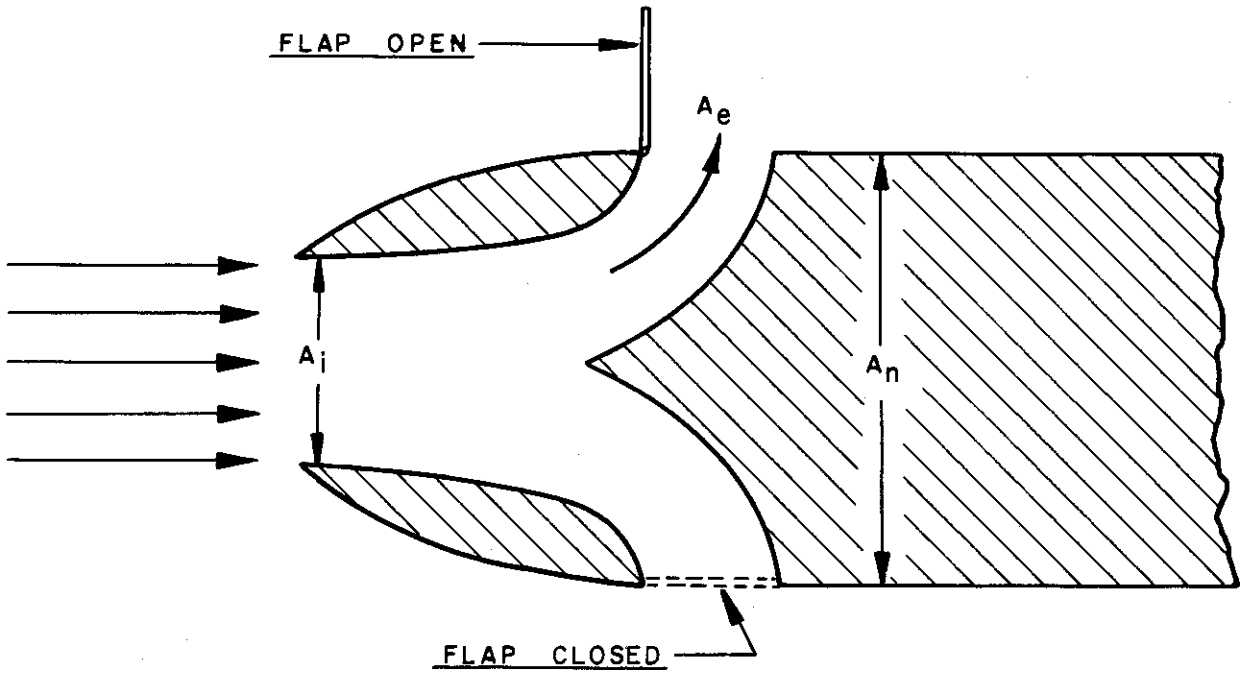

Figure 14. Cross Section of Momentum Exchange Device Using Four Exits Each $A_i/4$ Units in Size

In order that flow be maintained through the device it is probably necessary that the flow exit into a region of low pressure. This low pressure region may be created by deflecting flaps into the airstream ahead of the flow exits, thus putting the exits into the base pressure region behind the flaps.

Provided that flow can be maintained as indicated in the sketch the net force created by this device is equal to the change in momentum of the captured air. Thus the drag force is

$$D = \rho A_i V^2$$

Basing this drag on the usual drag coefficient and the inlet area, A_i

$$D = C_D \frac{1}{2} \rho V^2 A_i = \rho A_i V^2$$

or

$$C_D = 2$$

The drag coefficient of two is to be compared to the drag coefficient, 1.4, Figure 9, that can be achieved by blunting the nose to the area, A_i, at $M > 2.5$. The flow characteristics of this configuration must be studied experimentally in order to determine means of preventing choking which would render the device equivalent to the solid blunt nose configuration. Furthermore, since the device requires more space than does nose blunting, it must be determined, in the particular case, whether or not a penalty in frontal area is paid which more than overbalances the gain in drag coefficient. That is, in order to compare the momentum exchange device to simple nose blunting, the drag coefficients must be referred to the same area, for example, S_N, the area that must be available for the momentum device, and is, therefore, available for nose blunting.

The momentum device will benefit from the fore drag on the flaps which are placed ahead of the flow exits, adding another 1.6 units (at Mach 3) to the drag coefficient based on A_i.

5. Rotochute

The rotochute is a two or more bladed autorotating device that generates lift in the direction opposite the direction of motion. The axis of rotation of the rotochute is parallel to the longitudinal axis of the vehicle.

The rotochute has been investigated in wind tunnel and in drop tests at subsonic velocities. References 10 and 11 summarize the results of subsonic wind tunnel tests conducted at the NACA. At low speeds the deceleration force that may be developed is close to that obtainable with a parachute with an inflated area equal to the disk area of the rotochute.

The information on the rotochute is limited to subsonic speeds. At supersonic speeds the effectiveness of the rotochute may be expected to decrease since the rotochute depends on a high blade section lift-to-drag ratio for autorotation and for the generation of deceleration forces. At Mach 5.0 the maximum lift-to-drag ratio is in the order of 1/10 of the value at low speeds. Thus substantial reduction in performance may be anticipated. Furthermore, since the blades rotate, the actual speed at the blade tip will be the vector sum of the velocity of the vehicle plus the tip speed of the blade. The total velocity at the tips will then be higher than the equivalent of Mach 5.0 and the temperature problems in this region of the blades would intensify.

A detailed analysis of the rotochute as part of a study that examines braking devices generally is not possible. Such a detailed analysis, however, would be required in order to reach quantitative conclusions regarding its suitability as a high Mach number braking device. Problems of effectiveness, actuation, temperature, and packaging indicate considerable research and development would have to be pursued before its application could be accomplished. In view of the less difficult problems associated with dive brake or parachute systems, and the adequacy of these devices it is apparent that detailed investigation of rotochute is unnecessary at this time and that efforts should be concentrated on more clearly achievable systems.

6. Retrorocket and Thrust Reversal

A missile may be decelerated by means of directing motor thrust into the direction of motion. The weights of propellant required in the case of retrorockets is excessive; for example, 7000 pounds of propellant of specific impulse 180 are required to decelerate a 10,000 pound missile from M = 5 to M = 1. This fact renders retrorockets impractical for purposes of the present study.

Thrust reversal of the missile primary power plant cannot be relied upon for purposes of decelerating the missile, since, in general, the power plant may be inoperative, e.g., power plant failure, during that part of the flight in which recovery is desired to be made.

C. Trailing Devices

1. Parachutes

Figure 15 illustrates two possible types of metallic parachutes suitable for high load application. In order to estimate the supersonic drag coefficient of a parachute it is necessary to make several assumptions concerning the nature of flow.

A ribbon parachute, shown schematically in Figure 16, is assumed in this instance because of its simple configuration. Most ribbon parachutes exhibit satisfactory stability characteristics at low Mach numbers with 20 per cent porosity; consequently, this value will be used throughout the parachute drag and stability discussions.

The constructed or flat area of a parachute is given by

$$A_o = \frac{\pi d_o^2}{4}$$

However, since the porosity is 20 per cent, the open area is

$$A_e = 0.2 \times A_o = \frac{0.2\ \pi\ d_o^2}{4}$$

Assuming that the inflated diameter is two-thirds of the constructed diameter, the frontal area of the parachute mouth is given by

$$A_p = \frac{\pi}{4}(2/3\ d_o)^2 = \frac{\pi}{9} d_o^2$$

Thus the area ratio is $A_p/A_e = 2.22$.

The Mach number at which this area ratio becomes critical and at which choking takes place is M = 2.3. At Mach numbers lower than M = 2.3 the flow through the parachute will choke and there will be a detached shock from outside the canopy as shown in Figure 16. At

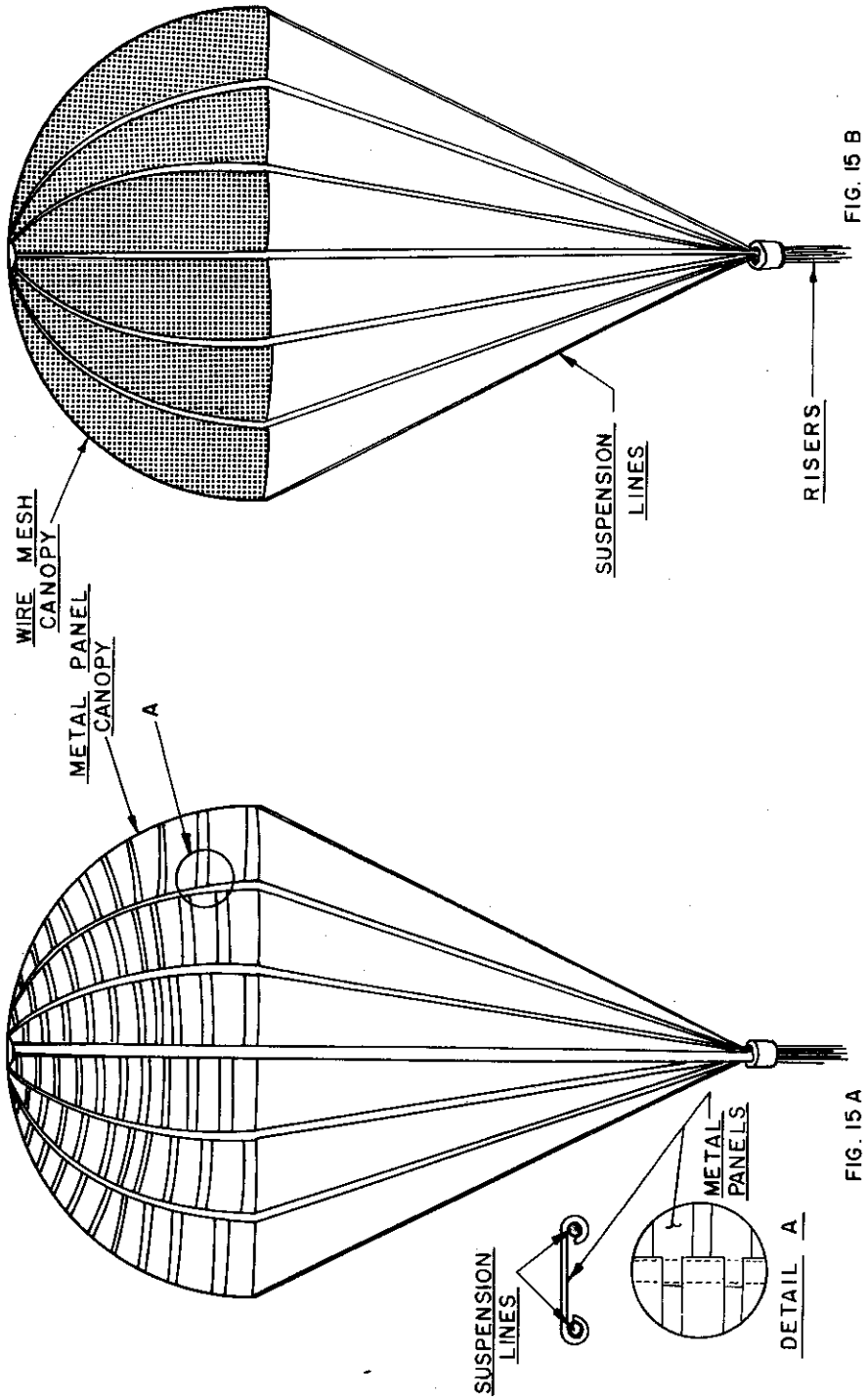

Figure 15. Metallic Parachute Concepts

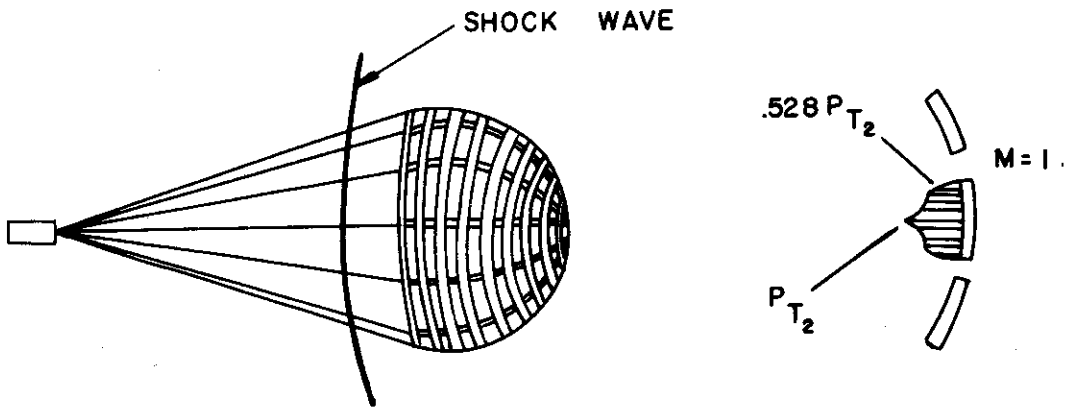

Figure 16. Airflow Through a Ribbon Parachute at High Mach Numbers

Mach numbers higher than the critical the shock wave front will probably be swallowed.

The foregoing discussion assumes that the entire surface of the canopy is equally effective in the venting of the parachute canopy. However, this assumption is doubtful because the openings more parallel to the stream, i.e., near the canopy skirt, are not as effective in venting of the parachute. Thus, the effective area ratio $\frac{A_p}{A_e}$ may be considerably lower and the shock front may choke at lower Mach numbers than predicted. However, even at Mach numbers above the critical, there will be a shock front inside the canopy caused not by mass flow considerations but by the obstructions to the flow in the form of parachute ribbons.

Thus the parachute ribbon should, in either case, experience the effects of a detached shock wave. For the purposes of drag performance prediction it may be assumed that the center of every ribbon in the parachute will experience full stagnation pressure available behind a normal shock, and that the flow will accelerate from the center of the ribbons towards the edges. The pressure distribution on the ribbons is then as shown in Figure 16. The pressure varies from stagnation at the ribbon center to that for sonic velocity at the ribbon edges.

The fore drag of the parachute may be determined by means of Equation (3) and Figure 1, by considering that the ribbon is a two-dimentional flat plate for which the value of K_2 is 0.96.

Thus,

$$C_{D_N} = (0.96 \frac{p_{t_2}}{p_\infty} - 1) \frac{2}{\gamma M^2} \sigma_R \frac{A_p}{A_o}$$

and $\frac{A_p}{A_o}$ is the ratio of inflated area to constructed area, and for a flat parachute equal approximately to $\frac{4}{9}$.

The base pressure ratio is assumed to be $\frac{p_B}{p_\infty} = 0.42$ as discussed in Part A. Thus the base drag coefficient is given by

$$C_{D_B} = \frac{0.83}{M^2}$$

The total drag coefficient for a parachute of solidity, $\sigma_R = 0.8$, is shown in Figure 17, where the subsonic drag coefficient is obtained from Ref. 12. The curve between M = 2 and subsonic velocities is interpolated.

The foregoing analysis neglects the possible effect of flutter and twist of the parachute ribbons. However, it may be presumed that a suitable parachute will be designed so as to minimize these difficulties.

Any type of trailing drag device improves the stability of a vehicle and therefore a parachute is quite favorable from this viewpoint. However, stability of the parachute about the attachment point must also exist. Limited tests at low supersonic speeds indicate that the stability of the parachute about its attachment point does not deteriorate with Mach number. Tests at high Mach numbers will be necessary to establish this type of stability.

At Mach numbers above the critical (swallowed shock wave), however, the inflation of a parachute may become quite difficult and exhibit still another type of instability.

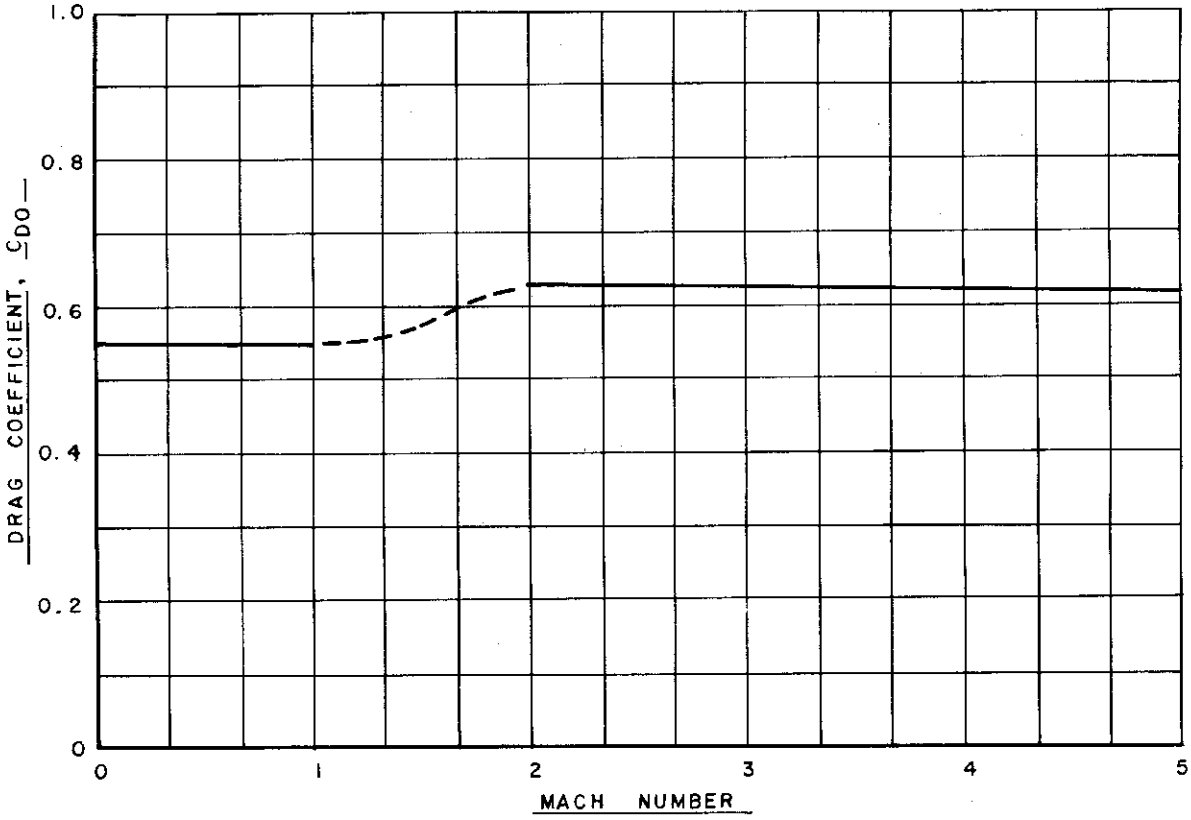

Figure 17. Drag Coefficient of Ribbon Parachute

Referring to Figure 18, when the free stream flow is above the critical Mach number the shock wave may be swallowed and the flow at

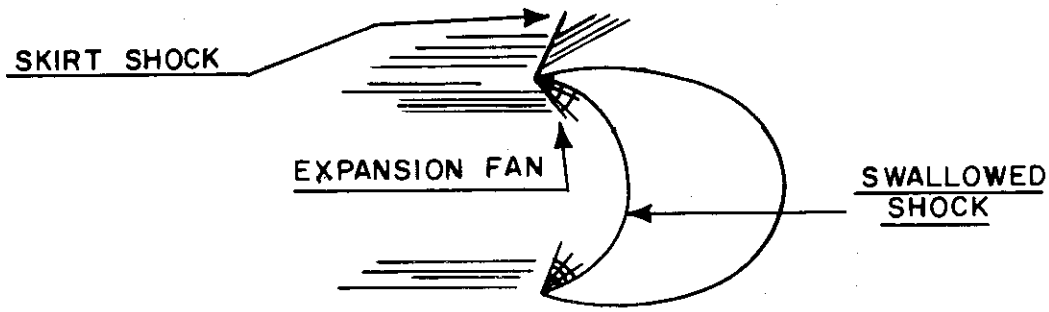

Figure 18. Supersonic Flow at the Lip of a Parachute

the skirt of the parachute may be supersonic. Since the mouth of the parachute is at an angle of attack there may exist a compression wave on the outer surface of the canopy (skirt shock) and an expansion wave on the inner surface. Thus a net force would act to squash the parachute. However, at the same time the pressure differential across the canopy near the mouth will produce mass flow into the canopy which may choke the parachute, consequently, expelling the shock front. When this event takes place the flow about the parachute becomes subsonic and the parachute reinflates with a subsequent repetition of the described cycle. This type of "inflation" instability could perhaps be remedied by reducing the porosity; however, tests would be necessary to establish a criterion for high-speed parachute design.

2. Drag Train

A drag train is a series of drag-producing bodies spaced at intervals along a cable, which trails the missile, Figure 19. The free

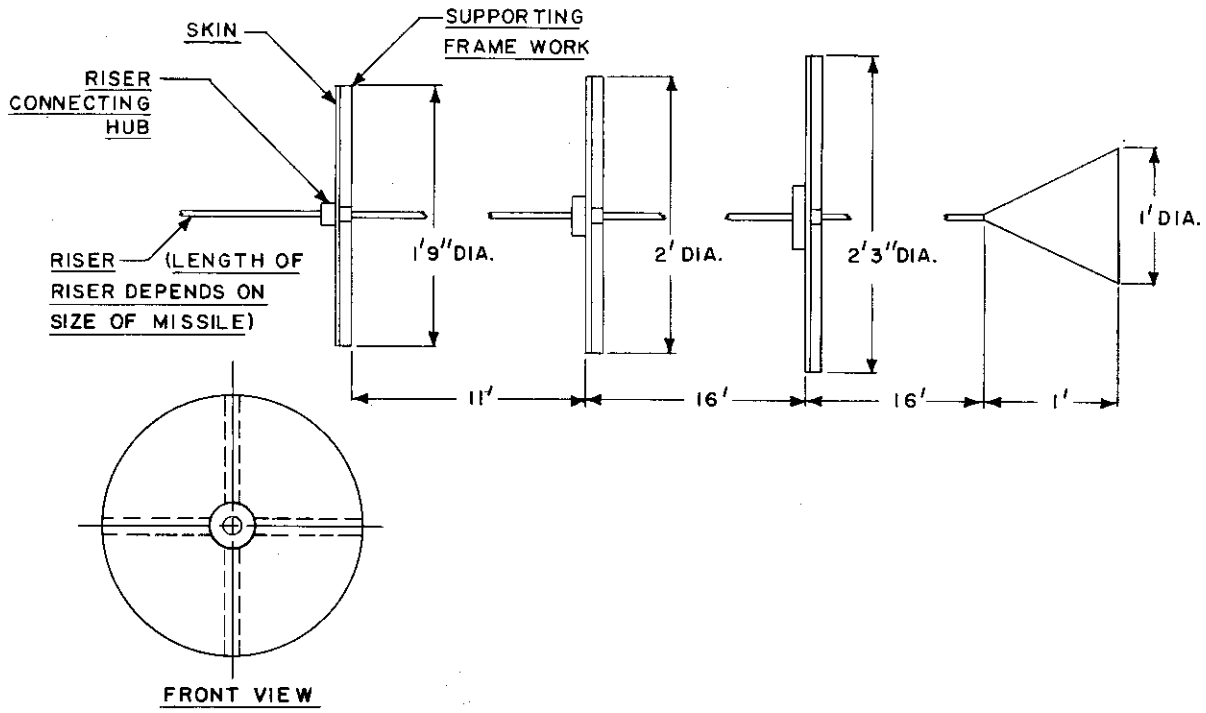

Figure 19. Drag Train

stream supersonic drag characteristics of the individual object making up the train can be assumed equal to those shown in Figure 7. However, considerable reduction in the drag coefficient may be expected when the individual elements are operating in a train, unless adequate spacing between the bodies is provided. This phenomenon was discussed in Part A where it was shown that wake effects result in a reduction of free stream dynamic pressure of 33 per cent even at down stream distances of 10 times the diameter of the preceding body, Refs. 5 and 6. At smaller distances these losses are even more severe, e.g., at a distance of five times the diameter the loss in dynamic pressure is 55 per cent, Ref. 5. It appears that to obtain reasonable drag producing efficiency it is necessary to separate the individual components of the train by 10 times the diameter of the preceding body.

The stability characteristics of the missile are improved by trailing devices by virtue of the fact that the drag force produces a restoring moment about the center of gravity of the vehicle. The train itself may be stabilized by attaching lifting surfaces or a cone to the end of the cable.

Additional wind tunnel data on wake characteristics are required in order to determine the spacing required between individual plates in the train. However, even in the absence of such data it is inevitable that drag trains will require riser lengths that exceed those required for parachutes. The effect of increased riser lengths on weight and bulk is shown in Chapter 5.

CHAPTER 4

THERMAL EFFECTS

Due to the processes of compression and friction, a body moving through the atmosphere accumulates as thermal energy a portion of its mechanical energy of motion. The accompanying temperature rise at high speeds can be great enough to reduce the strength of structural materials and even cause fusion.

The heating of a body moving through the atmosphere is a function of the forced convection heat transfer from the air to the body, the radiation heat transfer from the body to the atmosphere and space, and the solar heating due to radiation from the sun. Sufficient information is available to allow a reasonable prediction of heat transfer to flat plates parallel to the airstream and to certain configurations of bluff bodies. The heat gained and lost by radiation can be approximated by the Stefan-Boltzmann law. The solar heating of a body may be approximated from measured solar constants.

The temperature rise of the body may be predicted from the heat transfer, the specific heat of the material, and the weight of material under consideration. For structures fabricated of isolated thin sheets, the heat flow may be considered one-dimensional. This latter approximation is used throughout in calculating the temperature rises for the braking devices.

A. Heat Transfer Coefficient

For the drag devices being considered it was assumed that the shape of the device would most closely approximate a disk or flap plate normal to the airstream. This configuration would apply to spoilers or dive-brakes, trailing disks, and parachute-shaped drag devices. The heat transfer to the disk was approximated with Eber's equation for a cone as found in Ref. 13.

In Ref. 13 the Nusselt number for a cone shape is given as:

$$Nu = (0.0071 + 0.0154\beta^{0.5})R_e^{0.8}$$

The heat transfer coefficient may be written from the Nusselt number as

$$h = \frac{0.0071 + 0.0154\beta^{0.5}}{\ell_c^{0.2}} k \left(\frac{\rho_\infty V_\infty}{\mu}\right)^{0.8}$$

where the thermal conductivity of air is based on the boundary layer temperature. Application of this equation to a disk was made by expanding the apex angle, β, to π radians and letting ℓ_c be the disk radius. This modified equation is

$$h = \frac{0.0344\, k}{\ell_c^{0.2}} \left(\frac{\rho_\infty V_\infty}{\mu}\right)^{0.8}$$

Although this equation represents an extrapolation of the original equation, it is believed to represent adequately the heat transfer to a flat plate normal to the airstream. Values from the equation correspond reasonably well with values measured near the stagnation region of a hemisphere as shown in Ref. 14.

B. Boundary Layer Temperature

The increase in boundary layer temperature due to compression is a function of the local recovery factor on the surface. The temperature recovery for a disk is virtually complete, and a recovery factor of unity is used. Therefore, the boundary layer temperature assumed in the following calculations is that equal to the stagnation temperature of the flow. At high velocities ($M > 2$) the boundary layer temperature rise is sufficient that the specific heat of the air rises considerably over the ambient value and the stagnation temperature decreases. In order to account for this, average values of specific heat over the temperature ranges are used in computing the total temperature.

$$c_{Pav} = \frac{\int_{T_i}^{T} c_p(T)dT}{\int_{T_i}^{T} dT}$$

where $c_p(T)$ was taken from Ref. 15. The equation used for the boundary layer temperature is

$$T_B = T_A + \frac{0.2}{c_{p_{av}}} \left(\frac{V_\infty}{100} \right)^2$$

This equation approximates the value that would be obtained by an integration of the enthalpy over the range of temperature from T_A to T_B.

C. Derivation of Heat Flow Equation

The derivation of the temperature equation is equivalent to that presented in Ref. 13. The area on which the heat flow is based is taken as the frontal area of the brake. Convection and conduction heat transfer on the rear side of the brake is assumed to be zero, a reasonable approximation in view of the "deadwater" region at the base of the brake. Radiation heat transfer, on the other hand, takes place on both the front and rear surface of the brake, since the temperature distribution through the brake is fairly uniform for the skin thicknesses involved. Thus the terms in the heat flow equation expressing the effect of radiation contain a factor of two relative to the other terms.

The quantity of heat transferred to the front face of the disk from the air is

$$dQ = hS_D (T_B - T_S)\, dt.$$

The heat lost by radiation is

$$dQ = 2\, S_D \epsilon \sigma\, T_S^4\, dt.$$

The radiant heat absorbed from space and the outer atmosphere is

$$dQ = 2\, S_D \epsilon \sigma \lambda\, T_A^4\, dt$$

where λ is the sky radiation factor given numerically in Figure 7 of Ref. 13. The maximum amount of heat absorbed from the sun is

$$dQ = \epsilon\, S_D\, C\, dt.$$

The above radiation approximations should suffice for a simple analysis and are believed to be conservative.

The heat required to raise the temperature of the body is

$$dQ = c \delta w S_D \, dt$$

where δ is in ft, w is in lb/ft^3

Combining the above equations

$$c \delta S_D dT_S = hS_D(T_B - T_S)dt + 2S_D \epsilon \delta \lambda \, T_A^4 dt + S_D \epsilon C \, dt - 2S_D \epsilon \lambda T_S^4 \, dt$$

$$\text{or } \frac{dT_S}{dt} = \frac{h(T_B - T_S) - 2\epsilon\sigma (T_S^4 - \lambda T_A^4) + \epsilon C}{c \delta w} \qquad (5)$$

This differential equation may be solved by a step-by-step numerical integration to give a time history of the disk temperature for any given initial conditions and disk characteristics.

D. Numerical Calculations and Results

In order to gain some insight into the magnitudes of temperature rise to be encountered for representative supersonic vehicles in selected operating conditions, Equation (5) was solved on an IBM 650 digital calculator for both horizontal trajectories and inclined trajectories.

The temperature attained by the braking devices will depend on the manner in which it is stowed in the vehicle and the nature of the vehicle.

If, while stowed, the brake is in an insulated department or is protected with refractory material, the rises in the temperature of the brake before deployment will be small. The initial rate of temperature increase and the maximum temperature rise may be determined adequately by assuming that the temperature at deployment is equal to the ambient air temperature.

If the brake is not stowed in an insulated compartment or protected and the duration of flight at a constant altitude is long then the brake will reach an equilibrium temperature equal to the equilibrium temperature of the vehicle.

A plot of equilibrium temperatures is shown in Figure 20 as a function of Mach number for several altitudes. It is seen from this figure that at altitudes less than 100,000 feet sustained flight is unlikely. If such a vehicle could exist, it would need extensive heat protection. The brake would also need this same type of protection. Since that velocity will decrease after the deployment, the maximum temperatures attained by the brake are those given by Figure 20.

It is more realistic to assume that flight at high Mach number and medium altitude will be short in duration, and that, in these cases, the brake can be insulated or protected so that its temperature at deployment is approximately equal to the ambient air temperature. This is the initial condition assumed in the calculation of temperatures for horizontal and inclined trajectories contained in the following sections.

1. Horizontal Trajectories

In a horizontal or constant altitude flight path, the velocity variation is caused by the drag forces acting to slow the missile. The missile characteristics chosen as representative of the classes under consideration are as follows:

$C_D S_M$: 9.0 ft^2

Weight: 5,000 lb
17,600 lb
100,000 lb.

The ranges of operating conditions are:

Altitude - 0; 30,000 ft; 60,000 ft

Mach Number - 3.5

The thermal characteristics of the materials considered for the drag devices, given by the quantity, $F_s = c\delta w$ are tabulated in Table 1, where the material thicknesses are indicated for the range of F_s chosen.

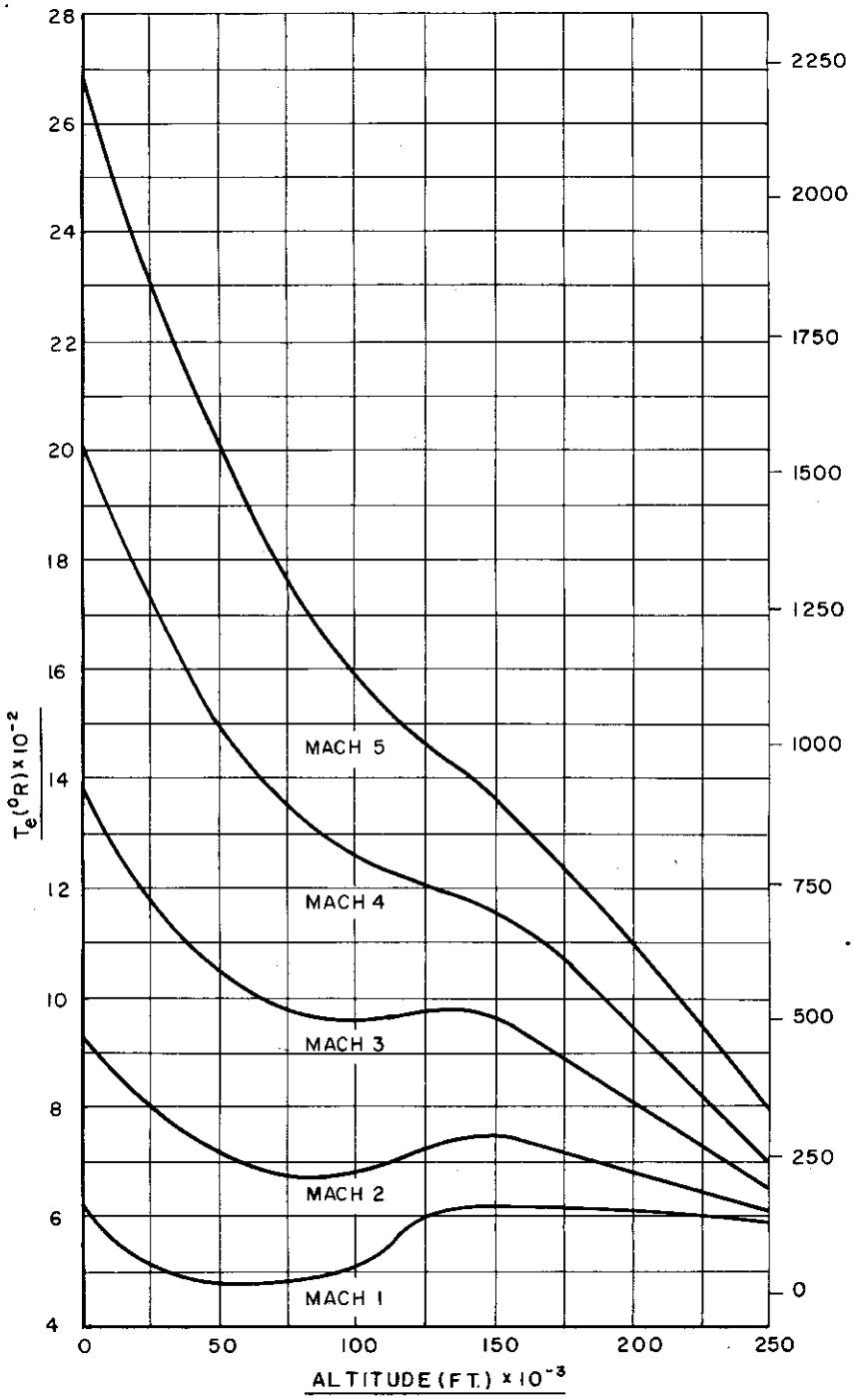

Figure 20. Equilibrium Temperature vs. Altitude for Various Mach Numbers

TABLE I

Thicknesses (in Inches) of Various Materials for Several Values of the Heat Capacity Parameter, F_s

F_s	Stainless Steel 17-7	Titanium	Aluminum
0.15	0.030	0.047	0.045
0.30	0.060	0.094	0.090
0.60	0.120	0.189	0.181
1.20	0.240	0.377	0.361

Chapter 5 investigates the thicknesses of the various surfaces exposed to heat, as a function of assumed loads. These loads are related to the operating conditions selected as parameters in the thermal heating study. That is, the load, D, is

$$D = C_D S \frac{\gamma}{2} p_\infty M^2$$

where the altitude effect is contained in the ambient atmospheric pressure, p_∞. The maximum load occurs at the highest (initial) Mach number, M_i. Thus, a brake designed on the basis of aerodynamic loading is designed for conditions at initiation of the braking phase. The thermal study determines whether or not the temperature rise on the brake, during the braking phase, is sufficiently great to affect, critically, the strength characteristics of the material chosen, at its design thickness.

The drag area of the braking device used for these calculations was 16 ft^2, thus, making the total drag area of the missile-drag device combination equal to 25 ft^2. All combinations of the variables could not be covered, but a sufficient number of cases was considered so that the effects could be determined.

The quantities which were calculated to represent the temperature

rise on the subject vehicle were:

(1) $(\frac{\Delta T}{\Delta t})_i$, initial rate of skin temperature rise

(2) (ΔT) max, maximum temperature rise attained

(3) ${}^t\Delta T_{max}$, time-to-maximum temperature rise.

These quantities are tabulated in Table 2 as functions of the important variables, the cases being arranged so as to exhibit, most readily, the effects of altitude and weight for given values of materials parameter, F_s and Mach number.

Inspection of Table 2 yields the following general conclusions as regards the behavior of the dependent quantities as functions of the important variables:

(1) Altitude Effect

$(\frac{\Delta T}{\Delta t})_i$ increases rapidly with decreasing altitude, varying by a factor of more than 10 from 60,000 feet to sea level.

$(\Delta T)_{max}$ is affected only slightly by altitude since the greater decelerations compensate the effect of increasing density of lower altitudes. (t) ΔT_{max} decreases with decreasing altitude, varying by a factor 10 from 60,000 feet to sea level.

(2) Effect of Vehicle Weight

$(\frac{\Delta T}{\Delta t})_i$ is affected not at all by weight of the vehicle.

$(\Delta T)_{max}$ increases rapidly with increasing weight, increasing approximately with the square root of the weight. (t) ΔT_{max} increases rapidly with increasing weight.

TABLE 2

Heating Characteristics, Representative Supersonic Vehicles, Digital Computer Solution, Equation (5), for Horizontal Trajectory

F_s	M_i	W pounds	Alt. $\times 10^{-3}$ ft	$\frac{\Delta T_i}{\Delta t}$ ^oF/sec	$^t\Delta T_{max}$ sec	$(\Delta T)_{max}$ ^oF
0.6	5	5,000	60	48.6	18	250
		5,000	30	186	5.4	217
		5,000	SL	535	2.1	218
		17,000	60	59.7	31	553
		17,600	30	200	9.2	512
		17,600	SL	592	3.6	453
		100,000	30	200	16.5	1110
		100,000	SL	600	6.6	1306
	3	5,000	60	20	40	97
		5,000	30	42.4	13.5	84
		17,600	60	16.6	49	213
		17,600	30	46.9	14.5	196
		17,600	SL	144	5.6	206
		100,000	SL	146	10.8	492
1.2	5	17,600	60	30.09	47	368
		17,600	30	100	14	328
		17,600	SL	297.6	5.4	342

TABLE 2 (cont'd)

Heating Characteristics, Representative Supersonic Vehicles,
Digital Computer Solution, Equation (5), for Horizontal Trajectory

F_s	M_i	W pounds	Alt. x 10^{-3} ft	$\frac{\Delta T_i}{\Delta t}$ ^oF/sec	$^t\Delta T_{max}$ sec	$(\Delta T)_{max}$ ^oF
		100,000	SL	304.2	10.6	997
	3	17,600	30	23.6	22.5	127
0.3	5	5,000	60	116.4	12.5	400
		17,600	60	117	19.0	762
		17,600	30	395	5.4	739
	3	17,600	60	28.8	31.0	296
		17,600	30	91.9	9.5	282
0.15	3	5,000	60	53.5	13.0	228
		5,000	30	182	3.8	211
		17,600	60	56.3	29.0	379
		17,600	30	190	6.2	375

(3) Mach Number Effect

$(\frac{\Delta T}{\Delta t})_i$ decreases with decreasing Mach number. $(\Delta T)_{max}$ increases approximately with M^2.
$(t)_{\Delta T_{max}}$ varies approximately inversely with M.

(4) F_s (Materials) Effect

$(\frac{\Delta T}{\Delta t})_i$ varies inversely with F_s.

$(\Delta T)_{max}$ varies inversely with $\sqrt{F_s}$.

$(t)_{\Delta T_{max}}$ varies with $\sqrt{F_s}$.

Of the four effects considered above, the least important, for horizontal trajectories, is the altitude effect. The greatest maximum temperature rises occur for the high weight, high Mach number conditions. Recovery weights of 100,000 pounds result in large temperature rises for all conditions.

The effect of weight is actually an indirect effect of velocity, since the vehicles of higher weight are not slowed by their drag as much as are lighter weight vehicles. Thus, flight at or near the assumed initial Mach numbers results in the longest durations of temperature rise and consequently, greatest maximum temperatures.

In order to relate the structural and thermal aspects of the design of the drag device, a series of computations have been made of maximum temperature rise, in horizontal flight on given dive brake and metallic parachute designs for a number of operating conditions.

Dive brakes (cf. Chapter 5) have been designed to provide drag forces of: (1) 592,000 pounds, (2) 176,000 pounds, (3) 42,000 pounds. The skin thicknesses required for these loads for the following materials: (1) 17-7 stainless steel, (2) titanium, (3) aluminum, when applicable, have been calculated, and the corresponding values of the heat

capacity parameter, F_s, computed. The maximum temperature rises obtained for several altitude-recovery weight combinations at M = 5.0 have been computed and are presented in Table 3. Only those materials which are practical in the particular instances were considered.

TABLE 3 Maximum Temperature Rises for Dive Brakes in Several Operating Conditions, M = 5

Load (lb)	Altitude (ft)	Recovery Wt. (lb)	Material	Thickness* (inches)	F_s	(ΔT) Max
592,000	0	5,000	Titanium	0.18	0.56	230
			Alum	0.20	0.68	210
		17,600	Titanium	0.18	0.56	460
			Alum	0.20	0.68	420
		100,000	Titanium	0.18	0.56	1340
			Steel	0.18	0.88	1140
176,000	30,000	5,000	Titanium	0.10	0.30	350
			Steel	0.10	0.48	249
			Alum	0.10	0.36	320
		17,600	Titanium	0.10	0.30	740
			Steel	0.10	0.48	570
		100,000	Titanium	0.10	0.30	1310
			Steel	0.10	0.48	1166

* Thicknesses only apply for one particular supporting structure operating at 65°F

It may be seen that large temperature rises are encountered in the extreme case of recovery weight equal to 100,000 pounds both at sea level and at altitude 30,000 feet. This case is of academic interest only because the brake drag area used with this large weight is inadequately small. For more representative recovery weights of 5000 pounds and 17,600 pounds an altitude or loading effect may be noted which enters through the value of F_s, that is, the lower loadings at altitude require smaller thicknesses of skin; hence lower values of F_s and larger values of temperature rise. In the case of recovery weight

100,000 pounds, however, this altitude, i.e., F_s effect is lost since the deceleration is less appreciable and the skin temperature has ample time in which to rise. The temperature rises in all cases are low enough to allow the use of steel materials without heat protection particularly when it is considered that the instants of maximum load and maximum temperature occur at different times.

The thickness of the ribbons in a metallic parachute is determined from fabrication considerations because the thickness required for maximum load conditions is smaller than can easily be handled. The thickness chosen for these computations was 0.020 inches and the material was titanium. The corresponding value of F_s is 0.064. Table 4 lists the maximum temperature rises for the metallic parachute in a number of operating conditions.

TABLE 4 Maximum Temperature Rises for Metallic Parachute in Several Operating Conditions; M=5, F_s=0.064 Material: Titanium, 0.020 inches Thick

Altitude	Recovery Wt.	(ΔT) max ^{o}F
0	5,000	950
	17,600	1500
	100,000	2050
30,000	5,000	840
	17,600	1258
	100,000	1573

Again the temperature rise for a weight of 100,000 is presented for completeness and does not represent a practical situation. The temperature rise in this case is virtually the equilibrium flight temperature that would be obtained with infinite weight or zero deceleration.

Of the remaining cases in Table 4, the combination of an altitude of 30,000 feet and a recovery weight of 5000 pounds at Mach 5.0 represents extreme capabilities for foreseeable level flight missiles. The maximum temperature attained in the case, assuming an initial temperature of $0^{o}F$, is well within the capabilities of steel or titanium.

2. Inclined Trajectories

In order to show the effects of heating at high speed, a hypothetical case of a 10,000 pound re-entry type missile was considered incorporating a drag device of 16 sq ft drag area. For this example it was assumed that the missile was falling vertically at a Mach number of 5 and that the drag device was deployed at an altitude of 250,000 feet.

Figures 21, 22, and 23 show the history of the fall from 250,000 feet to sea level. Figure 22 shows the variation of the drag force on the drag device with altitude and indicates the futility of deploying the brake at very high altitude. For comparison purposes, Figures 21 and 22 also show the fall of a 1000 pound missile with the same drag device. The range from 1000 pounds to 10,000 pounds represents probable limits of missile weight for a drag device with 16 sq ft drag area.

Figure 23 shows the temperature-time history of the drag device; the material used in this calculation of 0.04 inch thick steel. This thickness of material is greater by at least a factor of two than that which would be required from a purely structural loading and handling standpoint for metallic parachute canopies and similar devices.

From Figure 23 it is seen that temperatures exceeding 1000°F occur after 31 seconds of fall or at an altitude 80,000 feet. The reasons for these extreme temperatures are:

(1) The low drag generated by the device at high altitude actually allows the missile to accelerate to Mach 6 before beginning to slow down.

(2) The boundary layer temperature increases due to both the velocity and the ambient air temperature.

(3) The heat transfer coefficient increases due to increasing air density.

(4) The material thickness (0.040 inch) is incapable of storing the large quantities of heat transferred to it except through a rapid rise in its temperature.

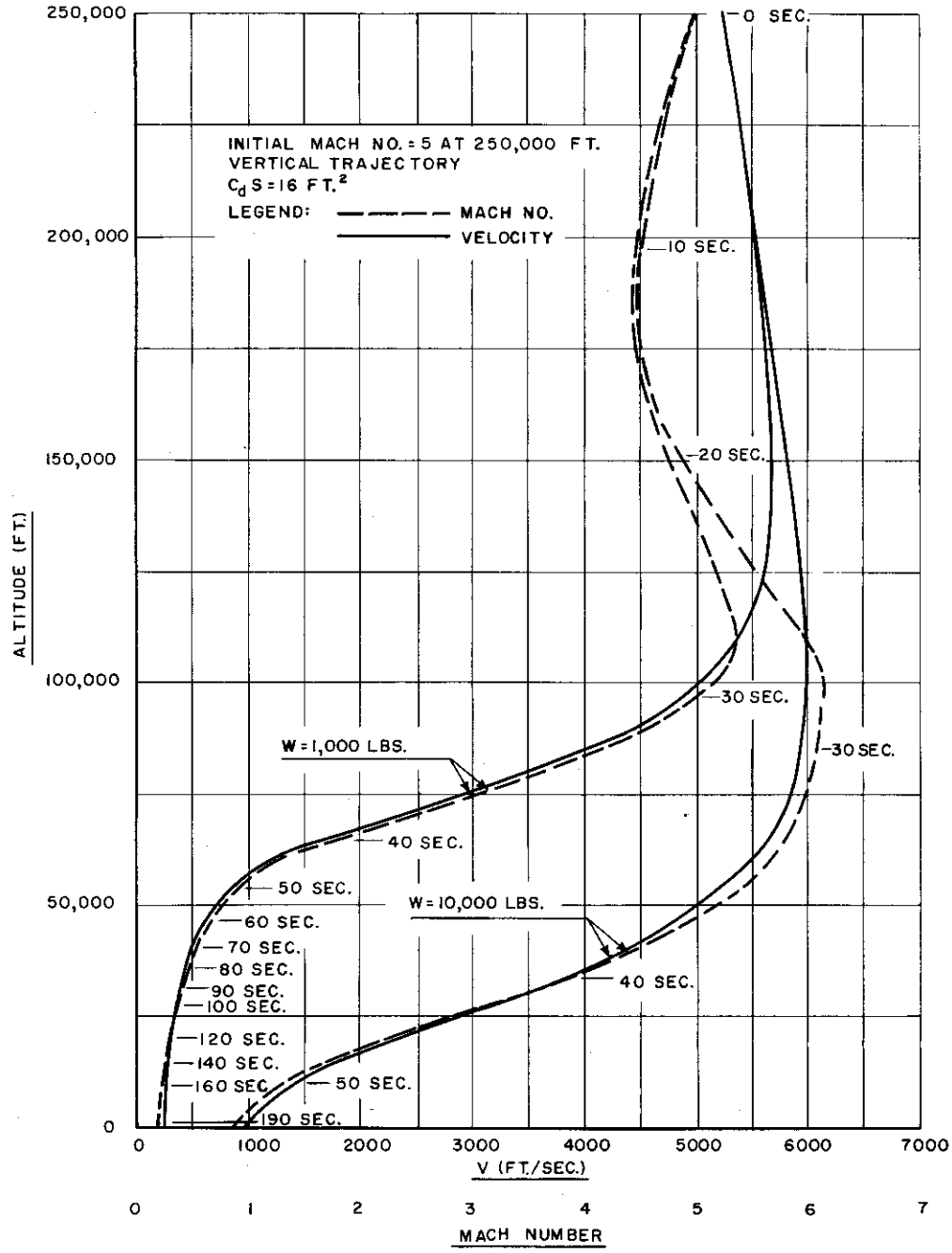

Figure 21. Velocity and Mach Number Variation with Altitude for Hypothetical Missile with Braking Device

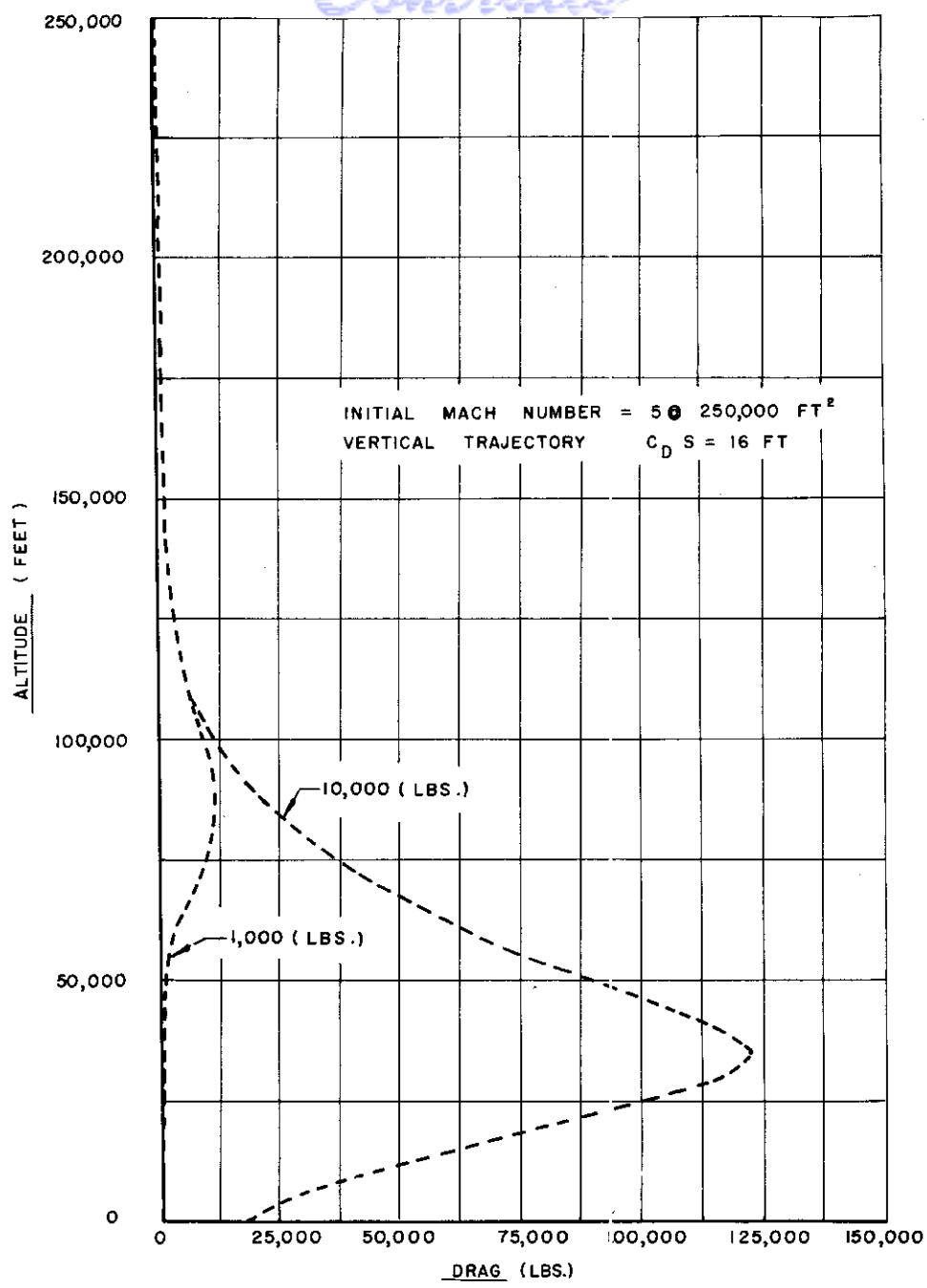

Figure 22. Drag Variation with Altitude for Hypothetical Missile with Braking Device

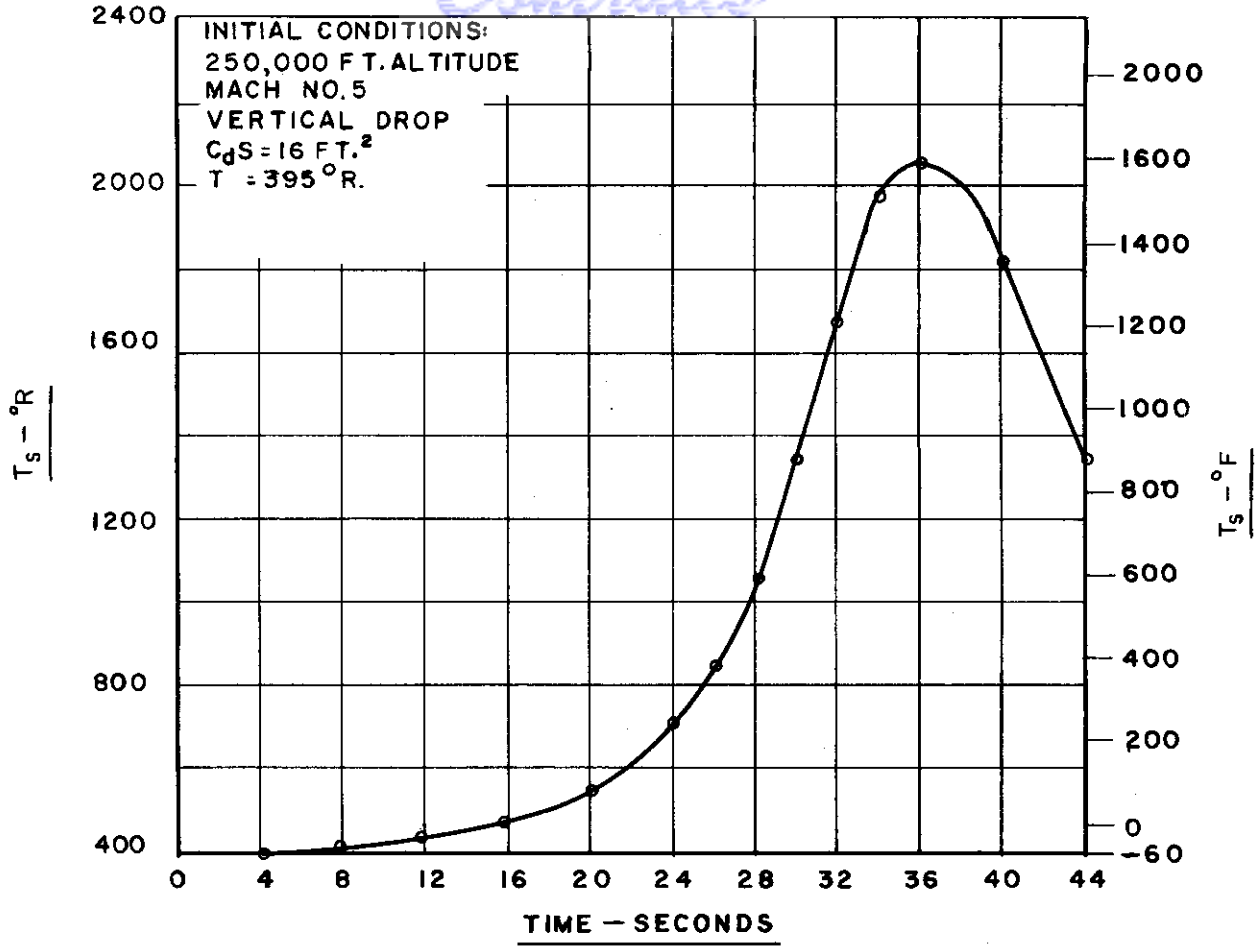

Figure 23. Temperature-Time History for Drag Device Attached to a 10,000 Pound Hypothetical Missile

Beyond 36 seconds the temperatures drop due to the reduction of speed under the decelerating influence of the increasing drag load.

It is to be noted that such extreme temperatures would not be encountered in the case of lower weight missiles since significant decelerations due to a 16 foot drag area would become effective at higher altitudes. The maximum temperatures obtained would also be reduced if thicker members were employed. However, substantial reduction of peak

temperatures, by adding material beyond the point of structural needs, reduces the drag-to-weight ratio, and other methods of controlling the temperatures such as cooling are more desirable.

A possible means of cooling the brake is to make it of hollow construction with the interior packed with coolant. The brake stowage compartment would be insulated so as to reduce heating prior to deployment. If the front face of the brake were made of a porous material the coolant would seep through the exterior surface providing transpiration cooling. This method is simple and very effective for short duration cooling requirements.

The most critical conditions of temperature are encountered in the cases of inclined or vertical trajectories. The severity of the temperature problem can be reduced by delaying the deployment of the brake to low altitudes and allowing the missile to decelerate due to its own drag area as it encounters higher density air. By deploying the brake at an altitude less than 40,000 feet, the effectiveness of the brake will be greater and the velocity at deployment will be lower, giving less time for aerodynamic heating to take place.

CHAPTER 5

DESIGN CONSIDERATIONS

The type of drag device which is most effective in meeting the requirements of a particular recovery problem will be determined by such factors as drag-weight and drag-bulk characteristics, adaptability to the vehicle, and the operating range over which the recovery will be attempted. In the following sections the characteristics of towed and immediately attached drag devices are analyzed. The salient features which measure the effectiveness of the device as part of a recovery system, are then determined.

A. Weight Analysis

The ability to withstand the effects of aerodynamic heating and the presence of high drag-weight ratio are predominating requirements of the structure of a drag device.

To determine the drag-weight ratio of a structure the general configuration of the drag device must first be developed so that a reasonably correct stress analysis can be made. Then with the drag coefficient of the device and the dynamic pressure, the drag load may be found and the weight of the structure computed. By expressing the drag load in terms of altitude and Mach number the weight of structure required for recovery at a given altitude and Mach number can also be found.

In the analysis, the load was considered to represent the sum of the steady state and dynamic loads. This was done since the effects of dynamic loading are difficult to establish without detailed knowledge of the elastic properties of a structure. In order to provide a common basis for comparing individual devices a drag area of 16 ft^2 was used in all cases.

Following is an analysis of drag principles which on the basis of the aerodynamic and thermodynamic characteristics are most desirable.

1. Immediately Attached Devices

Immediately attached devices will in general require a greater degree of tailoring in order to be adapted to a particular missile. Most of the devices in this category must be extended from the missile to be effective, and must be designed to withstand large bending moments.

Slats or spoilers are basically rugged structures and are capable of withstanding very high loads and temperatures that are at least as high as those that can be withstood by the missile itself. The actuating forces required are relatively low since extension can be accomplished by translation in a direction normal to the airstream, or the aerodynamic forces themselves can be used to extend them. The structural aspects of spoilers are similar to those of dive brakes. The structural characteristics of dive brakes are investigated as being typical of this class of devices.

Dive brakes have been used for many years on aircraft and considerable data already exist on various types of perforated brakes. The particular dive brake configuration investigated in this study is shown in Figure 24. This configuration assumes that the dive brake is divided into four separated flaps totaling 16 ft^2 of drag area. Structurally each flap is a stressed-skin design utilizing either aluminum, titanium or stainless steel.

In calculating the weight of the dive brake the skin of each flap was considered to be divided into a number of panels with fixed edges. The pressure distribution across the panel was assumed to be uniform. The framework was considered to consist of a number of hinged beams each of which had a uniform load acting along its length.

The weight of the skin is derived from Ref. 15, page 199, i.e.

$$W_s = nA\,w\,\left(\frac{0.5\,pb^2}{s_y\,(1+0.623\,\psi^6)}\right)^{\frac{1}{2}}$$

where w is in $lb/in.^3$.

The weight of the framework behind each panel in pounds may be obtained from Ref. 15, page 100, i.e.

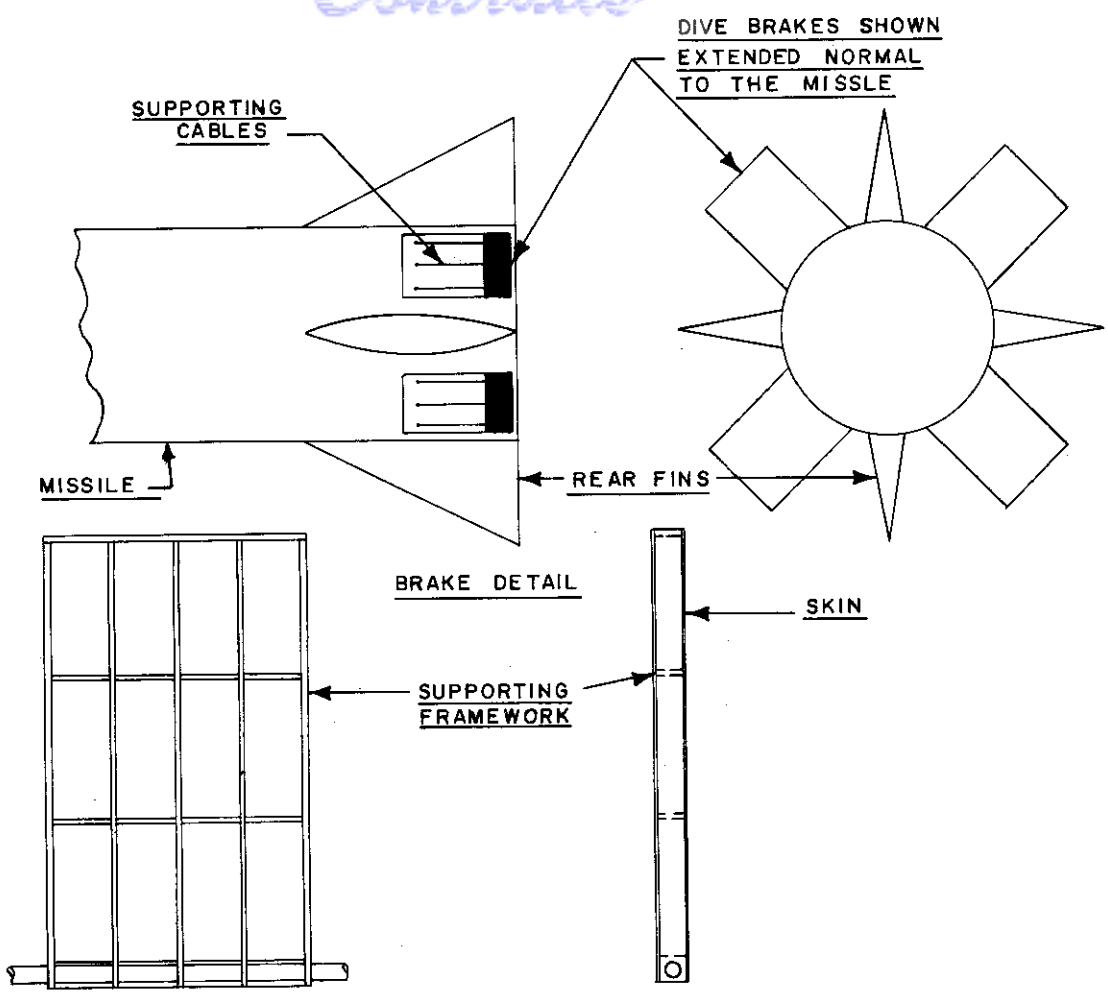

Figure 24. Dive Brakes

$$W_f = \frac{1}{5}\, ml\delta \left(\frac{30\,\omega l^2}{8 s_y}\right)^{2/3}$$

Plots of the drag-weight and weight-Mach number variations are given in Figures 25 and 26. Figure 27 is a plot of the drag-weight curves for titanium and stainless steel dive brakes and illustrates the effect of an elevated temperature on the load-weight ratios. It will be observed that up to temperatures of 800°F the load-weight ratio of titanium is superior to that of 17-7 stainless steel. Table 5 shows the required skin

TABLE 5

Summary of Thickness and Weights of Major Components of the Braking Devices

DIVE BRAKES

Total Drag Load x 10^{-5} lb	Skin Thickness-in.		Skin Weight-Lb		Structure Weight		Total Weight-lb	
	Titanium (5Al-2.5 Sn)	17-7 Stainless Steel	Titanium (5Al-2.5 Sn)	17-7 Stainless Steel	Titanium (5Al-2.5 Sn)	17-7 Stainless Steel	Titanium (5Al-2.5 Sn)	17-7 Stainless Steel
0.250	0.036	0.036	8.1	14.0	17.0	30.0	26.0	45.0
0.50	0.051	0.051	11.0	20.0	27.0	48.0	40.0	69.0
1.0	0.073	0.073	16.0	29.0	43.0	76.0	62.0	107.0
3.0	0.126	0.126	28.0	49.0	89.0	157.0	126.0	215.0
6.0	0.178	0.178	40.0	70.0	142.0	250.0	197.0	336.0

DRAG TRAIN

Total Drag Load x 10^{-5} lb	Average Skin Thickness-in.		Total Drag Plate Weight-lb		Risers						Total Weight-lb			
					Nylon**			Steel Cable***			Nylon Risers		Steel Cable	
	Titanium (5Al-2.5 Sn)	17-7 Stainless Steel	Titanium (5Al-2.5 Sn)	17-7 Stainless Steel	No.	Type-lb	Weight/ft	No.	Size-in.	Weight/ft	Titanium (5Al-2.5 Sn)	17-7 Stainless Steel	Titanium (5Al-2.5 Sn)	17-7 Stainless Steel
0.250	0.142	0.142	44.0	79.0	3	10,000	0.071	1	9/16	0.590	58.0	93.0	89.0	124.0
0.50	0.202	0.202	65.0	115.0	5	10,000	0.071	1	3/4	1.052	91.0	141.0	142.0	192.0
1.0	0.285	0.285	95.0	168.0	10	10,000	0.071	1	1-1/8	2.40	148.0	220.0	275.0	348.0
3.0	0.494	0.494	175.0	310.0				1	2	6.82			640.0	774.0
6.0	0.70	0.70	259.0	458.0				1	2-3/4	12.9			1115.0	1314.0

PARACHUTE WITH NYLON RISERS

Total Drag Load x 10^{-5} lb	Average Canopy Thickness-in.		Canopy Weight-lb		Suspension Line			Risers			Total Weight-lb		
					Nylon**			Nylon**					
	Titanium (5Al-2.5 Sn)	17-7 Stainless Steel	Titanium (5Al-2.5 Sn)	17-7 Stainless Steel	No.	Type-lb	Weight/ft	No.	Type-lb	Weight/ft	Titanium (5Al-2.5 Sn)	17-7 Stainless Steel	
0.250	0.020	0.015	11.0	14.6	12	3,000	0.036	3	10,000	0.071	24.0	27.0	$C_{D_O} = 0.55$
0.50	0.020	0.015	11.0	14.6	12	6,000	0.041	5	10,000	0.071	34.0	38.0	
1.0	0.020	0.015	11.0	14.6	12	10,000	0.071	10	10,000	0.071	57.0	61.0	

PARACHUTE WITH STEEL RISERS

Total Drag Load x 10^{-5} lb	Average Canopy Thickness-in.		Canopy Weight-lb		Suspension Line			Risers			Total Weight-lb		
					Steel Cable***			Steel Cable***					
	Titanium (5Al-2.5 Sn)	17-7 Stainless Steel	Titanium (5Al-2.5 Sn)	17-7 Stainless Steel	No.	Size-in.	Weight/ft	No.	Size-in.	Weight/ft	Titanium (5Al-2.5 Sn)	17-7 Stainless Steel	
0.250	0.020	0.015	9.6	12.7	12	1/8	0.035	1	9/16	0.59	46.0	49.0	$C_{D_O} = 0.63$
0.50	0.020	0.015	9.6	12.7	12	3/16	0.07	1	3/4	1.052	75.0	79.0	
1.0	0.020	0.015	9.6	12.7	12	9/32	0.183	1	1-1/8	2.40	161.0	164.0	
3.0	0.020	0.015	9.6	12.7	12	1/2	0.58	1	2	6.82	443.0	446.0	
6.0	0.020	0.015	9.6	12.7	12	3/4	1.09	1	2-3/4	12.9	830.0	833.0	

* Weight calculations were based on an ambient temperature of 75°F.
** Data obtained from spec MIL-W-4088.
*** Data obtained from ANC 5 and American Chain & Cable Catalog 4, July 1955.

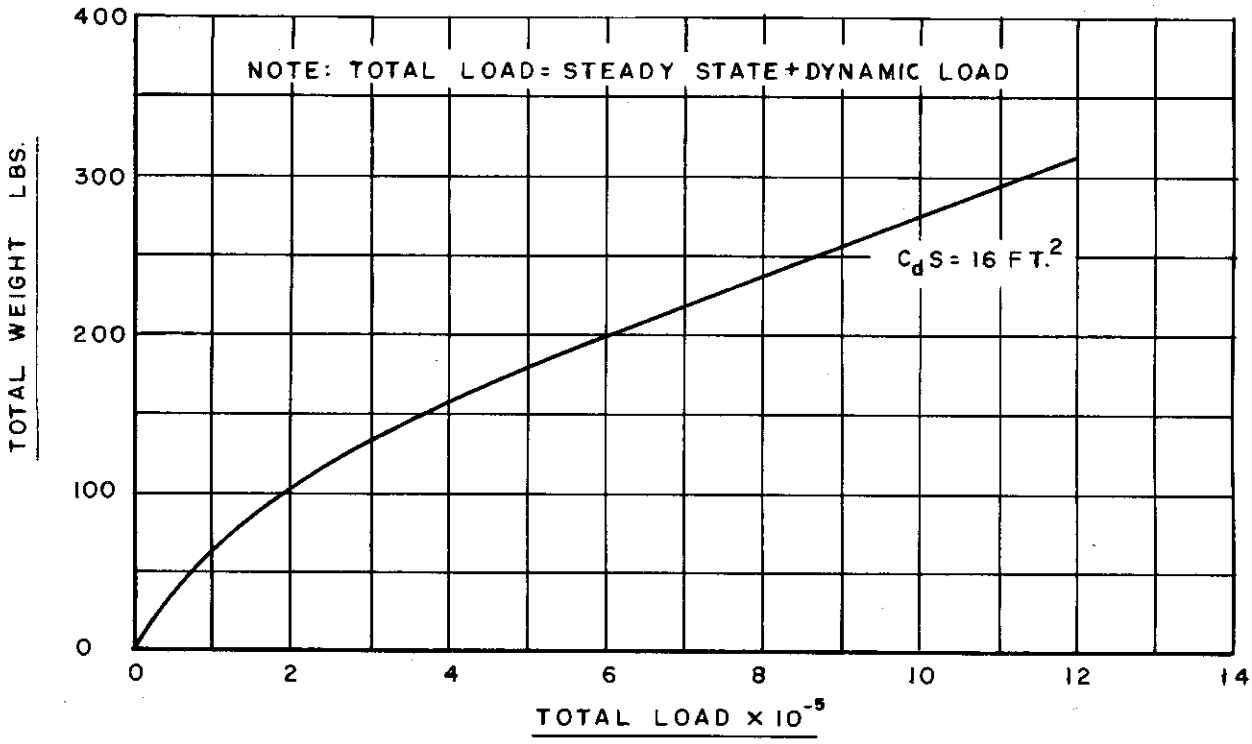

Figure 25. Weight of Titanium Dive Brakes vs. Load

thickness for the dive brake at various drag loads. This tabulation records the required skin thickness when titanium, and stainless steel are used at a temperature of 75°F.

2. Towed Devices

Towed devices such as parachutes and drag trains, are subject to the weight penalty of the structure required to trail the device at a suitable distance aft of the missile. The deployment of these devices will be critical and care must be taken so that excessive dynamic loads are not introduced.

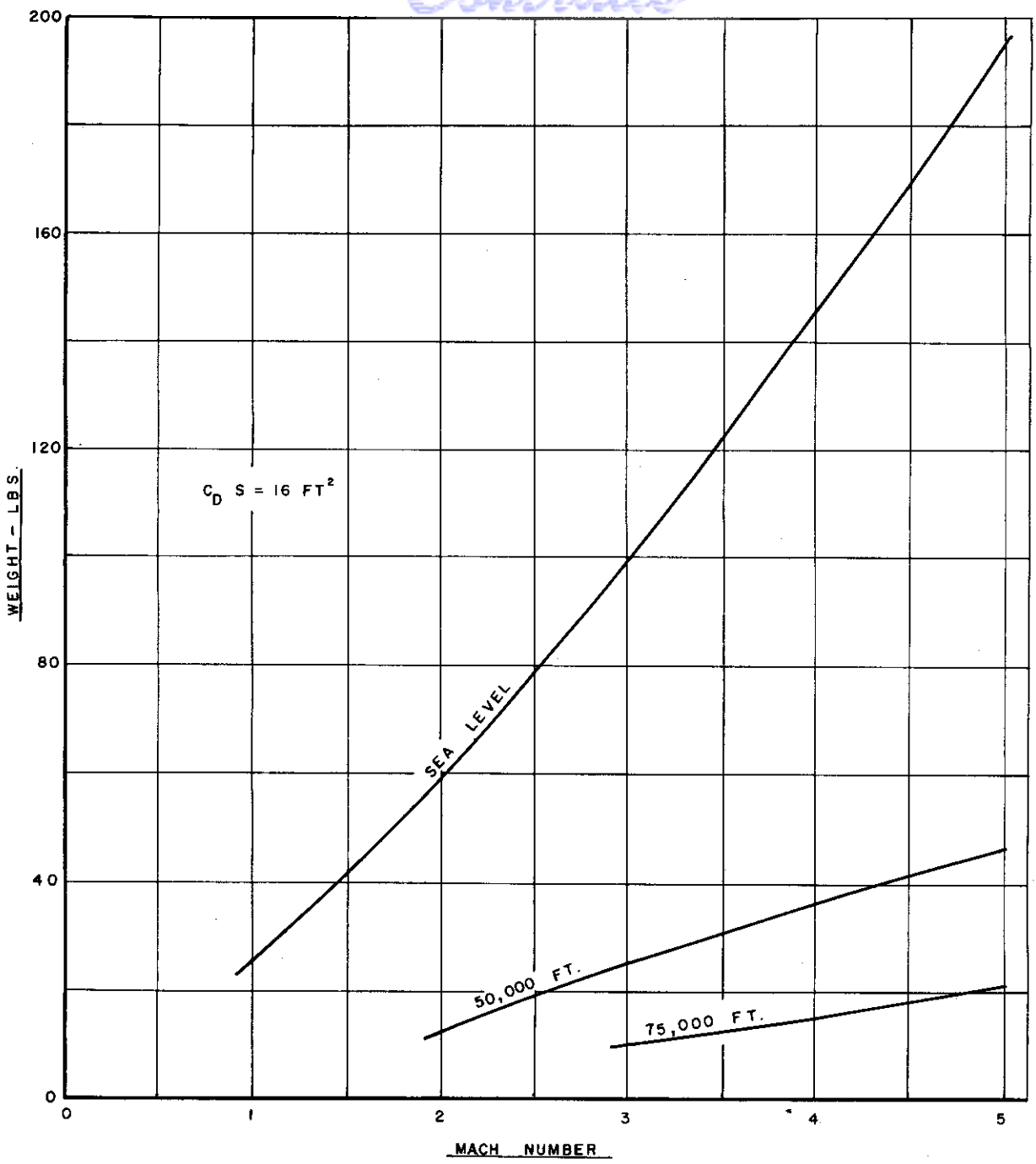

Figure 26. Weight vs. Mach Number for Titanium Dive Brakes at 75°F

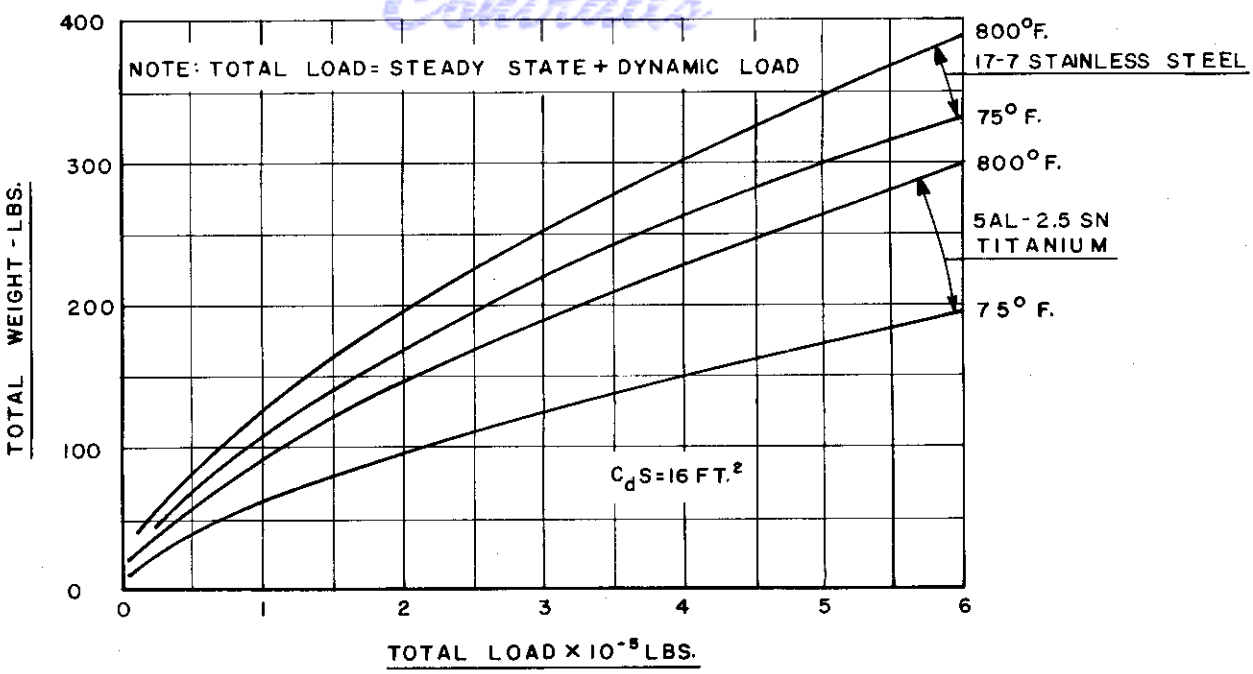

Figure 27. Effect of Temperature on Weight vs. Load Curves for Composite Dive Brakes

a. Parachutes

The fabric parachute in its many forms is well known. Perhaps the most suitable of these for high velocity application where intermediate stability is satisfactory is the ribbon parachute. At very high altitudes fabric parachutes may be employed at surprisingly high Mach numbers since under these conditions a low heat transfer coefficient and high radiation reduce the maximum temperatures attained. At lower altitudes an upper limit of Mach 2 seems to apply because of the high temperatures.

Parachutes made from temperature resistant materials such as Fiberglas or metal will push the critical temperature level to somewhat higher values. Fiberglas, however, is very susceptible to fatigue failure and it is doubtful that it can be used in situations where folding and packing are required.

The structures of two, 12 gore, flat circular type metallic parachutes are shown in Figure 15. Figure 15a is a panel assembly. The drag-weight characteristics of these parachutes are examined below.

Since the inflated diameter, d_p, of a flat parachute is two-thirds of its flat or constructed diameter, d_o, it follows that the parachute canopy gores must bow outward between the suspension lines. The shape of the inflated gore between the lines is very nearly semicircular in cross section; thus the ribbons or material which form the gores must sustain combined bending and axial stresses. Since the cross section of the gore is circular the bending stress in the ribbon for an, n, gore canopy is

$$S_B = \frac{nE\delta}{\pi d_p} = \frac{3nE\delta}{2\pi d_o}$$

The axial tension or hoop stress in the gore material is

$$S_T = \frac{p d_p}{2n\delta} \qquad \frac{\pi d_o p}{3n\delta}$$

Since the total stress must be less than the yield stress of the material

$$s_B + s_T = s < s_y$$

Solving for the thickness which develops fully the yield stress of the material

$$\delta = \frac{\pi d_o s_y}{3nE} \left(1 \pm \sqrt{1 - \frac{2E}{s_y^2} p} \right) \qquad (6)$$

This equation shows that there are two possibilities, one where the bending stress, the plus sign, predominates and the other where the tensile stress is larger, the minus sign. Any thickness between the values obtained from Equation (6) will result in stresses less than s_y.

The thicknesses obtained for the case where the stress is primarily tensile is so small that practical problems in handling

and fabrication preclude its use. For example, a parachute with a drag area of 16 sq ft, with a total load of 100,000 pounds would require steel ribbons only 0.002 inch thick. Thus the ribbons must be designed with the bending stresses predominant. In this case the average thickness of ribbons is 0.021 inch.

Since the discriminant in Equation (6) must remain greater than zero, the maximum pressure load that can be sustained is related to the modulus and yield stress of the material, thus

$$p_{max} < s_y^2/2E$$

Therefore, the maximum values of pressure loading are 200 lb/in.^{2} for 17-7 stainless steel and 380 lb/in.^{2} for titanium.

These pressure loadings correspond to total parachute loads of 298,000 pounds and 566,000 pounds, respectively. If higher parachute loads are required, or even when the above loads are approached, woven mesh flat cables should be employed for the ribbons. The advantage of this type structure is that very high values of the ratio s_y^2/E are obtainable.

A thickness of 0.020 inch for titanium and 0.015 inch for steel will be used here for the canopy weight estimates.

Since the canopy is of flat construction the weight is given by

$$W_c = \frac{\pi \sigma_R \, w \, \delta \, d_o^2}{4}$$

Thus for a 5.7 foot constructed diameter steel parachute with a solidity, σ_R, of 0.8 the weight of the canopy is 11.0 pounds.

In addition to the weight of the ribbons of the canopy, the weights of the suspension lines and the riser must be determined.

The load in each suspension line is

$$L_C = \frac{C_{D_o} A_o q}{n \cos \phi}$$

The size and weight of suspension lines required are obtained from Ref. 16, and are tabulated in Table 5.

For the purpose of calculating the riser weight, it was assumed that the vehicle was of the order of 5 to 6 feet in diameter and that, in the absence of firm wake survey data, it would be desirable to trail the drag producing device at a distance of 10 missile diameters aft. The weight of steel and nylon risers per foot of length is given in Table 5.

The total parachute weight, using both nylon and steel risers and suspension, is plotted vs. drag load and Mach number in Figures 28, 29, 30, and 31. From these curves it can be seen that when the total drag load is sufficiently low to permit the use of nylon suspension lines and nylon risers the system weight can be materially reduced. Figures 28 and 29 also give an indication of the weight penalty encountered by trailing these devices at a distance aft of the vehicle.

b. Drag Trains

The type of device referred to in this section is shown in Figure 19. The drag plates are added to the cable since without these, excessive cable lengths would be required. For example, a cable with an average diameter of 1 inch would need to be 2500 feet long and weigh 4700 pounds to produce a drag area of 16 sq ft.

By attaching drag plates the cable is greatly shortened and large drag coefficients per unit frontal area can be developed. The plates are spaced so as to reduce interference and wake effects. The succeeding plates along the cable are progressively increased in diameter to favor air capture. The drag coefficient of each plate is as shown in Figure 7. The 16 sq ft of drag area can be obtained with three drag plates spaced 8 diameters apart (see Figure 19). The first drag plate is located 10 missile diameters aft. Thus, for a 6 foot diameter missile, a total cable length of 98 feet is used. The diameter and weight of riser were determined in the same manner as for the case of the parachutes. The cone attached at the end

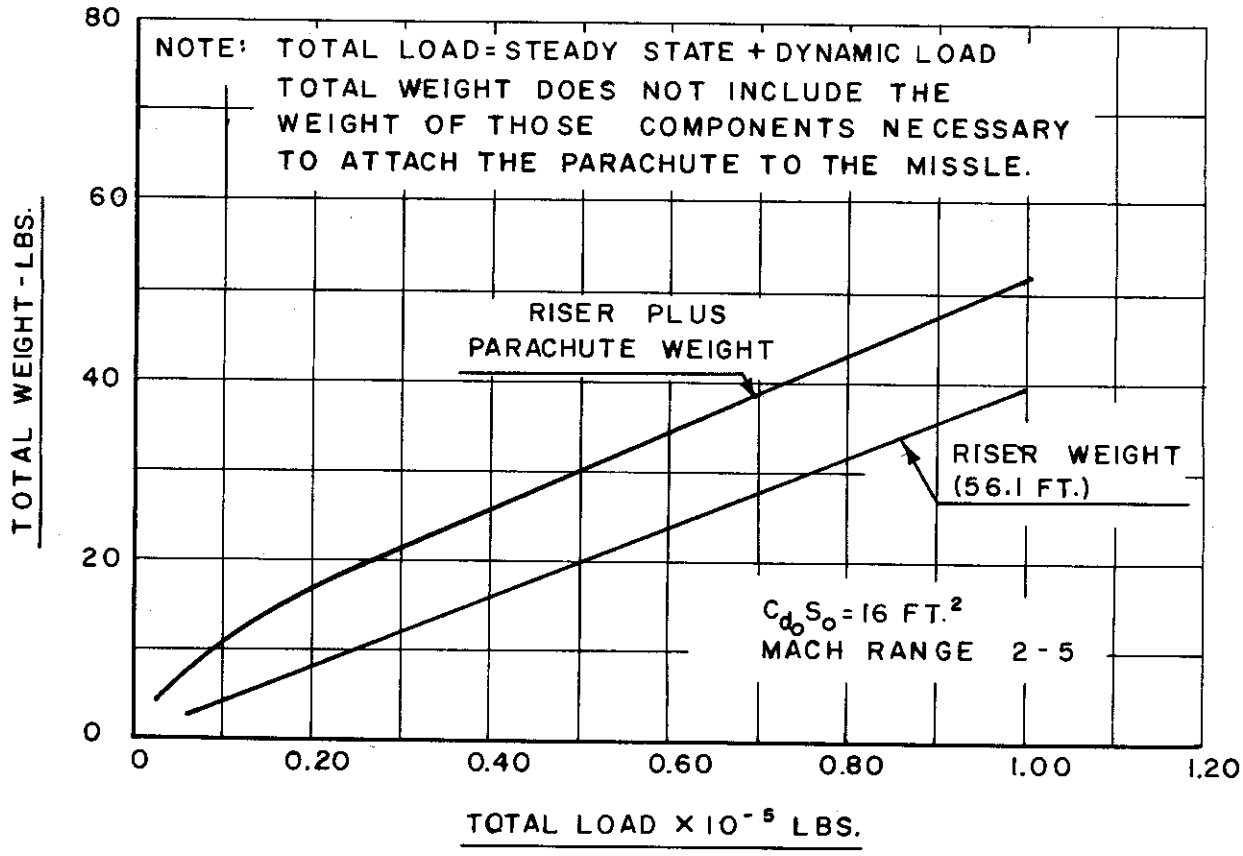

Figure 28. Weight vs. Load for Metallic Parachutes with Nylon Risers and Nylon Suspension Lines

of the cable is employed to stabilize the drag train by producing a restoring lift proportional to the angle between the cable axis and the relative airstream.

The drag plates were designed as reinforced flat plates with a simple center support. The skin of each plate was considered to be divided into four circular segments, each segment having fixed radial edges and unsupported circumferential edge. The

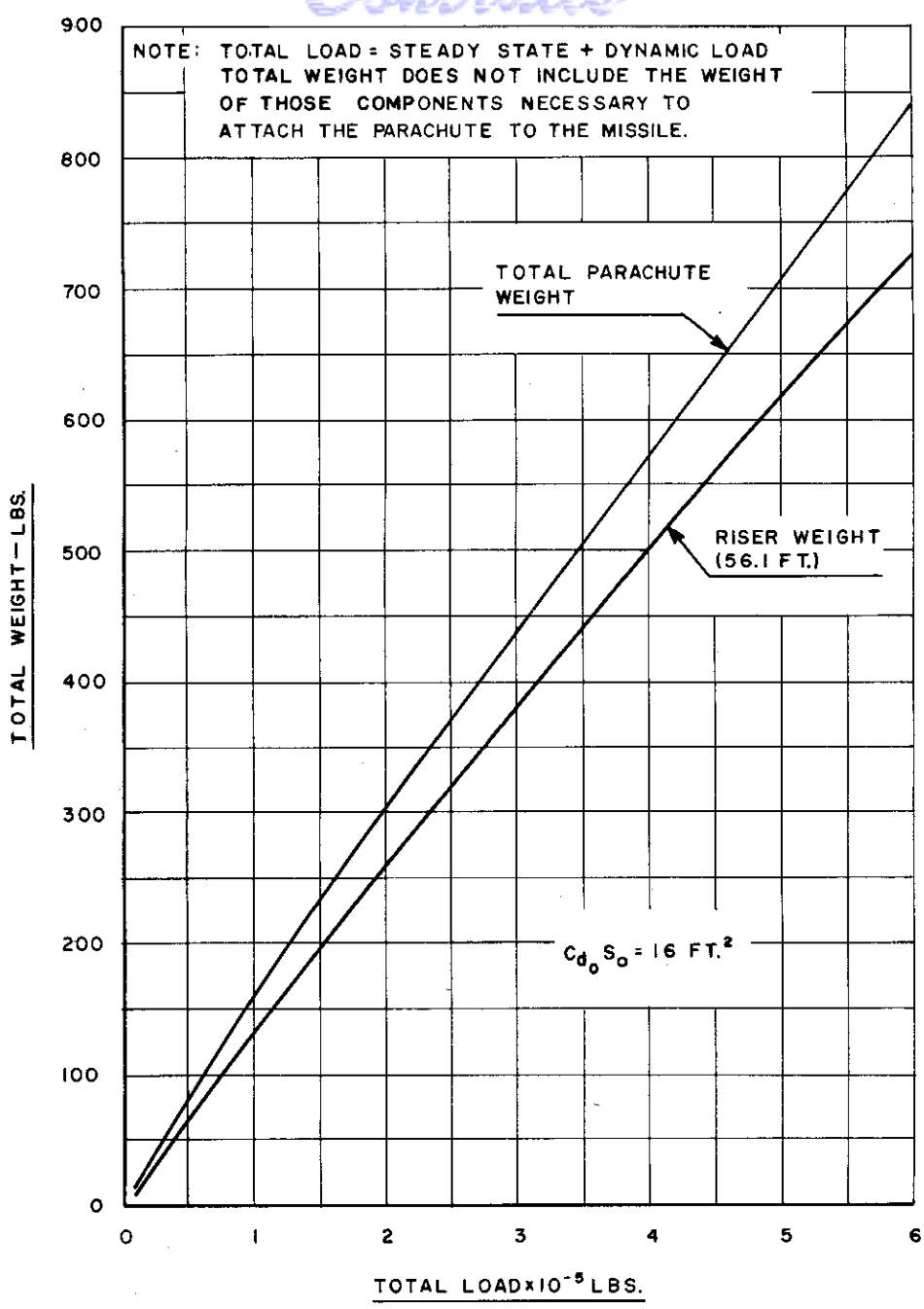

Figure 29. Weight vs. Load for Metallic Parachutes with Steel Risers and Steel Suspension Lines

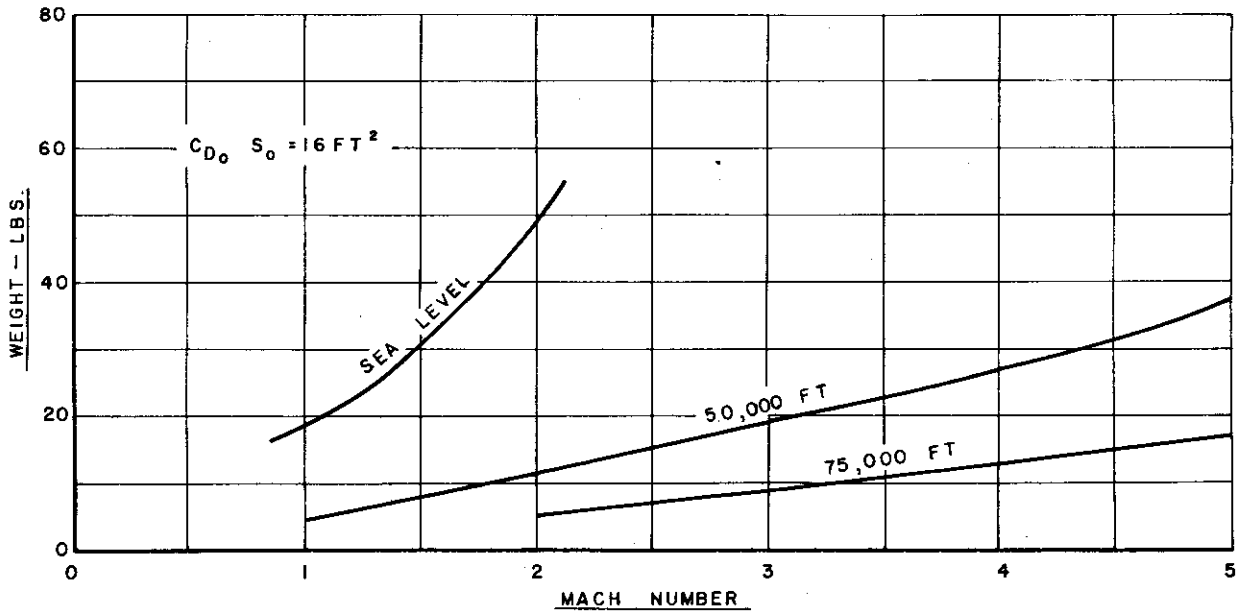

Figure 30. Weight vs. Mach Number and Altitude for Metallic Parachute with Nylon Risers and Nylon Suspension Lines

weight of the plates for various drag loads were obtained in the following manner. The pressure distribution across the plate was assumed to be uniform and the framework behind the skin was considered to consist of four centrally supported beams, each being uniformly loaded along its length. From Ref. 17, page 274, the weight of skin in pounds is given by the expression

$$W_s = wnA \left(\frac{0.7986\ pr^2}{S_y}\right)^{\frac{1}{2}}$$

The weight of the framework behind each drag plate as given by Ref. 15, page 98, is

$$W_F = 1/5\ wmr^3 \left(11.78\ \frac{p}{S_y}\right)^{2/3}$$

where m and n = 4.

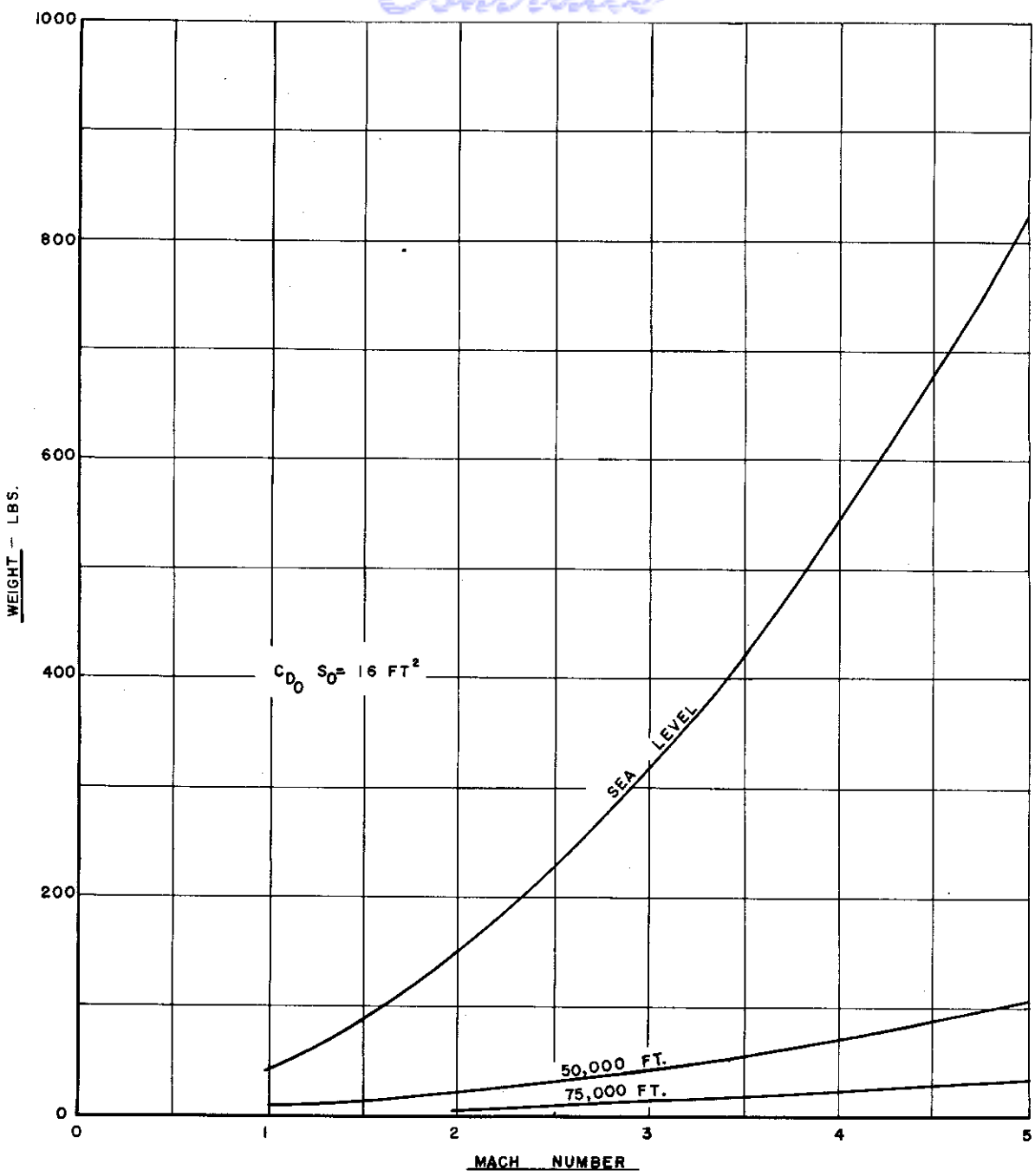

Figure 31. Weight vs. Mach Number and Altitude for Metallic Parachute at 75°F with Steel Risers and Steel Suspension Lines

The weight of these devices with both nylon and steel risers are plotted vs. drag load and Mach number in Figures 32 and 33. Figure 32 also gives an indication of the weight penalty encountered by trailing these devices at a distance aft of the vehicle. Table 5 gives the required thickness of the drag plate skin for various loads. This tabulation considers titanium and stainless steel at a temperature of 75°F.

B. Packageability

In any of the existing missiles, or recovery packages, the space available for a recovery system is extremely limited. The forward sections of a missile are generally completely occupied by the warhead and instrumentation while the central and aft sections are almost fully utilized by the fuel tanks and thrust units. Even if a missile were specifically designed with a recovery system in mind, the missile designers would view rather critically its space requirements. Therefore, the drag-bulk characteristic, or packageability, of a recovery system must be considered.

1. Immediately Attached Devices

One of the obvious advantages in using immediately attached devices is that they do not require any towing structure.

Slats, spoilers, and dive brakes have very desirable drag-bulk characteristics. This is especially true when it is considered that in their unoperated position they can be designed such that they form an integral part of the missile structure.

There is another advantage in that they can be located at almost any point on the outer periphery of the missile just as long as they do not interfere with its stability.

Particular locations that would be very desirable and probably very accessible, would be in that area just over the necked down section of the engine nozzle throat.

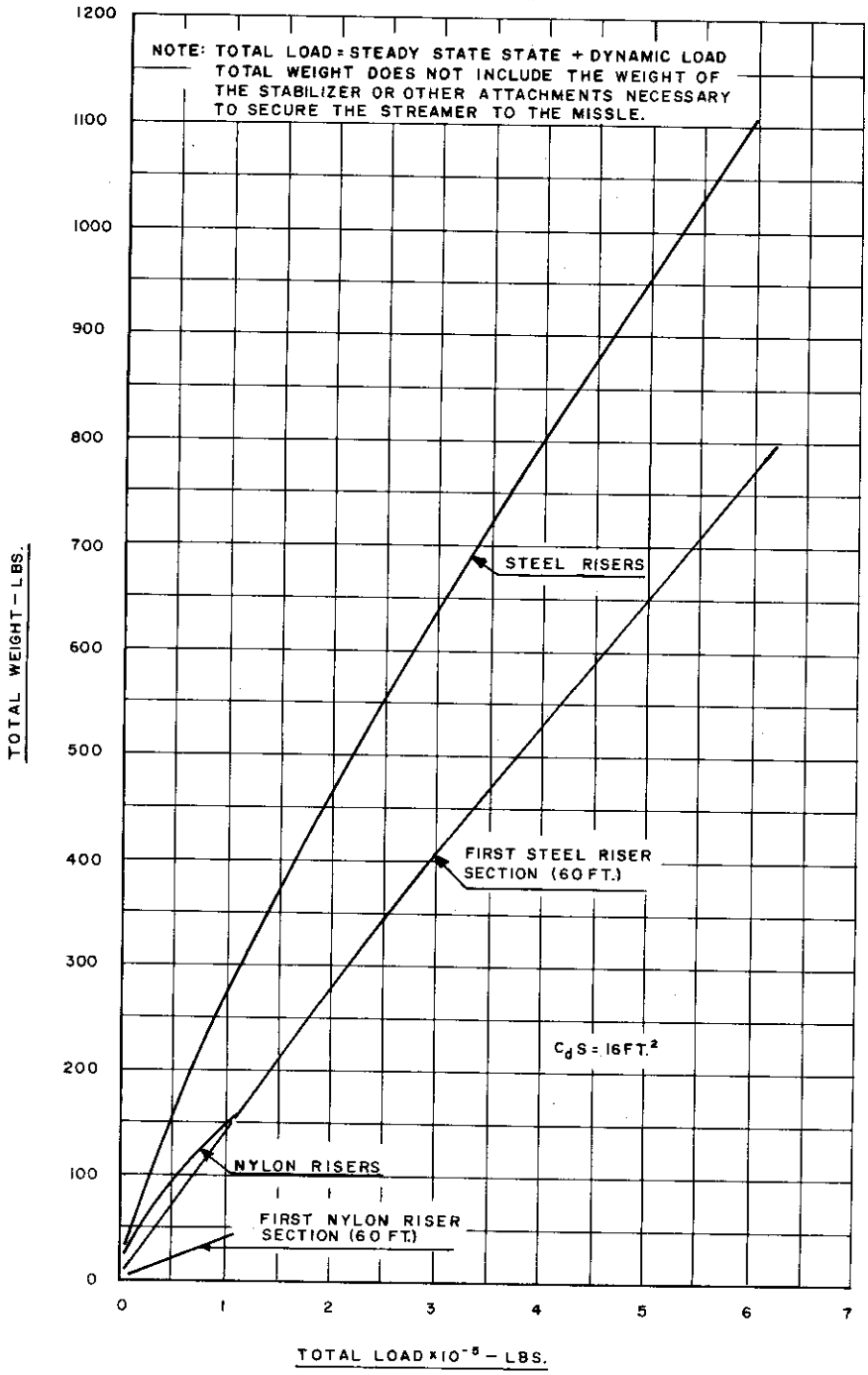

Figure 32. Weight vs. Load for Drag Train

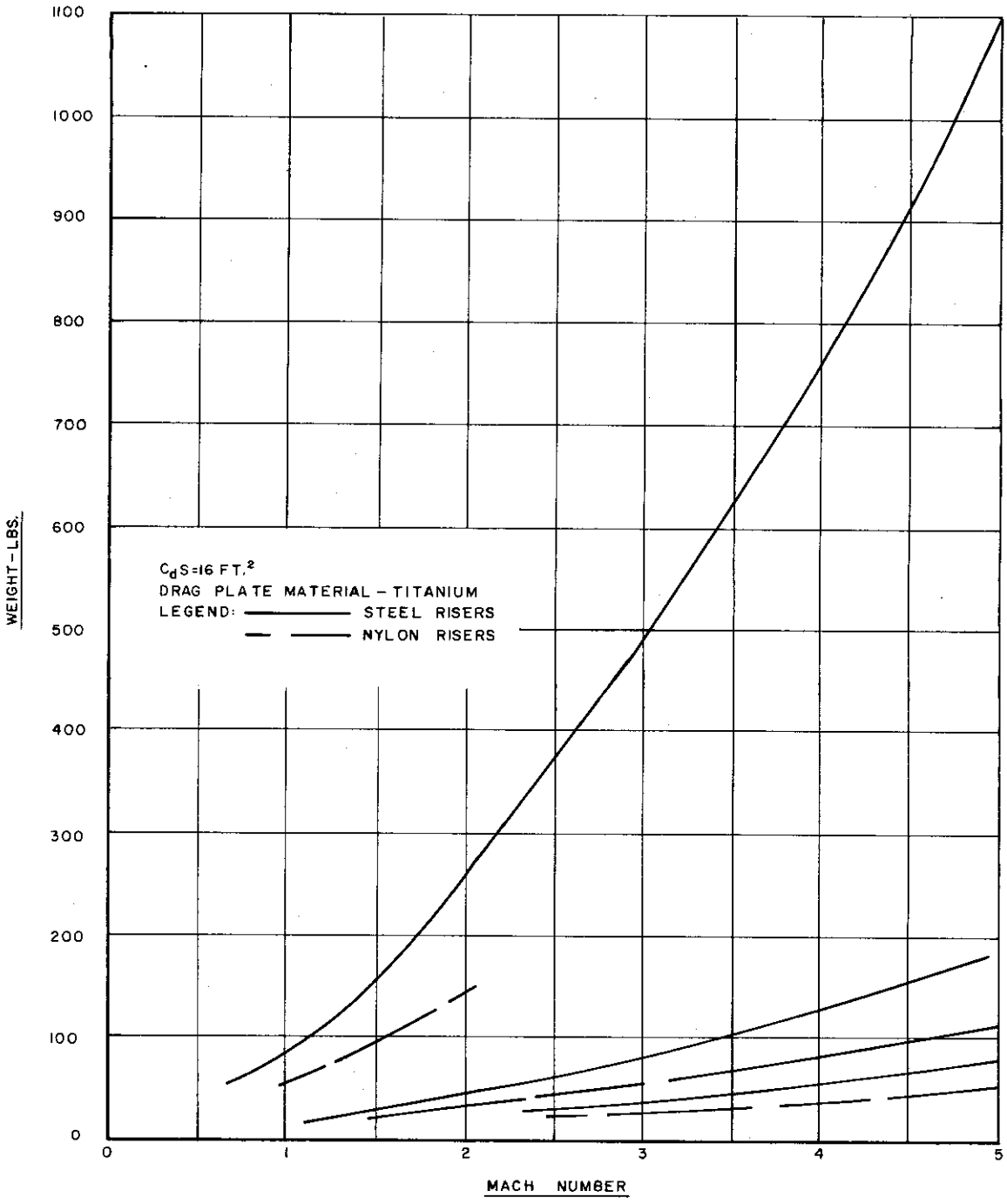

Figure 33. Weight vs. Mach Number for Drag Train

2. Towed Devices

A recovery system using the towing principle lends itself to some standardization and, within certain limits, may be adapted to various missiles with minor changes to itself and to the missile. However, the structure required to trail the drag devices aft of the missile imposes a rather severe space penalty, particularly at high drag loads. For example, a metallic parachute recovery system to sustain a load of 300,000 pounds requires a 2.0 inch diameter 6 x 37 cable as a riser. The only convenient way to package a cable is to coil it. The diameter of the coil is determined by the maximum permissible bending stress of the cable. The cable manufacturers recommend that the coiled diameter of a 6 x 37 cable be 18 to 27 cable diameters. For this particular case the packaging cylinder would be of the order of 3 to 4.5 feet in diameter. This diameter could be reduced by using several smaller cables rather than one large one. However, this might result in an increase in the weight of risers and attendant tie-down structure. Thus it is seen that some compromise must be made between the drag-weight and drag-bulk characteristics of these systems.

The above situation is alleviated considerably when the drag load becomes low enough so that fabric risers can be used. In the case of a drag train, however, the drag plates would be relatively large in diameter and would be extremely difficult to store in any of the smaller vehicles. The metallic parachute canopy would not be as difficult to store. The storage space of the canopy would be determined primarily by the minimum permissible coiled diameter of the suspension cables.

Thus one of the major problems of towed drag devices is maintaining packageability.

C. Materials

The aerodynamic heating which accompanies supersonic speeds introduces several structural problems. Probably the most familiar effect of elevated temperatures is the deterioration in the mechanical properties of materials. Another undesirable effect of an elevated temperature environment is the presence of temperature gradients within a structure. This produces different degrees of expansion, thus introducing thermal stresses. The

aeroelastic properties of a structure are also influenced by temperature; however, this can usually be traced to the presence of thermal stresses and the deterioration of materials at elevated temperatures.

In choosing materials which would be suitable for the various drag devices studies, the deterioration of the mechanical properties was considered to be by far the most important effect of an elevated temperature. The effect of thermal stresses and the other phenomena mentioned above are not nearly as important, since they can be minimized through proper design. A matter of fundamental importance in selecting materials is that of determining which of its properties, strength, stiffness or creep, will be critical in a design. Which property will dominate depends on many factors peculiar to each design. Since the operating time of the drag devices will be short, creep will not be an important factor. Aeroelastic phenomena, such as flutter, will be effected by the variation in the stiffness of a material; however, due to the nature of the drag devices considered, aeroelastic phenomena will not influence the designs to any great degree. It appears then that the strength, or more specifically, the strength-weight ratios will be the dominant design conditions.

Of the various materials available, nylon, dacron, aluminum, titanium, and stainless steel were considered to offer the most favorable strength density ratios. Figure 34 illustrates plots of the yield density ratios of aluminum, titanium, and stainless steel in the temperature range from 75° to 1000°F. It is apparent that up to 150°F aluminum offers the best strength-density ratio and beyond 150°F titanium or stainless steel are superior.

The fabrics, nylon and dacron, are ideally suited for parachute type recovery systems. There is also the possibility of using these fabrics as risers to tow metallic drag devices since the riser will be almost entirely within the wake of the missile and consequently exposed to less aerodynamic heating.

The drag-weight characteristics of several of the representative towed and rigidly attached drag devices are compared in Figure 35. Dive brakes or spoilers and metallic parachutes are seen to offer the most attractive possibilities. When the drag load is low enough so that nylon risers and nylon suspension lines can be used, the metal parachute has superior drag-weight properties. However, when the drag load is so high that steel risers are required,

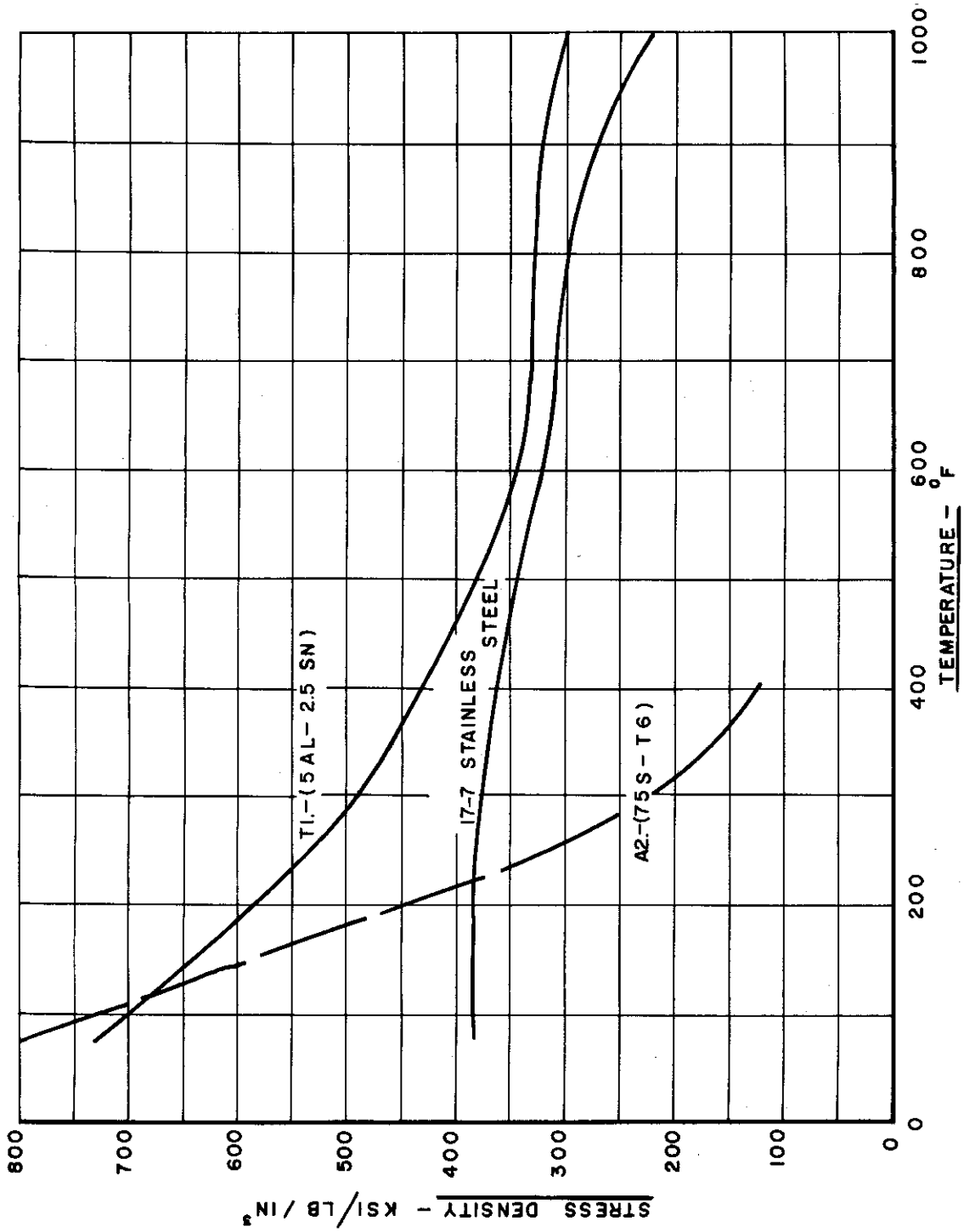

Figure 34. Yield Stress to Density Ratio vs. Temperature

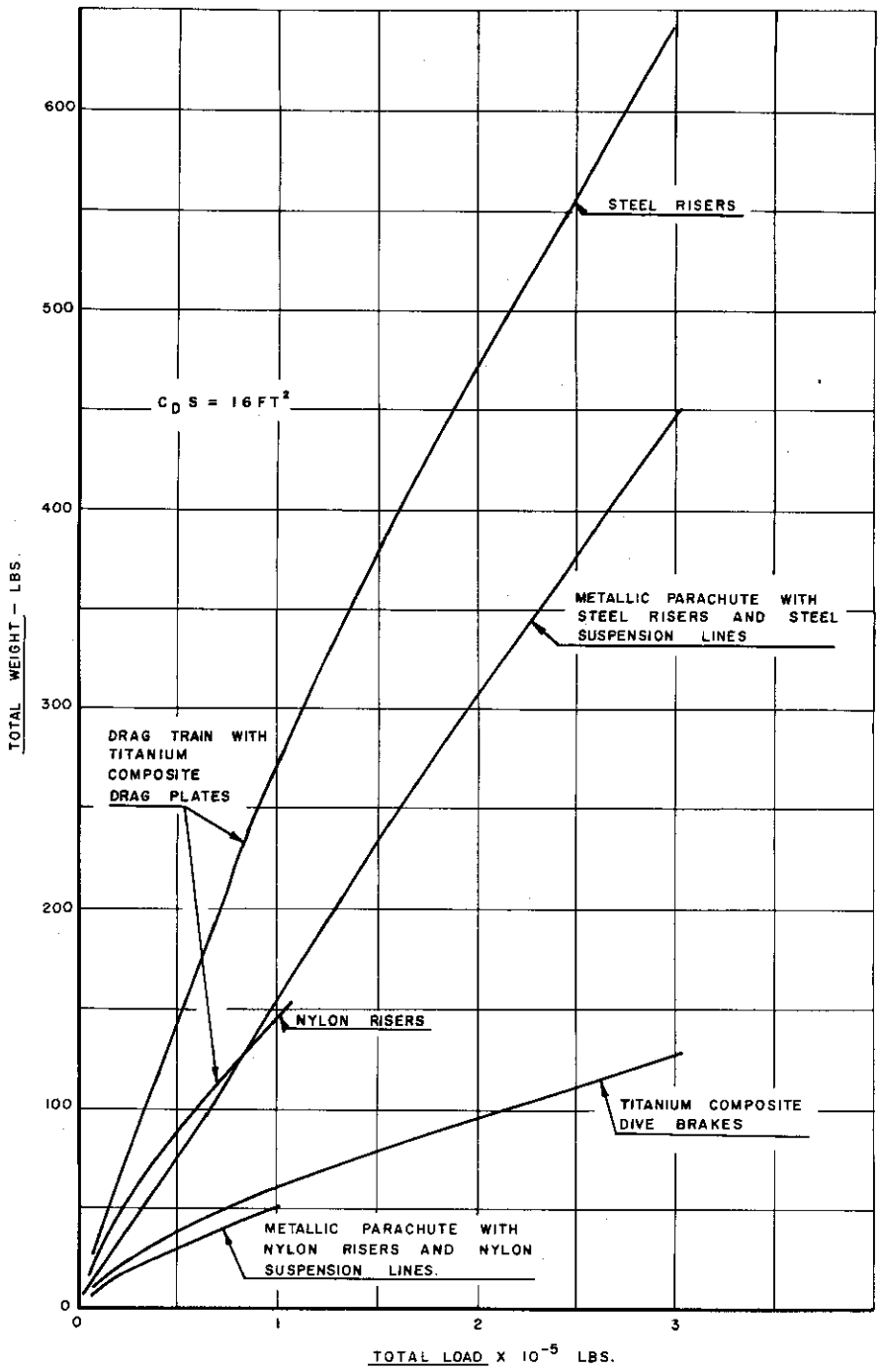

Figure 35. Weight vs. Load for Various Types of Braking Devices at 75°F

the drag-weight properties of the metal parachute drop off rapidly and dive brakes or spoilers then have the highest drag-weight ratio.

In general, it can be concluded that, of the immediate attached drag devices considered, spoilers and dive brakes represent the best general purpose first stage recovery system. For towed devices the parachute is considerably superior to drag trains, and basically, the attainment of drag by plates in the longitudinal direction increases the lengths of risers so much that weight and bulk become excessive. The parachute system considered in this study was towed 10 missile diameters aft of the missile to avoid the low energy wake regions. However, if the diameter of the canopy is increased to compensate for the wake losses close to the base of the missile, an overall reduction in weight and bulk would be realized. For example, from page 12, if the parachute area were increased by 50 per cent, the length of riser could be reduced by a factor of 2.0. Since the bulk and weight of the parachute system is largely due to the risers, the weight and bulk of the system would be decreased almost in proportion to the reduction in riser length. The reduction in weight achieved is shown in Figure 36, where the weight ratio is

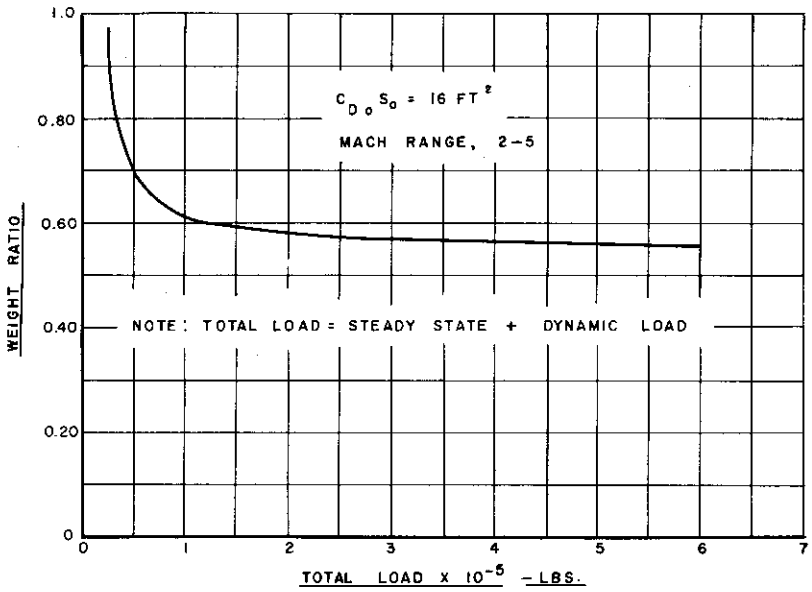

Figure 36. Weight Ratio vs. Load for Metallic Parachute with Steel Risers and Steel Suspension Lines

defined as the ratio of the weight of a parachute with a 25.4 foot riser and a 4.6 foot inflated canopy to the weight of a parachute with a 56.1 foot riser and a 3.8 foot inflated canopy.

CHAPTER 6

SCALING

The size or C_DS of braking devices required will depend upon the size, weight, and flight characteristics of the vehicle. The suitability of a specific braking principle will, in many cases, be governed by its size compared to the size of the vehicle. It is, therefore, necessary to establish some limitation between brake size and vehicle type in order to arrive at conclusions regarding the suitability of particular braking principles to specific objectives.

Since the combinations of vehicle size, weight, and flight characteristics are numerous, only limited conditions can be examined and the analysis accordingly restricted.

The most important characteristic of a first stage braking system is that it must be capable of reducing the velocity of the vehicle to a low enough value that conventional recovery devices may be deployed. The time or altitude loss during the first stage deceleration should be small and will depend on the type of trajectory.

The upper limit velocity at which conventional fabric parachutes can be deployed successfully will depend on the altitude. Recoveries have been successfully accomplished as high as Mach 2.4, at intermediate altitudes; however, the assumption of an upper velocity limit of 2000 fps at low altitudes appears realistic. The analysis of the size of brake required will be predicted on its capability to decelerate the missile to this velocity.

At very low altitudes and high velocities the recovery of a vehicle can be effected only if the missile is in near level flight. There are two ways in which the first stage deceleration may be accomplished. First, the vehicle may be assumed to continue in level flight after the deployment of the first stage brake, or second, the missile may be assumed to follow a ballistic trajectory. The latter procedure appears more realistic because in many

instances the deployment of the first stage may be contingent on malfunction of the vehicle, and presumably level flight cannot be maintained. In this case the time to decelerate the vehicle to 2000 fps must be very short or conversely the size of the brake may be large. This is the situation that is used to determine what proportions exist between a brake and the missile for low altitude conditions.

Since the deceleration due to the brake under these conditions will be large compared to the acceleration of gravity, the size of the brake required to decelerate the vehicle in a given time is determined on the basis of a rectilinear horizontal trajectory.

$$\frac{W}{g}\frac{dV}{dt} = - C_D S \frac{\rho V^2}{2}$$

Whence the time to decelerate from an initial velocity, Vi, to any chosen velocity, V, is

$$t = \frac{1}{\left(\frac{C_D S}{W}\right)_{Total}} \left(\frac{2}{\rho g}\right) \left(\frac{1}{V} - \frac{1}{Vi}\right)$$

The times to decelerate from 5000 to 2000 fps are plotted in Figure 37 vs. $\left(\frac{C_D S}{W}\right)_{Total}$ for altitudes of 0, 10,000 and 20,000 feet. The data of this figure are used with the relation

$$(C_D S)_{Brake} = W \left(\frac{C_D S}{W}\right)_{Total} - (C_D S)_{Missile}$$

to show the relative drag area proportion required of the brake as compared to the missile for missile weight as a function of missile cross-section area. The results are shown in Figure 38 where the time interval to decelerate from 5000 to 2000 fps was taken as 10 seconds for all altitudes. The curve in Figure 38 represents the boundary between the region of brake sizes which must exceed the missile cross-sectional area and the region where the brake size may be less than the missile cross-sectional area. The drag coefficient of the brake was taken as 1.7 and the drag coefficient of the missile as 0.2. The boundary was selected such that the area of the brake was equal to the

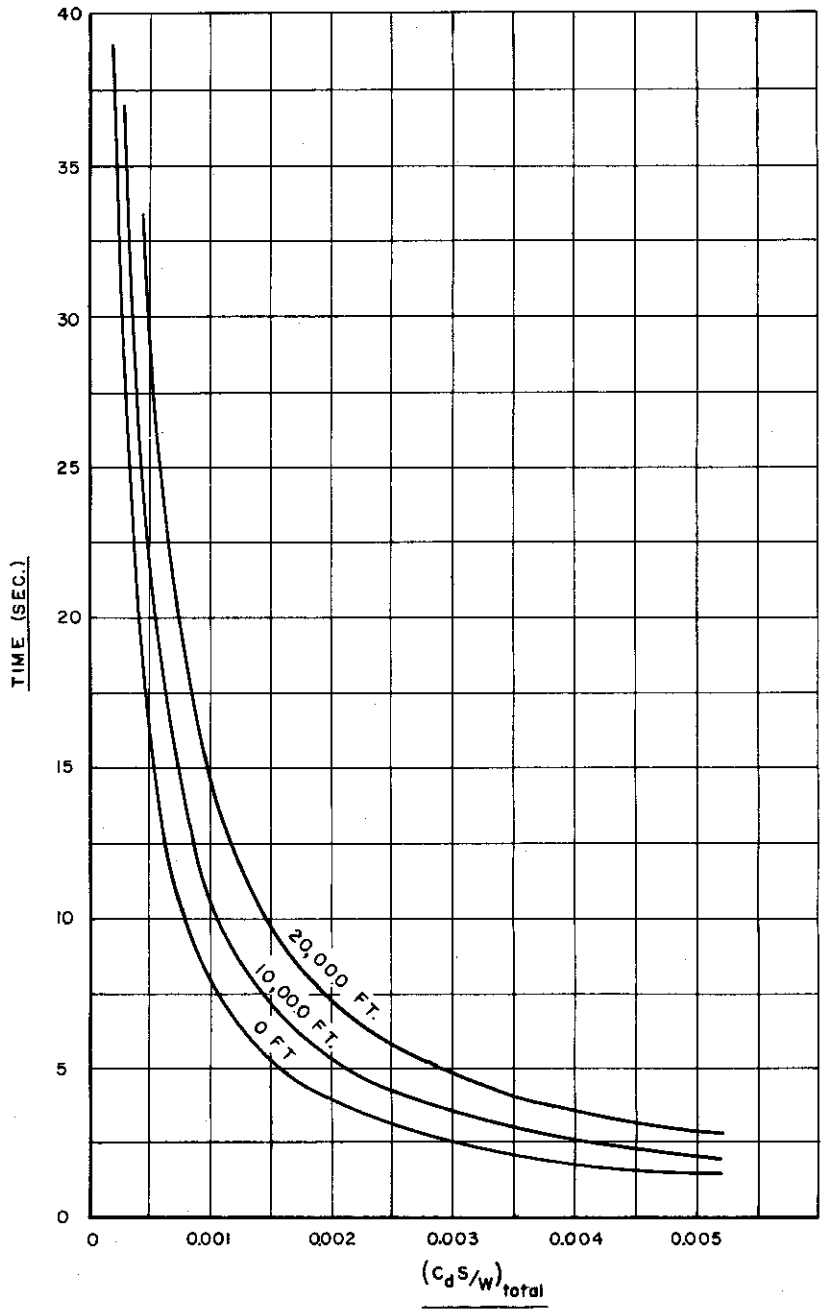

Figure 37. Time to Decelerate from a Velocity of 5000 fps to 2000 fps vs. $(C_DS/W)_{Total}$ and Altitude

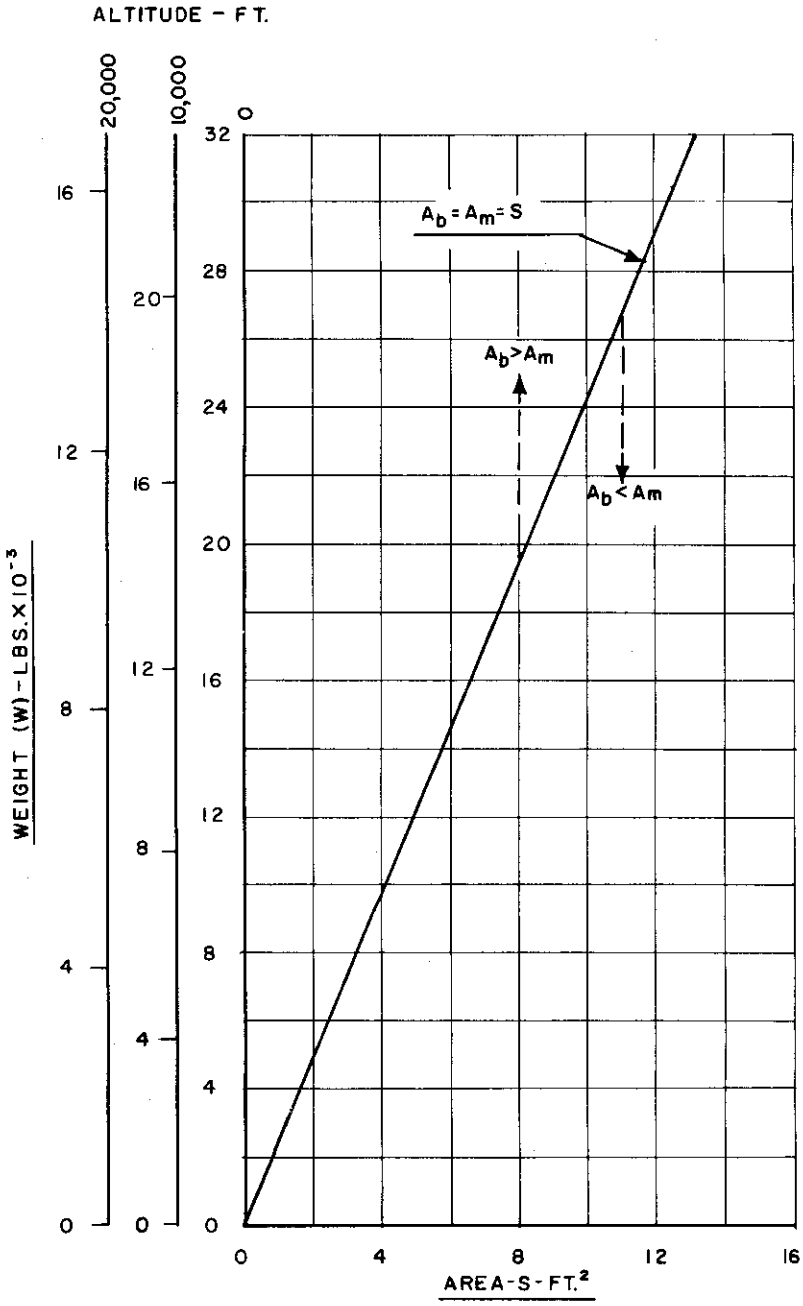

Figure 38. Constant Braking Area Required as Function of Vehicle Weight and Size to Decelerate from 5000 fps to 2000 fps in 10 Seconds (Horizontal Trajectory)

cross-sectional area of the missile because it is unlikely that the effective area of dive brakes, nose blunting, or slats could individually be larger than the missile cross-section area. Therefore, points in Figure 38 lying above the boundaries would probably require the use of devices which may be collapsed or folded while stowed in the missile and can be inflated or extended after deployment.

In the case of vertical trajectories, the altitude lost during first stage deceleration becomes of importance. A figure similar to the case of horizontal level flight is prepared and shown as Figure 39. The equation of motion for vertical flight is

$$\frac{W}{g} \quad \frac{dv}{dt} \quad = \; - \; C_D S \quad \rho \, \frac{V^2}{2} \; + W$$

This equation, assuming an exponential density atmosphere and a constant drag coefficient has the solution

$$V^2 = Vi^2 e^{-\frac{2c_o}{h}(e^{-hx} - e^{-hy})} + \frac{2ge}{h} e^{-\frac{2c_o}{h} e^{-hx}} \left[\overline{E}_i \left(\frac{2c_o}{h} e^{-hx} \right) - \overline{E}_i \left(\frac{2c_o}{h} e^{-hx} \right) \right]$$

where $\overline{E}_i$ (X) is tabulated in Ref. 20,

$$c_o = g \, \frac{C_D S}{2W} \quad \rho_i = \frac{g}{V_{To}^2} \qquad (V_{To} = \text{terminal velocity at a given altitude})$$

h is the rate of decay of ambient air density with increase in altitude, x is the altitude at which V is desired, and y is the release altitude.

Using values obtained from this relationship with $(C_D S)_B = W(\frac{C_D S}{W})_T - (C_D S)M$ yielded the plot of W vs. S for the vertical trajectory, (Figure 39). From this figure it is seen that if the cross-section loading $(\frac{W}{S_M})$ exceeds 240,

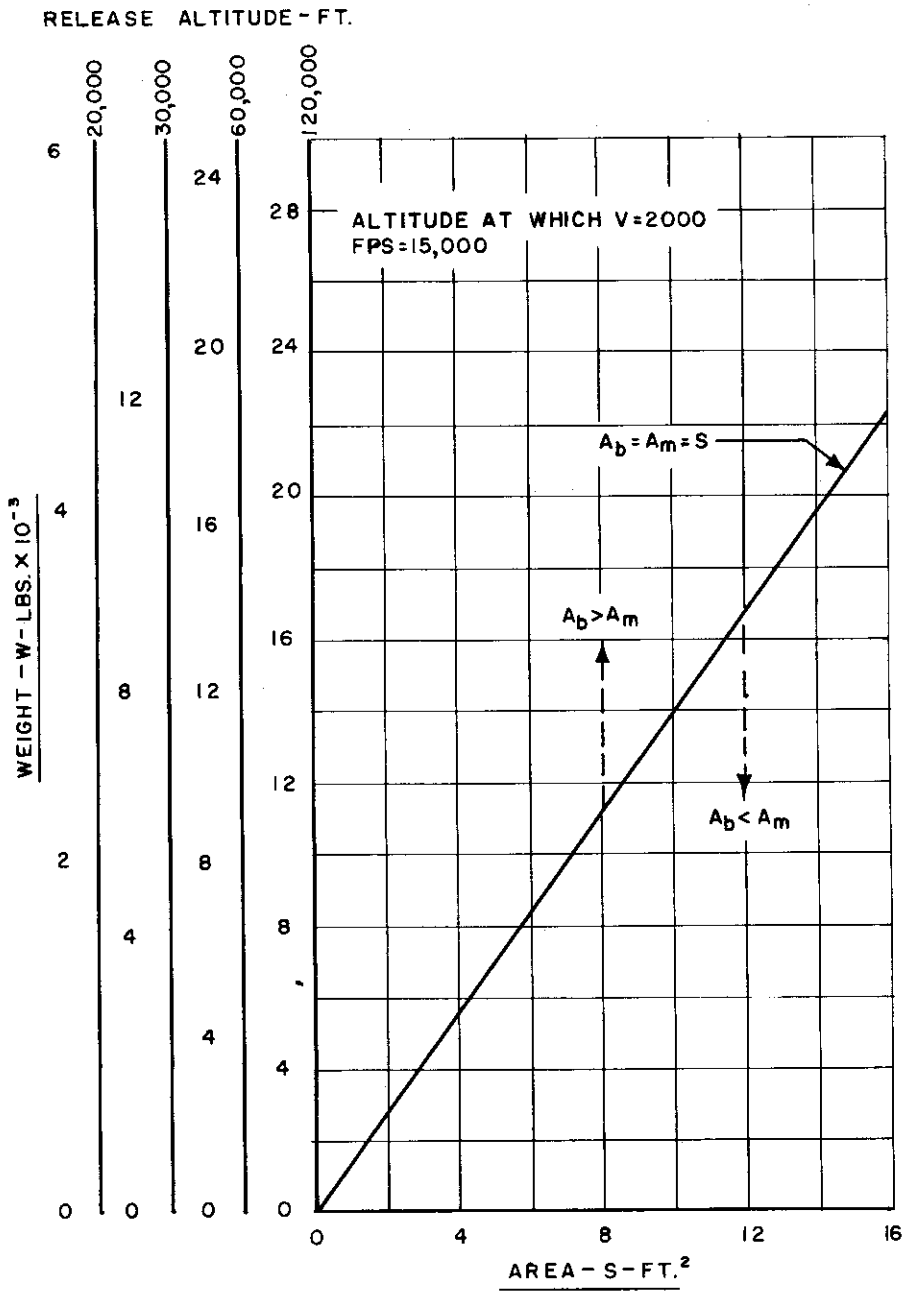

Figure 39. Brake Area Required as a Function of Vehicle Weight and Size to Decelerate from 5000 fps to 2000 fps in Time from Release Altitude to 15,000 ft (Vertical Trajectory)

800, 1200, or 1400, for release altitudes of 20,000, 30,000, 60,000 and 120,000 feet, respectively, then it is likely that trailing devices such as parachutes would have to be employed.

Various values of W/S_M for specific missile configurations are tabulated in Table 6. In comparing these values with the values obtained at the most critical altitude condition presented for horizontal trajectory calculations 20,000 feet (refer to Figure 38), it is seen that most of the missiles fall into the category where dive brakes or some other similar drag device may be employed satisfactorily. Furthermore, the deflection of dive brakes can be programmed so that their effective drag area may be varied to obtain a constant total drag for a given configuration, and thus a constant g value may be maintained throughout the first stage of the deceleration of a missile. In cases where the peak g values encountered in the deceleration of a missile with a constant brake drag area would exceed the g limit of the configuration, programmed dive brakes would be most effective.

In Figure 40, W vs. S for a constant g, first stage deceleration is shown for horizontal trajectory conditions at various flight altitudes. Referring to Table 6, it is seen that approximately 20 per cent of all the missiles and 33 per cent of the high performance missiles fall into the category where programmed dive brakes may be satisfactorily utilized to maintain a constant g deceleration ($W/S_M = 500$ at the most critical altitude condition presented). Thus, it is apparent that, in the case of a first stage deceleration in a horizontal trajectory, programmed drag devices such as dive brakes may be successfully employed by many configurations with minimum g loads being experienced.

However, referring again to the W/S_M values in Table 6, it is seen from Figure 39 for vertical trajectories that only approximately half of the configurations tabulated and 67 per cent of the high performance missiles fall into the category where S_B may be less than S_M for a first stage deceleration from 30,000 feet to 15,000 feet, ($W/S_M < 750$). Also, for vertical trajectories the time to decelerate a missile in its first stage may be quite small due to altitude restrictions, and thus the g loads imposed on a missile might easily be excessive. In order to reduce these g loads, programmed drag area devices might again be used for the first stage deceleration. On Figure 41, a plot of W vs. S for a constant g deceleration is presented for the conditions of vertical trajectories at various brake initiation altitudes. It is seen from

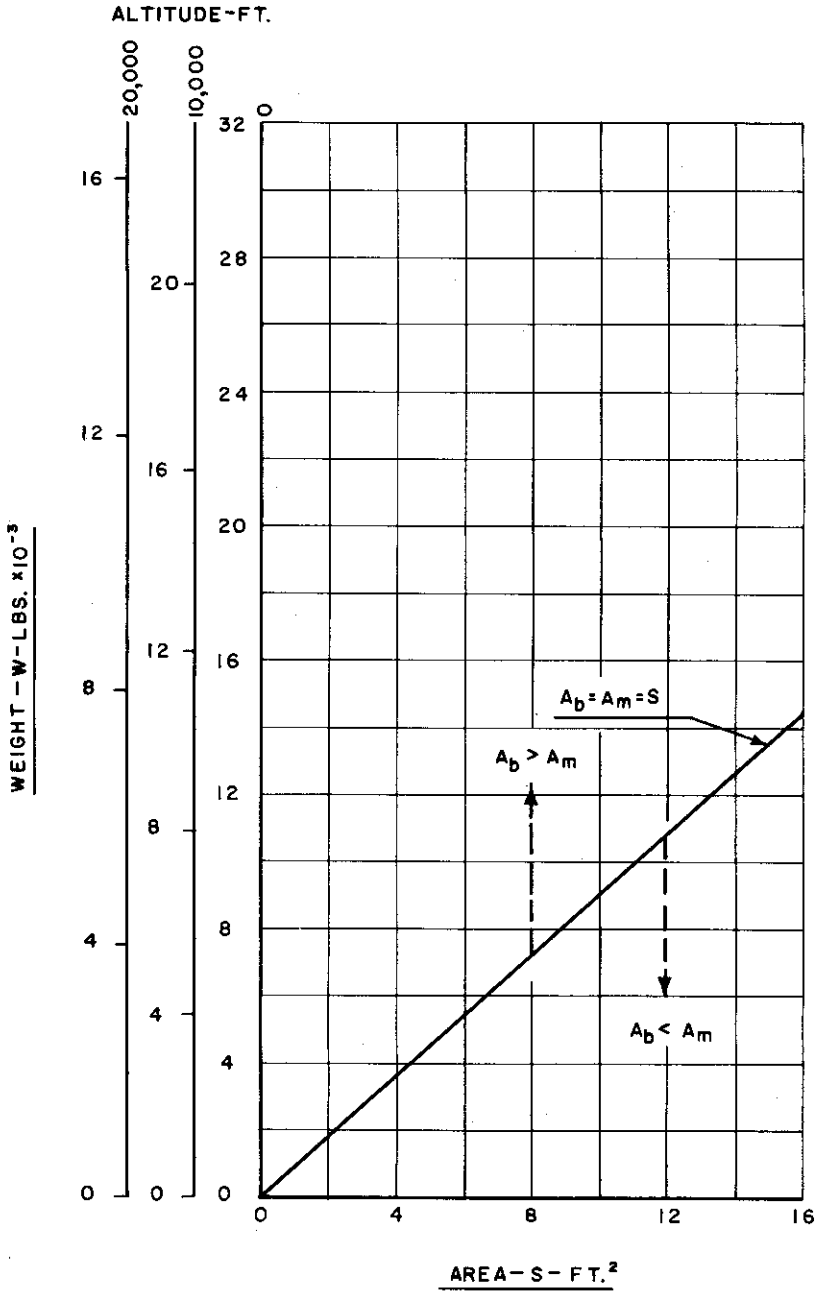

Figure 40. Brake Area Required as a Function of Vehicle Weight and Size to Decelerate from 5000 fps to 2000 fps in 10 Seconds at a Constant g (Horizontal Trajectory)

TABLE 6

Missile Gross Weight Per Unit
Cross-Sectional Area for Some Typical Configurations

Missile	Mach Number	$\frac{W^*}{S_M}$ in lb/ft^2
A	0.6	713
B	0.9	526
C	0.9	1400
D	1.0	1380
E	1.8	1300
F	2.0	550
G	2.0	740
H	2.0	404
I	2.0	459
J	2.0	1025
K	0.95 to 2.4	858
L	1.5 to 2.5	835
M	2.7	1464
N	2.75	648
O	3.0	500
P	3.5	684
Q	3.5	970
R	4.0	838
S	4.0	598
T	5.0	233
U	20.0	261

* Based on missile gross weight after burnout

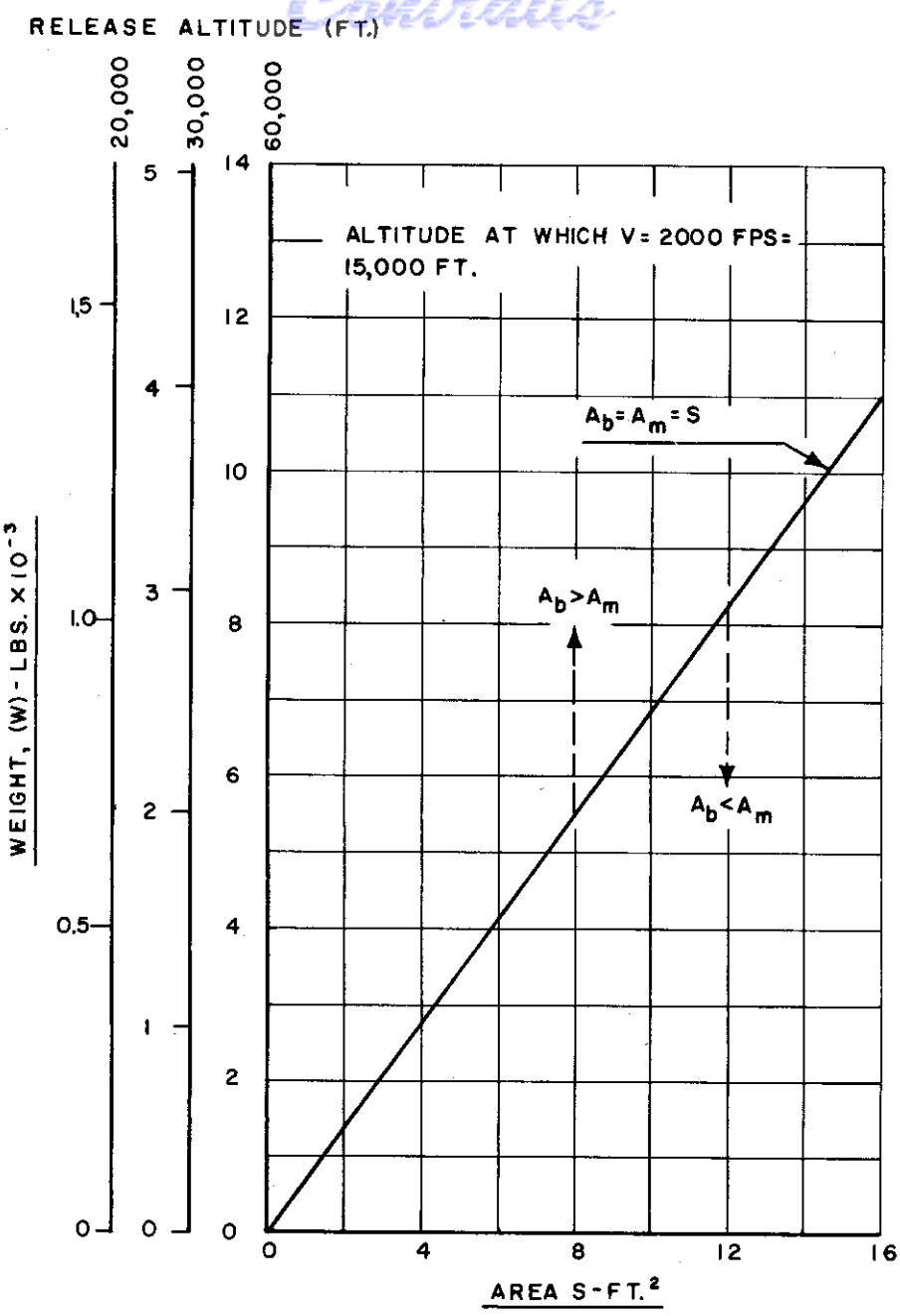

Figure 41. Brake Area Required as a Function of Vehicle Weight and Size to Decelerate from 5000 fps to 2000 fps in Time from Release Altitude to 15, 000 ft at a Constant g (Vertical Trajectory)

this figure that only one of the missiles would fall into the category where brake area could be less than the basic missile area ($W/S_M < 250$ at 30,000 foot altitude conditions) and therefore trailing devices such as parachutes are required. Since programmed actuation of trailing devices at these speeds does not seem feasible, a constant g deceleration does not appear possible for vertical trajectories requiring braking areas larger than the missile cross-sectional area.

CHAPTER 7

DISCUSSION

The important factors that have been considered in the investigation of braking principles have been drag, temperature effects, weight and bulk, and matching the size of the brake to the characteristics of the missile.

In general, the drag coefficient of the braking devices investigated when referred to their own projected solid area is about 1.7 at high velocities. The possibility of using unorthodox methods which may yield somewhat higher drag coefficients must be investigated experimentally because the theoretical analysis of such shapes would be inconclusive and possibly misleading.

Under conditions where the braking system must sustain extremely high loads, devices which are immediately attached to the missile are superior in terms of weight and bulk to trailing devices. Because, under these conditions, trailing devices require large and heavy cabling, stowage of this cabling presents considerable difficulty and the need to minimize snatch loads complicates the method of deployment.

By far the simplest means of decelerating high velocity missiles is to detach portions of the nose, fin leading-edge, etc. The method of deployment in these cases consists simply of an explosive charge being actuated at some time of initiation. For missiles which do not contain vital equipment in the nose or where the nose itself need not be recovered, this represents the simplest or most positive method of deceleration. Unfortunately these conditions are rarely satisfied. The influence of nose bluntness on the stability of the missile is minor and is even favorable at some velocities. The drag characteristics can be predicted adequately on the basis of existing data.

The use of dive brakes entails design problems for the actuating mechanisms and the selection of locations that minimize the effects on missile stability. The actuation of the dive brake can be accomplished with minimum auxiliary power if the brake is allowed to open by reacting with the airstream.

In this case frictional dampers must be installed in order to control the opening rate so as not to exceed the capability of the stops. If the dive brake were to open against the airstream, then power must be supplied to overcome the aerodynamic hinge moments during actuation. The power requirements in this case would increase the bulk and weight of the units and would probably result in a less compact system. The dive brakes must be positioned at fuselage stations that minimize the effects on the over-all stability of the vehicle. In this connection aft locations along the fuselage are favorable, but the optimum location will depend on the configuration of the missile. The maximum size of dive brakes that can be employed would extend into the airstream about 1/2 missile diameter and occupy approximately two-thirds of the total missile circumference, when retracted. Thus the maximum usable (effective) area of dive brakes would be approximately equal to the cross-sectional area of the missile.

Leading edge slats may be used to increase the drag of the fins. The maximum height of slats that can be used must be determined experimentally although slat heights approximately equal to the maximum thickness of the fin are probably tolerable. Slats are probably useful only as secondary or auxiliary devices because the drag area obtainable by this means is relatively small.

Rotochutes are somewhat limited at high Mach number, low altitude operation due to the large bending moments induced in the long cantilevered blades. The deployment characteristics of the rotochutes impose severe restrictions on locations along the missile. Since the rotochute depends on centrifugal forces or rotation to effect its extension, it must occupy positions which are free from obstructions due to fins and other protuberances. Nose locations or special attachments would be required. The effectiveness of the rotochute at high Mach numbers will be reduced considerably due to the deterioration of lift-to-drag ratio with Mach number. Considerable research and development of the rotochute would be required in order to evaluate its effectiveness and to determine its adaptability to high-speed missile recovery problems.

Where the area of the brake must considerably exceed the cross-sectional area of the missile, trailing devices must be employed. In such circumstances the load on the brake may be extreme, and consequently the weight and bulk of risers will be great. Under extreme loads, metal risers may be necessary. The low extension characteristics of steel cables compared to nylon lines present snatch problems, and methods of controlling the differential velocity during deployment may be necessary. More crucial than these design

problems are the characteristics of parachutes themselves at high Mach numbers. The inflation characteristics of fabric type parachutes at high Mach numbers are relatively unknown, and it is anticipated that the inflation characteristics of parachutes made of metal will be more difficult. Data on these characteristics must be obtained by conducting wind tunnel or flight tests.

CHAPTER 8

CONCLUSIONS

The more significant conclusions derived from the preceding study are enumerated as follows:

1. It is clear that several braking principles may be applied to accomplish the first stage deceleration of vehicles in altitude ranges from sea level to 250,000 feet and Mach 1 to 5. Devices can be constructed to withstand high loads and the temperatures generated under these conditions. Under conditions of extreme velocities and low altitudes, the loads imposed by the brake on the vehicle will probably substantially exceed the capabilities of the vehicle itself. The recovery procedure must consider the capabilities of the vehicle. Because of foreseeable limitations imposed by the missile, it is unlikely that extremely massive or rugged brakes will be necessary or desirable.

2. Under most conditions of first stage deceleration, the time to decelerate must be short. The temperatures obtained during this interval can be controlled with simple methods of evaporation or transpiration cooling.

Temperature rises become an important consideration for first stage decelerations that are initiated at extremely high altitudes and high Mach numbers. Under these conditions the dynamic pressure is small and the brake is ineffective in reducing velocity. However, long times are available for aerodynamic heating to take place and the temperature problem assumes greater importance. This method of first stage deceleration does not appear desirable. It appears preferable to delay the initiation of braking to a lower altitude where practical deceleration forces can be achieved. If the brake is not initially cooled or contained at essentially ambient air temperatures in an insulated compartment in the vehicle, then the brake must be able to withstand the same temperatures experienced by the vehicle. Protection of the brake structure

with a heat resistance layer such as magnesium oxide or Fiberglas may be desirable in these cases. This method would be applicable to dive brakes and drag trains, etc.

3. For first stage decelerations which require a braking area less than the cross-sectional area of the missile, dive brakes, leading edge slats or nose blunting are possible and are more advantageous from the standpoints of simplicity, bulk, and weight. Dive brakes in particular can be programmed to maintain a constant deceleration force on the vehicle and minimize high peak loads that are difficult to eliminate with other devices.

4. For first stage decelerations which require braking areas exceeding the cross-sectional area of the missile devices which can be towed by the missile and extended or inflated after deployment are required. In view of limit load capabilities of vehicles, it is likely that nylon risers with heat protection can be used. Parachute-like devices are superior to drag trains and should be employed.

5. A considerable amount of research and development work will be required to evaluate the suitability of rotochute type devices to the first stage deceleration of vehicles. Problems of actuation and adaptation of the rotochute to vehicles of arbitrary configuration need careful consideration. In view of the apparent superiority of dive brakes and metal canopy parachutes, investigation of rotochutes should be deferred until these other devices are evaluated.

During the project the need for information on several critical questions arose. These problems must be investigated experimentally. The investigations that are required are indicated in the final section of this report.

CHAPTER 9

RECOMMENDATIONS

Below are recommendations for conducting wind tunnel sled tests to investigate experimentally characteristics of specific braking principles:

1. Investigation of Parachutes

The inflation of conventional fabric parachutes at high supersonic Mach numbers is unknown. It is recommended that wind tunnel tests be conducted to photograph the inflation characteristics and shock wave formations around parachutes at Mach numbers in the order of 3.0 drag. Opening shock factors should also be measured. The Unitary Wind Tunnel at the Lewis Laboratories of the NACA is a typical facility which can accomplish these tests.

2. Wake Survey

The information on the energy distribution in the wake of bodies at supersonic speeds has been obtained by measuring total and static pressure. The analysis of these data to obtain wake dynamic pressure is difficult and uncertain. In order to obtain wake data that are more directly applicable to determine forces generated by parachutes, etc., in the wake of a vehicle, it is recommended that wind tunnel tests be conducted. These tests would consist of measuring the drag force on a circular plate at several down stream positions behind the body. The diameter of the disk should be between 1 and 1-1/2 diameters of the wake producing body.

3. Dive Brake Locations

The drag characteristics of dive brakes can be estimated from existing data; however, their location along the missile axis will have an influence on the stability of the vehicle. Wind tunnel tests should be

conducted with dive brakes located at axial positions for an idealized configuration to indicate the influence of dive brake location on the stability of the vehicle.

4. Metal Parachute Canopies

The performance of parachute canopies made of metal bands or wire mesh cloth can be investigated by conducting sled tests. The test conditions required are high dynamic pressure rather than high Mach number. It is recommended that two sled runs be conducted to determine the magnitude of the problem in employing metal parachute canopies.

REFERENCES

1. Hoerner, S. F., Aerodynamic Drag, The Otterbein Press, Dayton, Ohio, 1951.

2. NACA Report 1135, Equations, Tables and Charts for Compressible Flow, 1953.

3. Griffith, W., "Shock Tube Studies of Transonic Flow Over Wedge Profiles", Journal Of The Aeronautical Sciences, April, 1952.

4. Chapman, D. R., Wimbrow, W. R., and Kester, R. H., Experimental Investigation of Base Pressure on Blunt - Trailing - Edge Wings at Supersonic Velocities, NACA TN 2611, January 1952.

5. Howarth, D., Modern Developments in Fluid Dynamics of High-Speed Flow. 2 Volumes. Oxford University Press, 1953

6. Redman, E. J. and Walter, L. W., Investigation of the Flow in the Wake of a Circular Cylinder at Mach Number 2.86, Navord Report 3705, 4 August 1954.

7. Stephenson, J. P., The Effects of Aerodynamic Brakes on the Speed Characteristics of Airplanes, NACA in 1939, Sept. 1949.

8. NACA RM L55K23, CONFIDENTIAL

9. Walchner, O., Systematic Wind Tunnel Measurements on Missiles, NACA TM 1122, March 1947.

10. NACA RM SL 54FLO, CONFIDENTIAL

11. NACA RM SL 54 D 13a, CONFIDENTIAL

12. Cook Research Laboratories, Chicago, Illinois, Recovery Systems for Missiles and Target Aircraft, Phase II, to be published as AF Technical Report by WADC.

13. Huston, W. B., Warfield, C. N., Stone, A. Z., A Study of Skin Temperatures of Control Bodies in Supersonic Flight, NACA RM L7J21.

14. Stalder, J. R. and Nielsen, H. V., Heat Transfer from a Hemisphere - Cylinder Equipped with Flow Separation Spikes, NACA TN 3287, 1954.

15. R. J. Roark, Formulas for Stress and Strain, McGraw - Hill, New York, 1943.

16. ANC-5 Strength of Metal Aircraft Elements, March 1955

17. S. Timoshenko, Theory of Plates and Shells, McGraw - Hill, New York, 1940.

LIST OF SYMBOLS

A	Area of a panel or skin segment (in.^{2})
A_e	Open area of a parachute
A_o	Constructed area of a parachute
A_p	Projected area of a parachute
b	Height of a panel (in.)
C	Solar constant = (0.1192 BTU/ft^2-sec)
C_D	Drag coefficient
C_{D_N}	Nose drag coefficient
C_{D_B}	Base drag coefficient
C_M	Moment coefficient
c	Specific heat (BTU/lb$^\circ$R)
c_p	Specific heat at constant pressure
c_v	Specific heat at constant volume
D	Drag force
D_N	Drag force due to the nose of a body
d	Diameter
d_o	Constructed diameter of parachute
d_p	Projected diameter of parachute
E	Modulus of elasticity

F_S	Heat capacity parameter = $c\delta$ $\left(\frac{\text{BTU-ft}}{\text{lb}^{\circ}\text{F}}\right)$
g	Acceleration of gravity
h	Heat transfer coefficient $\left(\frac{\text{BTU}}{\text{ft}^2\text{-sec-}^{\circ}\text{R}}\right.$
K_3	Shape factor, three-dimensional equation
K_2 and K_2'	Shape factor, two-dimensional equation
k	Thermal conductivity $\left(\frac{\text{BTU}}{\text{ft-sec-}^{\circ}\text{R}}\right)$
L_c	Suspension line load
ℓ	Length (in.)
ℓ_c	Length of generatrix of a cone (ft)
M	Mach number
m	Number of frame beams
N_u	Nusselt number
n	Number of panels, skin segments, or gores
p	Pressure
p_B	Base pressure
p_∞	Atmospheric pressure (free stream static pressure)
p_{t2}	Stagnation pressure after a normal shock
Q	Heat transferred(BTU)
q	Dynamic pressure
q_c	Compressible dynamic pressure

q_w	Dynamic pressure in wake
R_e	Reynold's number
r	Radius (in.)
S	Frontal area of a body
S_B	Brake area
S_D	Disk area
S_M	Frontal area of missile
S_N	Nose area
s	Stress
s_B	Bending stress
s_T	Tensile stress
s_Y	Yield stress
T	Temperature ^oR
T_A	Ambient air temperature ^oR
T_B	Boundary layer temperature ^oR
T_S	Skin temperature ^oR
t	Time
V	Velocity
V_∞	Free stream velocity (fps)
W	Weight

W_c	Weight of canopy
W_f	Weight of frame
W_s	Weight of skin
w	Specific weight
α	Angle of attack
β	Total apex angle of cone (radians)
γ	Ratio of specific heats = $\frac{c_p}{c_v}$
δ	Thickness
ϵ	Emissivity of surface
θ	Semi vertex angle of wedge
λ	Sky radiation factor
μ	Viscosity of air ($\frac{\text{lb-sec}}{\text{ft}^2}$)
ρ	Density
ρ_∞	Free stream density ($\frac{\text{slugs}}{\text{ft}^3}$)
σ	Stefan Boltzman radiation constant = (0.47594×10^{-2} BTU/ft^2 sec $^\circ$R^4)
σ_R	Solidity ratio
ϕ	Semi angle between parachute suspension lines
ψ	Ratio of height to width of panel
ω	Load per unit length of frame beam ($\frac{\text{lb}}{\text{in.}}$)